ABERRATION FIELD PROPERTIES OF SIMPLE NON-AXIALLY SYMMETRIC OPTICAL SYSTEMS.

JEWELL, TATIANA EMELIANOVNA

ABERRATION FIELD PROPERTIES OF SIMPLE NON-AXIALLY SYMMETRIC OPTICAL SYSTEMS

THE UNIVERSITY OF ARIZONA M.S. 1984

PLEASE NOTE:

In all cases this material has been filmed in the best possible way from the available copy. Problems encountered with this document have been identified here with a check mark __✓__.

1. Glossy photographs or pages _____
2. Colored illustrations, paper or print _____
3. Photographs with dark background _____
4. Illustrations are poor copy _____
5. Pages with black marks, not original copy _____
6. Print shows through as there is text on both sides of page _____
7. Indistinct, broken or small print on several pages ✓
8. Print exceeds margin requirements _____
9. Tightly bound copy with print lost in spine _____
10. Computer printout pages with indistinct print _____
11. Page(s) _____ lacking when material received, and not available from school or author.
12. Page(s) _____ seem to be missing in numbering only as text follows.
13. Two pages numbered _____. Text follows.
14. Curling and wrinkled pages _____
15. Other _____

ABERRATION FIELD PROPERTIES OF SIMPLE NON-AXIALLY SYMMETRIC OPTICAL SYSTEMS

by

Tatiana Emelianovna Jewell

A Thesis Submitted to the Faculty of the

COMMITTEE ON OPTICAL SCIENCES (GRADUATE)

In Partial Fulfillment of the Requirements
For the Degree of

MASTER OF SCIENCE

In the Graduate College

THE UNIVERSITY OF ARIZONA

1 9 8 4

STATEMENT BY AUTHOR

This thesis has been submitted in partial fulfillment of requirements for an advanced degree at The University of Arizona and is deposited in the University Library to be made available to borrowers under rules of the Library.

Brief quotations from this thesis are allowable without special permission, provided that accurate acknowledgment of source is made. Requests for permission for extended quotation from or reproduction of this manuscript in whole or in part may be granted by the head of the major department or the Dean of the Graduate College when in his or her judgment the proposed use of the material is in the interests of scholarship. In all other instances, however, permission must be obtained from the author.

SIGNED: Tatjana Emelianovna Jewell

APPROVAL BY THESIS DIRECTOR

This thesis has been approved on the date shown below:

Roland V. Shack — 8/16/84

R. V. Shack
Professor, Optical Sciences

Date

ACKNOWLEDGMENTS

I would like to express my appreciation to the faculty and staff at the Optical Sciences Center, but especially to my advisor Professor Roland V. Shack for his initial suggestion of this topic. I was very lucky to have his friendship and guidance during this work and my time at the Optical Sciences Center.

To my husband, Jack, I would like to express my gratitude for his patience, encouragement, and faith in me.

A special thanks goes to Maggie Whitney for her invaluable help in the preparation of the final typewritten form of the thesis.

TABLE OF CONTENTS

TABLE OF CONTENTS—Continued

LIST OF ILLUSTRATIONS

Figure Page

LIST OF TABLES

ABSTRACT

The first- and third-order properties of simple tilted and decentered optical systems were analyzed. The basic optical systems chosen were the usual components of symmetric optical systems, namely the plane-parallel plate, the thin refractive prism, the mirror (including aspherics), and the thin lens.

The emphasis was placed on the development of insights enabling the designer to use these components as parts of larger tilted and decentered systems.

Aberrations of a thin lens were analyzed using an approach of a centered system with eccentric pupil, rather than the tilted and decentered system approach.

Since a vector form of the wave aberration expansion was used, the tilts and decenters of the components were not restricted to be coplanar.

A few interesting special cases involving combinations of the components were discussed. Some of these special cases were evaluated with an exact ray trace using a computer design program and found to be in good agreement with the theoretical third-order predictions.

CHAPTER 1

INTRODUCTION

An aberration theory of perturbed optical systems has been developed by K. Thompson (1980) from earlier work by R. Shack. This theory has made it possible to develop an understanding of all of the aberration terms through fifth order in tilted and decentered systems. The emphasis was on studying each term in the wave aberration expansion without specifying the system.

The purpose of this work is to study the aberrations through third order of simple tilted and decentered optical systems. The systems to be examined here are the plane-parallel plate, the thin refractive prism, the mirror, and the thin lens.

Some work in this area has been previously published. Prasad et al. (1975) dealt with an arbitrary number of tilted plane surfaces separated by media of different refractive indices. Based on an exact ray-trace scheme, he developed the expressions for coma and astigmatism, but his treatment assumed only coplanar tilt of the surfaces, and the rays were traced in the same plane.

Shearer (1950) used the parabasal astigmatism formulas, known as the Coddington equations, to show that the reference axis astigmatism of one concave spherical mirror can be eliminated by cross-tilting it with a second concave spherical mirror.

Other related work was done by R. Buchroeder (1970, 1976), although his approach did not provide the description of aberrations over the entire image field. He developed the means to correct third-order aberrations along the reference axis and could describe the aberrations in the meridional plane.

King (1974) and Gelles (1974, 1975) applied the technique described by R. Buchroeder to design tilted and decentered mirror systems with the third-order aberrations corrected at the center of the image field.

In this work we present the description of the first-order properties and the third-order aberrations of tilted components of an optical system over the entire field. The results of this work will provide an optical designer with useful insights enabling him or her to use simple systems as components of a design. The designer can lay out the system and balance third-order aberrations of the tilted components in the system. Then computer programs can be used for optimization once the system has been laid out.

Since we use paraxial equations, the component tilts are assumed to be small. For large tilt angles, the solutions obtained using this approach will not be exact, but sufficiently close for use as a starting point of optimization with computer design programs.

This thesis is structured as follows. Since this work is based largely on the theory developed earlier (Thompson 1980), Chapter 2 reviews the first- and third-order properties of general perturbed

optical systems. To develop gradually an understanding of the behavior of each component, we start with the simplest one. In Chapter 3 we examine the behavior of the tilted plane-parallel plate. Chapters 4, 5, and 6 deal with the thin refractive prism, the mirror (including aspherics), and the thin lens. Each chapter establishes the first- and third-order properties and treats some interesting special cases, which provide understanding in using these components as part of an optical system design.

In Chapter 7 we examine a few of these special cases with a computer optical design program (Super Oslo) to confirm the theory developed in the previous chapters.

Finally, Chapter 8 summarizes the results and indicates where this work may be continued.

CHAPTER 2

REVIEW OF FIRST ORDER PROPERTIES AND THIRD ORDER ABERRATION FIELDS IN TILTED AND DECENTERED OPTICAL SYSTEMS

Before the discussion of the components, it would be appropriate to review briefly the first- and third-order behavior of tilted and decentered general optical systems. The development of the first- and third-order theory of perturbed optical systems was done by K. Thompson in his dissertation, "Aberration fields in tilted and decentered optical systems." In this chapter we simply summarize the contents of two chapters of his dissertation.

First-Order Theory

The properties of interest are image displacement, pupil displacement, Gaussian image plane (GIP) tilt, optical axis ray trace, and aberration field decentration, calculated surface by surface.

The reference axis (RA) of a perturbed system is the axis about which all of the elements are rotationally symmetric in the aligned system. This is the axis from which the surface tilts and decenters, object, image, and pupil decenters and Gaussian image plane tilt are measured.

The local axis (LA) of a surface is defined as the line containing the vertex and the center of curvature of a surface. The

tilt of a surface is given by the angle between the LA and the reference axis of the system.

A spherical surface does not have a unique axis. Any line through the center of curvature intersecting the surface may be taken to be the local axis of that surface. Therefore we define the local axis for a spherical surface as the line containing the center of curvature and the center of the object field. The properties of a surface in a perturbed system are uniquely determined by the displacement of the center of curvature from the reference axis.

The equivalent tilt paramter, $\vec{\beta}_0$, is related to the displacement of the center of curvature $\vec{\delta}c$, and to the conventional tilt and decenter parameters $\vec{\beta}$ and $\vec{\delta}v$ by

$$\vec{\beta}_0 = \vec{\beta} + c\vec{\delta}v = c\vec{\delta}c \tag{2.1}$$

as shown in Fig. 2.1.

For a plane surface, the local axis can be defined as the normal to the surface passing through the center of the object. The tilt of a plane surface is given by the angle between the local axis of this surface and the reference axis as shown in Fig. 2.2.

In an optical system, any surface (denoted by j) has associated with it an object/image, and entrance/exit pupil, either or both of which may be real or virtual. The image and exit pupil for the j-th surface become the object and entrance pupil for the (j + 1)-th surface.

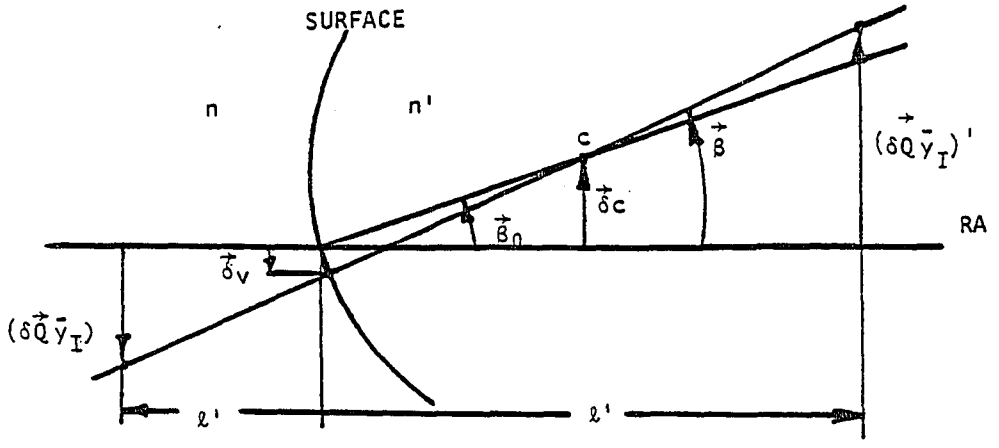

Fig. 2.1. The equivalent tilt parameter and the image displacement for a spherical surface.

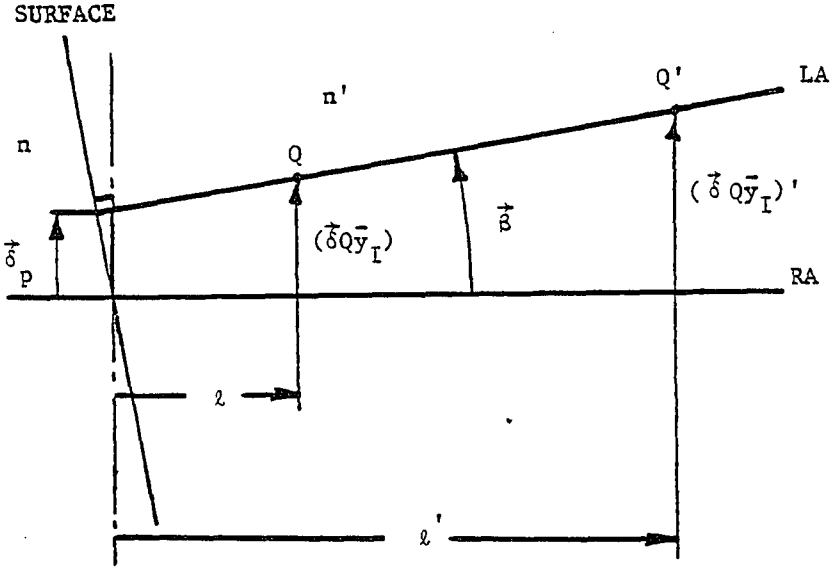

Fig. 2.2. The tilt and the image displacement for a plane surface.

For the spherical surface the relative image displacement, $\vec{\delta}Q'$, (image displacement normalized by the image height in the centered system) is given by

$$\vec{\delta}Q' = \vec{\delta}Q + \frac{y\Delta(n)}{\mathcal{H}}\vec{\beta}_0 \ . \tag{2.2}$$

Here $\vec{\delta}Q$ is the relative object displacement for the surface, y is the marginal ray height at the surface in the centered system, $\Delta(n) = n' - n$, the difference between image space index of refraction and the object space index, and $\mathcal{H} = n\bar{u}y - nu\bar{y}$ is the Lagrange invariant (u is the marginal ray angle preceding the surface, $\bar{u}$ is the chief ray angle preceding the surface, $\bar{y}$ is the chief ray height at the surface in the centered system).

The notation here is slightly different from that in the original work by K. Thompson. Here $\vec{\delta}Q$ and $\vec{\delta}Q'$ are already normalized quantities (compare with $(\vec{\delta}Q/\bar{y}_I)$ and $(\vec{\delta}Q/\bar{y}_I)'$ in the original). Also, here all the equations are presented in vector form, since it was shown in the original work that the development need not be restricted to the meridional plane. The tilts and decenters can be nonmeridional and noncoplanar.

For a plane surface the expression 2.2 becomes

$$\vec{\delta}Q' = \frac{n'}{n}\vec{\delta}Q + \frac{\Delta(n)u}{\mathcal{H}}\vec{\delta}_p, \tag{2.3}$$

where $\vec{\delta}_p$ is the distance from the reference axis to the intersection of the local axis with the surface as shown in Fig. 2.2.

Similarly, the entrance and exit pupils throughout the system can be found using the expression

$$\vec{\delta}E' = \vec{\delta}E - \frac{\bar{y}\Delta(n)}{n'c}\vec{\beta}_0 \ . \tag{2.4}$$

Here $\vec{\delta}E$ and $\vec{\delta}E'$ are relative entrance and exit pupil displacements (normalized by the entrance and exit pupil radii).

The optical axis ray (OAR) by definition passes through the centers of the object/image planes and the pupils for all surfaces of the system. This ray is the paraxial equivalent to a zero field, zero aperture ray in a real ray trace.

The intersection of this ray with the image plane of the unperturbed system gives the image displacement and the location of the center of the Gaussian image plane. Given the centers of the object, the image, and the pupils, the paraxial height $\vec{\bar{y}}^*$ at a surface, and the paraxial ray angle $\vec{\bar{u}}^*$ preceeding the surface for the OAR are given by

$$\vec{\bar{u}}^* = \bar{u}\,\vec{\delta}Q + u\vec{\delta}E \tag{2.5}$$

$$\vec{\bar{y}}^* = \bar{y}\,\vec{\delta}Q + y\vec{\delta}E, \tag{2.6}$$

where both quantities are measured with respect to the reference axis.

The wave aberrations are measured with respect to the Gaussian image plane, therefore it is important to find the tilt of the Gaussian image plane. The tilt of this plane with respect to the RA for any surface is

$$u'\vec{\theta}' = u\vec{\theta} + \vec{\beta}\Delta(u), \tag{2.7}$$

where $\Delta(u) = u' - u$, and $\vec{\theta}$ and $\vec{\theta}'$a are the tilts of object and Gaussian

image planes with respect to the RA. For a spherical surface $\vec{\beta} = \vec{\beta}_0 - c\vec{\delta}v$, as before, and for a plane surface $\vec{\beta}$ is the tilt of the local axis. The tilt of the Gaussian image plane for a spherical surface is shown in Fig. 2.3.

The center of the aberration field contribution for any surface in the system lies along the line that connects its center of curvature, located by $\vec{\beta}_0$, and the center of the pupil, located by the OAR. For a plane surface, since the center of curvature is at infinity, it is along the normal to the surface which passes through the center of the pupil. Referring to Fig. 2.4, the displacement, measured from the OAR, is given by

$$\vec{a} = -\vec{\bar{i}}^*/\bar{i} \tag{2.8}$$

Here

$$\bar{i} = \bar{u} - \bar{y}c, \tag{2.9}$$

$$\vec{\bar{i}}^* = (\vec{\bar{u}}^* + \vec{\bar{y}}^*c) - \vec{\beta}_0, \tag{2.10}$$

$\vec{a}$ is the relative (normalized by the image height) displacement of the aberration field contribution due to a surface measured in the Gaussian image plane, $\vec{\bar{i}}^*$ is the angle of incidence of the OAR on the surface, and $\bar{i}$ is the angle of incidence of the chief ray on the surface in the centered system.

For a plane surface

$$\vec{a} = (\vec{\beta} - \vec{\bar{u}}^*)/\bar{u} \ . \tag{2.11}$$

When an aspheric is added to a surface, it provides an additional contribution to the aberration field in the image plane. The center of

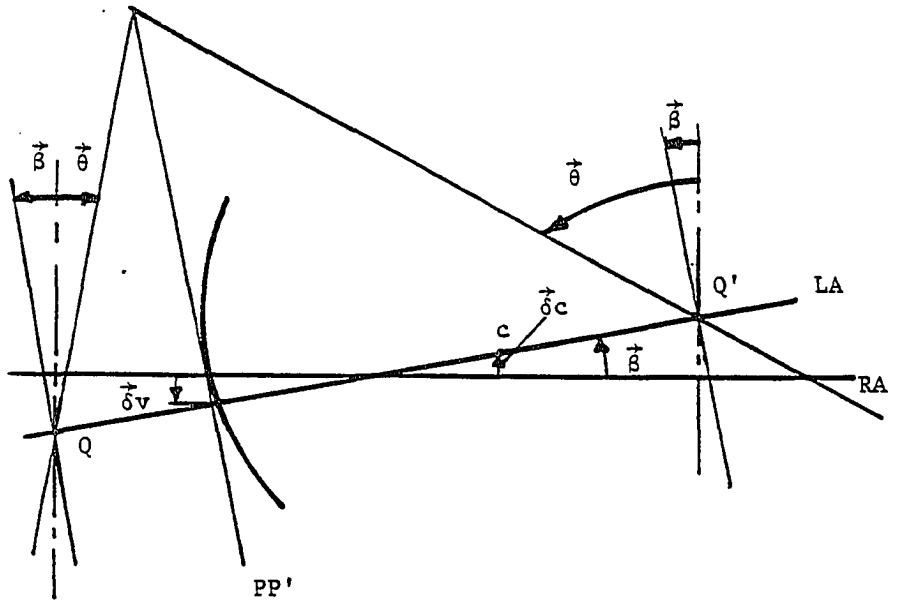

Fig. 2.3. Tilt of the Gaussian image plane.

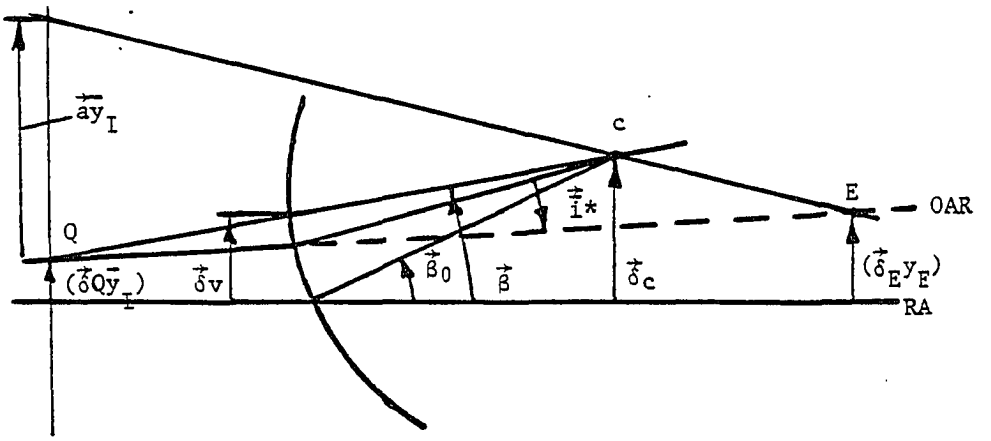

Fig. 2.4. Displacement of the aberration field contribution of a surface.

the aberration contribution due to the aspheric is along the line connecting the vertex of the aspheric cap with the center of the pupil

$$\vec{a}_A = (\vec{\delta V}_A - \vec{\bar{y}}^*)/\bar{y} \ . \qquad (2.12)$$

Here $\vec{a}_A$ is the relative displacement of the aberration field contribution due to the aspheric, $\vec{\delta V}_A$ is the displacement of the vertex of the aspheric cap from the RA. This displacement is independent of the tilt of the surface that contains the aspheric.

Third-Order Aberration Fields

In a centered system, the aberration contribution for each surface is centered on axis. In a perturbed system, the aberration contributions from each surface will not change to the first approximation, but will be displaced from the reference axis. There are no new types of aberrations, instead the field dependence is changed.

The wave aberration expansion to third order including tilts and decenters is given by

$$W = \Delta W_{20}(\vec{\rho}\cdot\vec{\rho}) + \Delta W_{11}(\vec{H}\cdot\vec{\rho}) + \sum_j W_{040j}(\vec{\rho}\cdot\vec{\rho})^2$$

$$+ \sum_j W_{131j}\left[(\vec{H} - \vec{a}_j)\cdot\vec{\rho}\right](\vec{\rho}\cdot\vec{\rho}) + \sum_j W_{222j}\left[(\vec{H} - \vec{a}_j)\cdot\vec{\rho}\right]^2$$

$$+ \sum_j W_{220j}\left[(\vec{H} - \vec{a}_j)\cdot(\vec{H} - \vec{a}_j)\right](\vec{\rho}\cdot\vec{\rho}) \qquad (2.13)$$

$$+ \sum_j W_{311j}\left[(\vec{H} - \vec{a}_j)\cdot(\vec{H} - \vec{a}_j)\right]\left[(\vec{H} - \vec{a}_j)\cdot\vec{\rho}\right],$$

where $\vec{H}$ is the field vector in the aligned system, $\vec{\rho}$ is the exit pupil vector in the aligned system, and vector $\vec{a}_j$ locates the center of each surface contribution to the aberration field in the image plane.

The spherical aberration term

$$W = \sum_j W_{040j}(\vec{\rho}\cdot\vec{\rho})^2 \qquad (2.14)$$

is independent of the field and independent of $\vec{a}_j$. This means that the (non-oblique) spherical aberration is unaffected by tilt and decenter perturbations.

The next term is coma,

$$W = \sum_j W_{131j}\left[(\vec{H} - \vec{a}_j)\cdot\vec{\rho}\right](\vec{\rho}\cdot\vec{\rho}) = W_{131}\left[(\vec{H} - \vec{a}_{131})\cdot\vec{\rho}\right](\vec{\rho}\cdot\vec{\rho}), \qquad (2.15)$$

where

$$\vec{a}_{131} = \frac{\vec{A}_{131}}{W_{131}} \tag{2.16}$$

and

$$\vec{A}_{131} = \sum_j W_{131j}\vec{a}_j \ . \tag{2.17}$$

The effect of tilts and decentrations is to displace the total coma field for the centered system to the point located by the image plane vector $\vec{a}_{131}$. The magnitude of coma is $W_{131}|\vec{H} - \vec{a}_{131}|$ and the orientation is along the vector $\vec{H} - \vec{a}_{131}$. A special case for coma occurs when $W_{131} = 0$, i.e., the system is corrected for coma. Then

$$W = -(\vec{A}_{131}\cdot\vec{\rho})(\vec{\rho}\cdot\vec{\rho}) \ . \tag{2.18}$$

This is constant coma, i.e., the magnitude and orientation of coma are independent of the field point. The magnitude of coma is $-|\vec{A}_{131}|$ and coma is oriented along the vector $\vec{A}_{131}$.

Field curvature and astigmatism are given by

$$W = \Delta W_{20}(\vec{\rho}\cdot\vec{\rho}) + \sum_j W_{220Mj}\left[(\vec{H} - \vec{a}_j)\cdot(\vec{H} - \vec{a}_j)\right](\vec{\rho}\cdot\vec{\rho})$$

$$+ \frac{1}{2}\sum_j W_{222j}\left[(\vec{H} - \vec{a}_j)^2\cdot\vec{\rho}^2\right] \ . \tag{2.19}$$

Here

$$W_{220M} = W_{220} + \frac{1}{2}\ W_{222} \ . \tag{2.20}$$

The medial focal surface can be described as

$$-\Delta W_{20} = W_{220M}\left[(\vec{H} - \vec{a}_{220M})\cdot(H - \vec{a}_{220M}) + b_{220M}\right] , \tag{2.21}$$

where

$$\vec{a}_{220M} = \frac{\vec{A}_{220M}}{W_{220M}} \tag{2.22}$$

$$\vec{A}_{220M} = \sum_j W_{220Mj}\vec{a}_j \tag{2.23}$$

$$b_{220M} = \frac{B_{220M}}{W_{220M}} - \vec{a}_{220M}\cdot\vec{a}_{220M} \tag{2.24}$$

and

$$B_{220M} = \sum_j W_{220Mj}(\vec{a}_j\cdot\vec{a}_j) . \tag{2.25}$$

The focal surface is still quadratic with the field, but now the vertex is located transversely from the OAR in the Gaussian image plane by the vector $\vec{a}_{220M}$. In addition, a longitudinal shift occurs along the optical axis from the scalar term $b_{220M}\ W_{220M}$. In linear units this shift is

$$\delta z_{220M} = -8(\text{f-number})^2 W_{220M} b_{220M} . \tag{2.26}$$

When the system has a flat medial focal surface ($W_{220M} = 0$), it can be described by

$$-\Delta W_{20} = -2\vec{H}\cdot\vec{A}_{220M} + B_{220M}. \tag{2.27}$$

In general, the flat medial surface is tilted and defocused relative to the Gaussian image plane.

Astigmatism with respect to the medial surface is given by

$$W = \frac{1}{2}W_{222}\left[(\vec{H} - \vec{a}_{222})^2 + \vec{b}^2_{222}\right]\cdot\vec{\rho}^2, \tag{2.28}$$

where

$$\vec{a}_{222} = \frac{\vec{A}_{222}}{W_{222}} \tag{2.29}$$

$$\vec{b}^2_{222} = \frac{\vec{B}^2_{222}}{W_{222}} - \vec{a}^2_{222} \tag{2.30}$$

$$\vec{A}_{222} = \sum_j W_{222j}\vec{a}_j \tag{2.31}$$

and

$$\vec{B}^2_{222} = \sum_j W_{222j}\vec{a}_j^2 \ . \tag{2.32}$$

This is binodal asigmatism, i.e., astigmatism with respect to the medial surface is zero at two points in the image plane. These two points are located by the vectors $\vec{a}_{222} + i\vec{b}_{222}$ and $\vec{a}_{222} - i\vec{b}_{222}$. For a more detailed description of binodal astigmatism, see K. Thomspon (1980). Figure 2.5 illustrates the location of the nodes of binodal astigmatism. In a system with binodal astigmatism, two focal surfaces touch at the points where astigmatims is zero. They do not cross.

When the aligned system is corrected for astigmatism ($W_{222} = 0$) the astigmatism of the perturbed system will be linear;

$$W = \frac{1}{2}\left[-2\vec{H}\vec{A}_{222} + \vec{B}^2_{222}\right]\cdot\vec{\rho}^2, \tag{2.33}$$

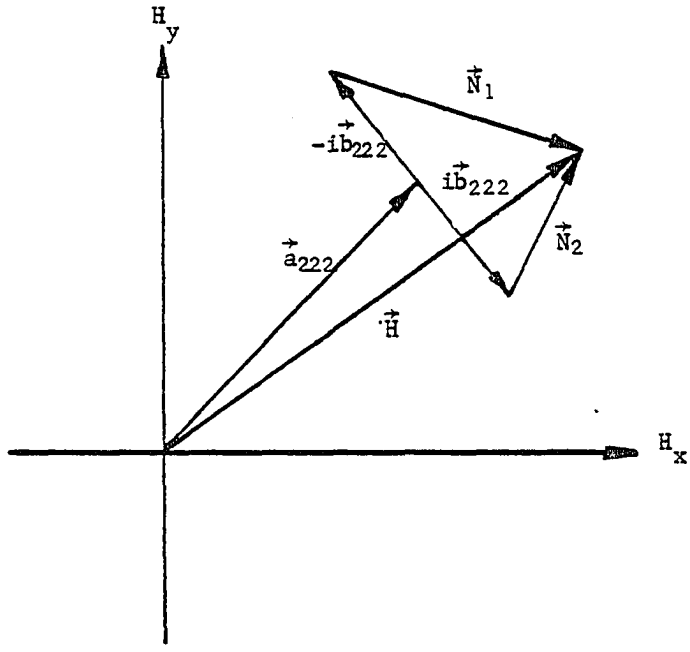

Fig. 2.5. Location of the nodes of binodal astigmatism. $\vec{N}_1$ and $\vec{N}_2$ are the node vectors.

and if $\vec{A}_{122} = 0$, it becomes constant

$$W = \frac{1}{2}\vec{B}_{122}^{2}\cdot\vec{\rho}^{2} \quad . \tag{2.34}$$

The magnitude of binodal astigmatism is given by the product of the distances from the field point of interest to each of the nodes. The orientation of the line foci on one of the focal surfaces are along the line bisecting the angle between the node vectors. The line foci on the other focal surface are at right angles to these.

The last term is distortion. This aberration results only in image displacement and therefore it is better treated and interpreted in terms of the properties of the transverse aberration. The expression for distortion in a tilted and decentered system is given by

$$(n'u')\vec{\epsilon} = W_{311}\left[(\vec{H}_{311}^{2} + \vec{b}_{311}^{2})\vec{H}_{311}^{*}\right] + W_{111E}\vec{H}_{111E} \tag{2.35}$$

where

$$\vec{H}_{311} = \vec{H} - \vec{a}_{311} \tag{2.36}$$

$$\vec{H}_{111E} = \vec{H} - \vec{a}_{111E} \tag{2.37}$$

$$\vec{a}_{311} = \frac{\vec{A}_{311}}{W_{311}} \tag{2.38}$$

$$\vec{a}_{111E} = \frac{W_{311}}{W_{111E}}\left(\vec{C}_{311} - \vec{b}_{311}^{2}\vec{a}_{311}^{*}\right) \tag{2.39}$$

$$W_{111E} = \Delta W_{11} + 2W_{311}b_{311} \tag{2.40}$$

$$b_{311} = \frac{B_{311}}{W_{311}} - \vec{a}_{311}\cdot\vec{a}_{311} \tag{2.41}$$

$$\vec{b}^2_{311} = \frac{\vec{B}^2_{311}}{W_{311}} - \vec{a}^2_{311} \tag{2.42}$$

$$\vec{c}_{311} = \frac{\vec{C}_{311}}{W_{311}} - (\vec{a}_{311}\cdot\vec{a}_{311})\vec{a}_{311} \tag{2.43}$$

$$\vec{A}_{311} = \sum_j W_{311j}\vec{a}_j \tag{2.44}$$

$$B_{311} = \sum_j W_{311j}(\vec{a}_j\cdot\vec{a}_j) \tag{2.45}$$

$$\vec{B}^2_{311} = \sum_j W_{311j}\vec{a}^2_j \tag{2.46}$$

$$\vec{C}_{311} = \sum_j W_{311j}(\vec{a}_j\cdot\vec{a}_j)\vec{a}_j \tag{2.47}$$

and the asterisk denotes the conjugate vector.

The vector $\vec{a}_{111E}$ locates the first-order node. The third-order nodes are located by the vectors $\vec{a}_{311} + i\vec{b}_{311}$ and $\vec{a}_{311} - i\vec{b}_{311}$. An additional node is located at the point specified by $\vec{a}_{311}$ due to multiplication by $\vec{H}^*_{311}$.

When the system is corrected for distortion, we should use the expression

$$W = -2(\vec{H}\cdot\vec{A}_{311})(\vec{H}\cdot\vec{\rho}) - (\vec{H}\cdot\vec{H})(\vec{A}_{311}\cdot\vec{\rho}) + 2B_{311}(\vec{H}\cdot\vec{\rho}) + \vec{B}^2_{311}\cdot(\vec{H}\vec{\rho}) - \vec{C}_{311}\cdot\vec{\rho} \tag{2.48}$$

which can be written in scalar form:

$$W = -2H^2A_{311}\rho\cos(\theta - \varepsilon)\cos(\theta - \phi) - H^2A_{311}\rho\cos(\varepsilon - \phi)$$
$$+ 2B_{311}H\rho\cos(\theta - \phi) + B_{311}^2H\rho\cos[2\alpha - (\theta + \phi)]$$
$$- C_{311}\rho\cos(\beta - \phi) \qquad (2.49)$$

Here each of the vectors is associated with its angle as shown in Table 2.1.

Table 2.1. The vectors and the angles associated with them.

Vector	$\vec{H}$	$\vec{\rho}$	$\vec{A}_{311}$	$\vec{B}_{311}$	$\vec{C}_{311}$
Angle	θ	ϕ	ε	α	β

Now by taking the derivative of the wavefront aberration function and decomposing the transverse ray aberration into two components, radial (in the direction of $\vec{H}$) and tangential (perpendicular to $\vec{H}$), we obtain the expression for the radial component ($\phi = \theta$).

$$D_R = -2H^2A_{311}\cos(\theta - \varepsilon) - H^2A_{311}\cos(\theta - \varepsilon) + 2B_{311}H$$
$$+ B_{311}^2H\cos2(\theta - \alpha) - C_{311}\cos(\theta - \beta) \qquad (2.49)$$

and the tangential component ($\phi = \theta + 90°$)

$$D_T = H^2A_{311}\sin(\theta - \varepsilon) - B_{311}^2H\sin2(\theta - \alpha)$$
$$+ C_{311}\sin(\theta - \beta). \qquad (2.50)$$

The term in the radial component $2B_{311}H$ represents a change of the magnification with the field.

Two terms, $C_{311}\cos(\theta - \beta)$ and $C_{311}\sin(\theta - \beta)$, represent the shift of the entire field in the direction of the vector $\vec{C}_{311}$.

The terms $B_{311}^2 H \cos 2(\theta - \alpha)$ and $-B_{311}^2 H \sin 2(\theta - \alpha)$ show the anamorphism present when the magnification differs in two orthogonal directions. They do not result in a departure from collinearity, i.e., a square object will be imaged as a rectangle with the long side along the x or y axis depending on the sign of the wave aberration coefficient.

The two last terms are $-3H^2A_{311}\cos(\theta - \epsilon)$ and $H^2A_{311}\sin(\theta - \epsilon)$. The magnitude of these terms varies quadratically with the field, and the magnitude of the tangential component is one-third of the radial one for the same zone in the field. A straight line here will no longer be imaged as a straight line.

CHAPTER 3

THE PLANE-PARALLEL REFRACTIVE PLATE

The plane-parallel plate has no power and, as an image-forming system by itself, is not very interesting. Since it is usually used as a component in a system, we will examine it in this context.

Since a plane-parallel plate has its centers of curvature at infinity, it can only be tilted with respect to the reference axis. A convenient reference axis in this case is the optical axis of the system containing the plate.

If the plane-parallel plate is located in a space where the object or image is at infinity, it does not introduce aberrations. In a telecentric space (pupil at infinity), a plane-parallel plate does introduce aberrations, but they are constant over the field. Here we consider the tilted plane-parallel plate in a space where both the image and the pupil are at finite distances.

First-Order Properties

First let us locate the centers of the object, image, and pupils for the plane-parallel plate itself. Since the plate has surfaces parallel to each other, the tilt of the plate is the common tilt of both surfaces.

Both object and image centers are located on the local axis of the surface. Since the surfaces of the plate are parallel, a single local axis applies to both surfaces.

Applying Eq. 2.3 to both surfaces we can obtain an expression for the relative image displacement for a plane-parallel plate

$$\vec{\delta}Q' = \vec{\delta}Q + \frac{u\Delta(n)n}{n'\mathscr{C}} \vec{\beta}t \ , \tag{3.1}$$

as shown in Fig. 3.1.

Here t is the thickness of the plate, $\vec{\beta}$ is the tilt angle, $\Delta(n) = n' - n$, the difference between the refractive indices of the plane parallel plate n' and the medium n (in the case of air n = 1).

The same argument applies to the pupils

$$\vec{\delta}E' = \vec{\delta}E - \frac{\bar{u}\Delta(n)n}{n'\mathscr{C}} \vec{\beta}t \ . \tag{3.2}$$

Given the centers of the object, image, and pupils, the paraxial ray height $\vec{\bar{y}}^*$ at the surface and the paraxial ray angle $\vec{\bar{u}}^*$ preceding the surface for the OAR can be determined using Eqs. 2.5 and 2.6.

Applying Eq. 2.7 to both surfaces of the plate, we find that

$$u'\vec{\theta}' = u\vec{\theta} \ . \tag{3.3}$$

We can say that for the plane-parallel plate, the tilt of the object plane defines the tilt of the image plane, i.e., the tilted plate does not change the tilt of the Gaussian image plane.

Next we find the center of the aberration field contribution for each surface in the tilted plate. As seen in Fig. 3.2, the displacement

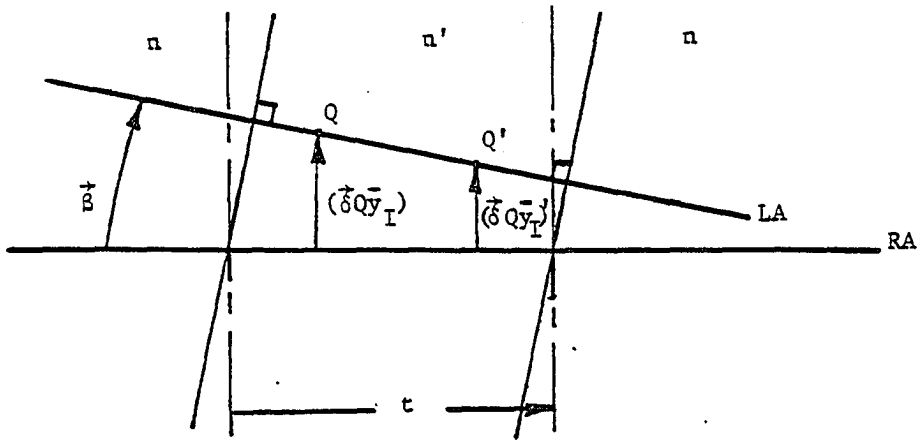

Fig. 3.1. Displacement of the image for a plane-parallel plate.

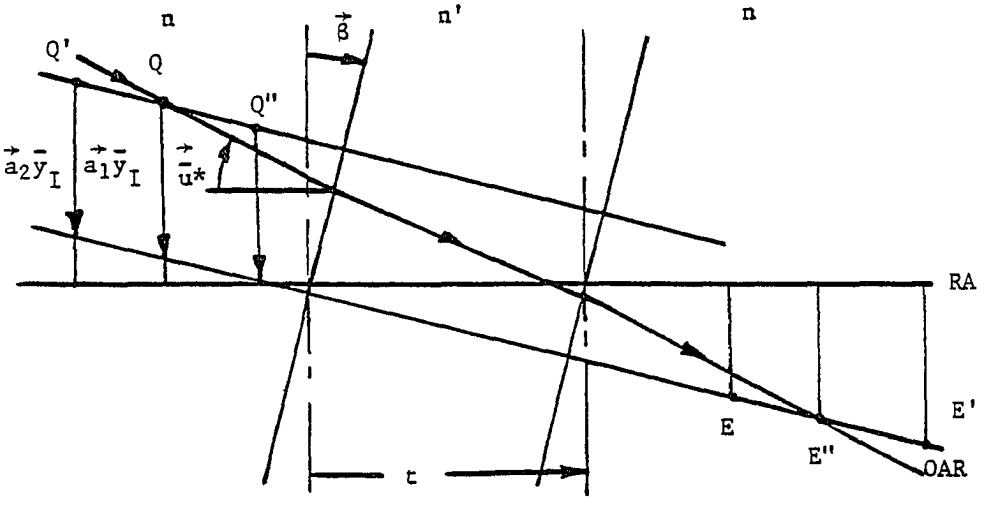

Fig. 3.2. Displacement of the center of the aberration field of a plane-parallel plate.

of the center of the aberration field is the same for each surface of the plate and can be determined by either Eq. 2.8 or 2.11. This displacement depends only on the tilt of the plate and the distance between the pupil and the image in the space where the plate is located. For a single plane-parallel plate, the only case where this displacement is zero is when the center of the object and the center of the pupil are located on the normal to the plate ($\vec{i}^* = 0$).

The first-order properties of the tilted plane-parallel plate described above are well known, except the concept of the displacement of the center of the aberration field.

We can summarize these properties. We know that the plane-parallel plate placed in a system with no aberrations and squared on the axis introduces aberrations. They are spherical aberration, coma, astigmatism, and distortion. There is no Petzval term. The plate also produces equal longitudinal displacement of the image and pupil planes.

If we tilt the plate, the center of the image and the pupil will be displaced. In addition, the center of the aberration fields will also be displaced. The displacement of the aberration center will be in the same direction, and the magnitude of this displacement can be determined by

$$(\vec{a}\ \overline{y_I}) = S\vec{\beta} \tag{3.4}$$

as shown in Fig. 3.3. Here S is the distance from the entrance pupil to the object. Equation 3.4 is essentially the same as 2.11 with $\vec{u}^* = 0$.

If we place a second plate in the system, it will introduce an additional displacement of the image and the center of the aberrations. The net displacement of the image field can be found by adding the component displacements vectorially. The centers of the aberration fields for each plate are displaced from the net center of the field as shown in Fig. 3.4.

Third-Order Aberration Fields of a Tilted Plane-Parallel Plate

Since the displacement of the center of the aberration field contribution for each surface is the same, the effect of the tilt is to displace the center of symmetry of all third-order aberrations due to the plane-parallel plate to the point in the image field located by the vector $\vec{a}$. All third-order aberrations will have a common center (the node). If we change the tilt angle, the aberration center will move to a new point, as will the center of the field. The magnitude of the aberrations with respect to the new center will not change (since it depends only on the first-order properties of the system and the thickness of the plate), but the magnitude of the aberrations on the RA will change.

In the treatment above we assumed that the plane-parallel plate was placed in a system not having aberrations of its own. Once we know what aberrations are introduced by a tilted plane-parallel plate, we can determine the effect of placing a plate in a system with aberrations.

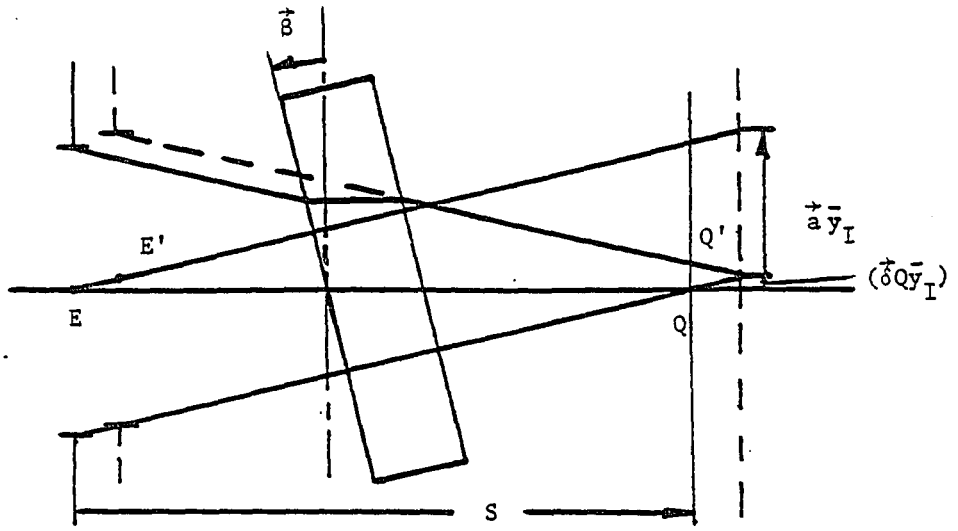

Fig. 3.3. Displacement of the image, the pupil, and the center of the aberrations in a single tilted plane-parallel plate.

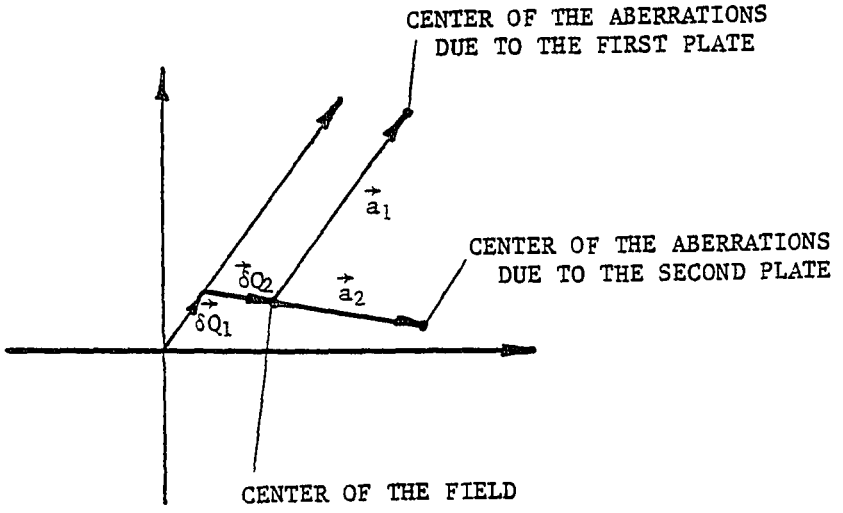

Fig. 3.4. The centers of the aberrations of two tilted plane-parallel plates.

If the plate is not tilted, we know that the centers of the aberrations due to the system and due to the plate are in register at the center of the field. If we tilt the plate, the center of the image field will be displaced together with the center of the aberrations due to the system. The center of the aberrations due to the plate will be displaced from that point.

The resulting aberration fields in general will then be as follows. The coma field will be the ordinary linear coma shifted in the image plane. Astigmatism will be binodal, and distortion will have three third-order nodes. The magnitude and location of the nodes of these resulting aberration fields will depend on the magnitudes of the component fields and the tilt angle of the plate. By varying the tilt of the plate, we can vary the magnitude of the aberrations at the center of the field. A few interesting special cases follow.

Case I.

The system and the plane-parallel plate are corrected together with the plate untilted. If we tilt the plate, the centers of the aberration fields will separate as shown in Fig. 3.5. We know that spherical aberration is not affected by the tilt, therefore it will be zero.

Since the aberrations of the system and the plane-parallel plate are equal and opposite in sign, the resulting coma field will be constant. This is easily seen in Fig. 3.5. Indeed, at point P (the

center of aberrations for the plate) we have coma due to the system whose magnitude is $|W_{131}\vec{a}|$. Take the case where the direction of this coma is opposite to the vector $\vec{a}$. Then at point S (aberration center for the system) the magnitude and the orientation of coma due to the plate will be the same as at point P, because the system and the plate have aberrations that are equal and opposite in sign.

The same result can be obtained using Eq. 2.18

$$W = -(W_{131}\,\vec{a}\cdot\vec{p})(\vec{p}\cdot\vec{p}) \tag{3.5}$$

with $\vec{A}_{131} = W_{131}\vec{a}$. W_{131} is the wave aberration coefficient of the plate. The resulting astigmatism will be linear, since the quadratic terms cancel. It is not difficult to see that the node of the astigmatic field will be midway between the two centers of the component fields since at that point they have equal magnitude and the corresponding line foci are normal to each other.

Using Eq. 2.33 with $\vec{A}_{222} = W_{222}\vec{a}$ and $\vec{B}^2_{222} = W_{222}\vec{a}^2$, we obtain the expression for astigmatism with respect to the medial surface

$$W = \frac{1}{2}\, W_{222}[-2\vec{a}\vec{H} + \vec{a}^2] \cdot \vec{p}\ . \tag{3.6}$$

Using Eq. 2.27 with $\vec{A}_{220M} = W_{220M}\vec{a}$ and $B_{220M} = W_{220M}\,|\vec{a}|^2$, we obtain the expression for the medial focal surface

$$-\Delta W_{20} = W_{220M}\,[\,-2\vec{H}\cdot\vec{a} + |\vec{a}|^2]. \tag{3.7}$$

It is a flat surface and is tilted and defocused. Linear astigmatism is illustrated in cross-section in Fig. 3.6. Two astigmatic

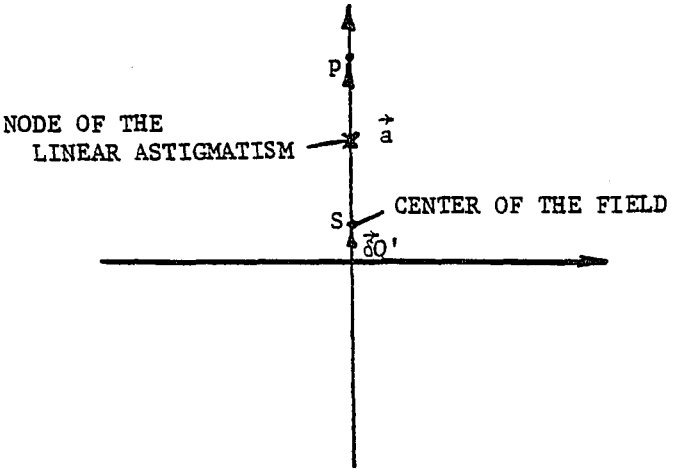

Fig. 3.5. Case I.

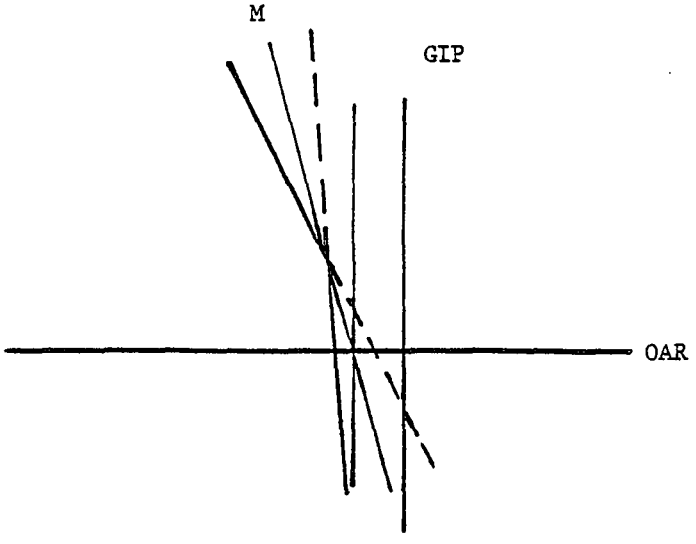

Fig. 3.6. Linear astigmatism of Case I.

focal surfaces are cones. The medial flat focal surface bisects the cross-sectional angle between them.

Distortion will not be treated in detail here because not only is it significantly more complex, but it is also usually less important in optical systems. However, enough information has been included so that details can be worked out if desired.

Case II.

Two plane-parallel plates are placed in a system with no aberrations and tilted in opposite directions by the same angle. They have the same thickness and are made of the same glass. The first plate moves the center of the image field and the center of the aberrations in one direction. The second plate moves them the same amount in the opposite direction. The center of the image field will not be displaced from the reference axis, but the centers of the aberrations due to each plate are displaced by equal amounts in opposite directions as shown in Fig. 3.7. The aberrations due to each plate in this case have equal magnitude and the same sign.

We can find the node for the resulting coma field if we notice that at the point midway between the aberration centers the coma contributions are of the same magnitude and opposite directions. The magnitude of the resulting coma field will be twice the magnitude of either one.

To find a node for astigmatism, we must find a point in the field where the corresponding line foci of the component fields are normal to each other and have the same magnitude. In this case, we can find two such points. Therefore, the astigmatism is binodal with the nodes located on the line normal to the line connecting two aberration centers and passing through the center of the field (Fig. 3.7).

The expression for astigmatism with respect to the medial focal surface can be obtained using Eq. 2.28.

In this case, $\vec{a}_{222} = 0$ and $\vec{b}^2_{222} = \vec{a}^2$ and Eq. 2.28 becomes

$$W = \frac{1}{2} W_{222}(\vec{H}^2 + \vec{a}^2)\cdot\vec{\rho}^2 \tag{3.8}$$

where W_{222} is the wave aberration coefficient of the system.

The medial focal surface is a quadratic surface centered on the OAR but defocused from the GIP as can be seen from the following expression:

$$-\Delta W_{20} = W_{220M}\,\vec{H}\cdot\vec{H} + |\vec{a}|^2, \tag{3.9}$$

which was obtained from Eq. 2.21 with $\vec{a}_{220M} = 0$, $\vec{b}_{220M} = |\vec{a}|^2$, and $W_{220M} = W_{220} + \frac{1}{2}W_{222}$.

Case III.

The system is the same as in Case II, only now the plates are cross-tilted. In this case, the centers of the aberration and the image fields will be displaced from the reference axis orthogonally as shown in Fig. 3.8.

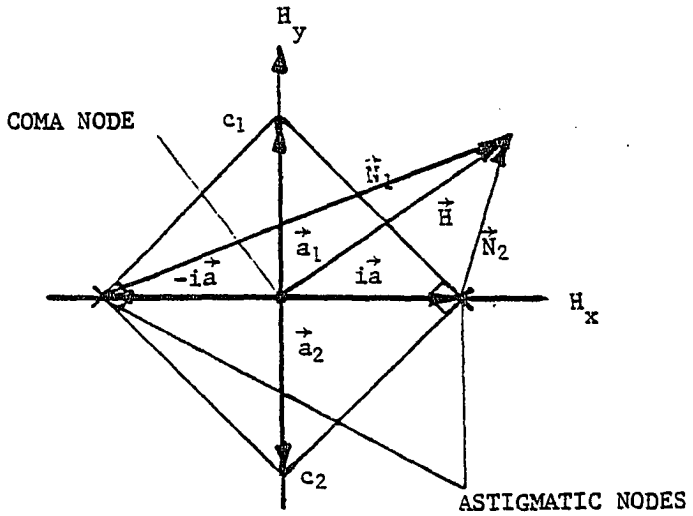

Fig. 3.7. Binodal astigmatism of Case II.

C_1 and C_2 are the aberration centers of the plates.

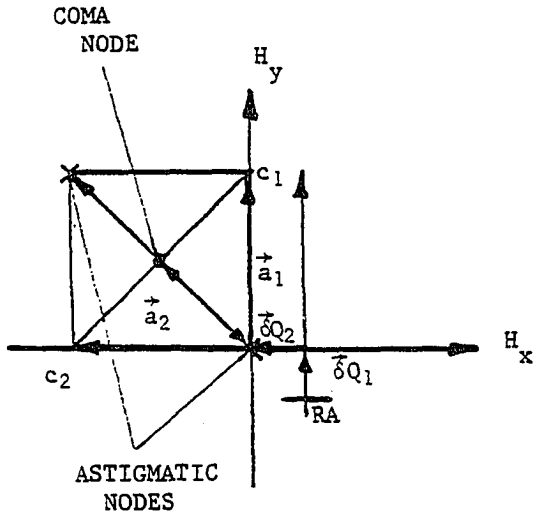

Fig. 3.8. Coma and binodal astigmatism of Case III.

C_1 and C_2 are the aberration centers of the plates.

The coma field will have a node midway between the centers of the component fields and can be described by

$$W = W_{131}\left[\left[\vec{H} - \frac{\vec{a}_1 + \vec{a}_2}{2}\right]\cdot\vec{\rho}\right](\vec{\rho}\cdot\vec{\rho}) \qquad (3.10),$$

where W_{131} is the wave aberration coefficient of the system. As can be seen from Eq. 3.10, the coma fields no longer cancel at the center of the field.

Astigmatism will again be binodal with one of the nodes at the center of the field. The nodes can be located as in Case II. The astigmatism with respect to the medial surface will be

$$W = \frac{1}{2}W_{222}\left[\left[\vec{H} - \frac{\vec{a}_1 + \vec{a}_2}{2}\right]^2 + \frac{(\vec{a}_1 - \vec{a}_2)^2}{4}\right]\cdot\vec{\rho}^2 \qquad (3.11)$$

where W_{222} is the wave aberration coefficient of the system. The medial focal surface is centered at the point $\vec{H} = (\vec{a}_1 + \vec{a}_2)/2$ and defocused from the GIP by the amount $W_{222M}\,|\vec{a}|^2/2$ where $|\vec{a}|$ is the magnitude of either displacement vector.

Case IV.

Next we consider the system with two plane-parallel plates of the same thickness where the aberrations are zero with untilted plates. If we tilt the plates by the same angle in opposite directions, this case is similar to Case II. The difference is that in this case we have the aberrations due to the system of magnitude, twice the magnitude of either plate and opposite in sign. The center of the image field will be

on the reference axis, as will be the center of the aberrations due to the system (Fig. 3.9).

We know from Case II that the resulting coma field due to two plates will have a node midway between their aberration centers, at the center of the field. Since they have equal magnitudes and opposite sign, they cancel each other. Therefore coma will be zero across the entire field.

From Case II, we also know that astigmatism due to two tilted plates will be binodal with the nodes located as shown in Fig. 3.7. Now the regular quadratic astigmatism of opposite sign and centered at the center of the image field will be added to it. The resultant astigmatism will be constant. It can be seen as follows. If we take the point at the center of the image field we know that the only astigmatism there is the binodal astigmatism of the two plates. Setting $\vec{H} = 0$ in Eq. 3.8, we obtain the expression

$$W = \frac{1}{2}(W_{222}\vec{a}^2)\cdot\vec{\rho}^2, \tag{3.12}$$

where W_{222} is the wave aberration coefficient of the two plates.

If we take one of the nodes of binodal astigmatism due to the plates, we can see that the only astigmatism there is the astigmatism due to the system, which will have the same magnitude as at the center of the image field. The orientation of the line foci at this point is

the same as for the center of the image field. The same argument can be applied to the second nodal point. Therefore we have constant astigmatism.

The same result can be obtained using Eq. 2.33. In this case $\vec{A}_{222} = 0$, $\vec{B}^2_{222} = W_{222}\vec{a}^2$. The medial focal surface is a flat surface defocused from the Gaussain image plane by $|\vec{a}|^2$. Using Eq. 2.27, the equation for the medial focal surface is obtained:

$$-\Delta W_{20} = |\vec{a}|^2. \tag{3.13}$$

Case V.

The last case is the same as above, but the plates are cross-tilted. As before, we can see that this case is similar to Case III with the aberrations due to the system added. The center of the image field is displaced from the reference axis as in Case III. From Case III, we know that the resulting coma field due to the plates has its node at point P as shown in Fig. 3.10. At this point, the only coma will be that due to the system which is

$$W = W_{131}\,\frac{\vec{a}_1 + \vec{a}_2}{2} \tag{3.14}$$

where W_{131} is the wave aberration coefficient of the system. At point C_3 (the node for the coma field of the system), the only coma is due to the resultant field of the plates, which is of the same magnitude and opposite sign of coma due to the system. Since this coma has the opposite sign, the direction will be the same as at point P. Therefore

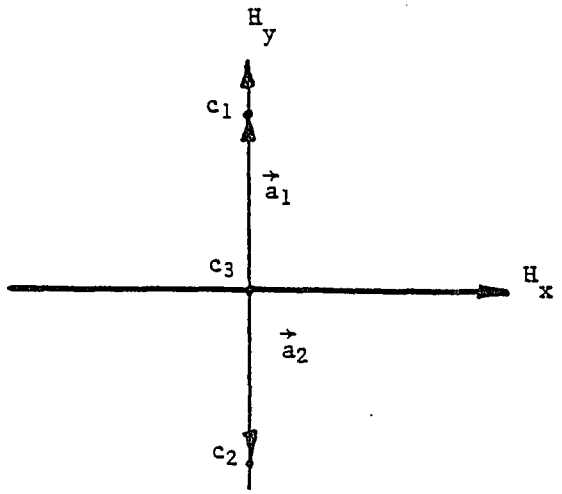

Fig. 3.9. Case IV.

C_1 and C_2 are the aberrations centers of the first and the second plates.

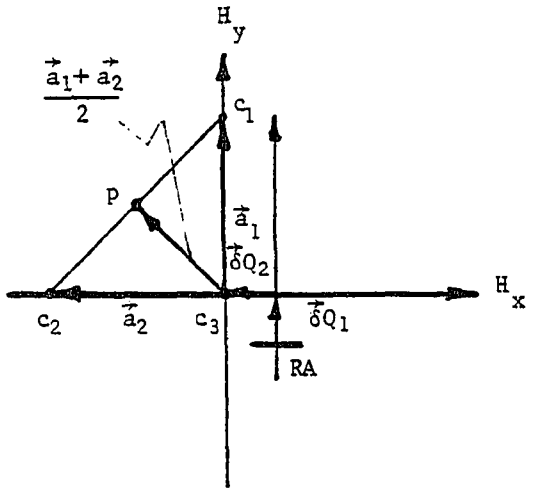

Fig. 3.10. Case V.

C_1 and C_2 are the aberration centers of the plates; C_3 is the aberration center of the system.

we have here a constant coma field with direction of -45° to the y-axis in the image field. Eq. 3.14 can be obtained using Eq. 2.18.

Since the system was corrected for astigmatism before the plates were tilted, we should expect the astigmatism to be either linear or constant (see Eq. 2.33). But we can see immediately that at point C_3 the astigmatism will be zero, since at this point are located the node of the binodal astigmatism due to the plates and the center of the quadratic astigmatism of the system. The other node of binodal astigmatism will have astigmatism due to the system. Therefore the total astigmatic field must be linear with the node located at point C_3.

The magnitude of this linear astigmatism with respect to the medial focal surface can be found using Eq. 2.33 with $\vec{A}_{222} = W_{222}(\vec{a}_1 + \vec{a}_2)$, where W_{222} is the wave aberration coefficient of one of the plates and $\vec{B}^2_{222} = 0$, since $\vec{a}_1^{\,2} = -\vec{a}_2^{\,2}$. The expression for the resultant astigmatism with respect to the medial focal surface is

$$W = -W_{222}\vec{H}(\vec{a}_1 + \vec{a}_2) \tag{3.15}$$

and the orientation of sagittal line foci are along the vector

$$-\left[(\vec{a}_1 + \vec{a}_2)\vec{H}\right]^{1/2} .$$

The expression for the medial focal surface can be obtained using Eq. 2.27 with $\vec{A}_{220M} = W_{220M}(\vec{a}_1 + \vec{a}_2)$ and $B_{220M} = 2W_{220M}|\vec{a}|^2$ where W_{220M} is the wave aberration coefficient of one of the plates.

The expression for the medial focal surface becomes

$$-\Delta W_{20} = 2W_{220M}\left[-\vec{H}\cdot(\vec{a}_1+\vec{a}_2)+|\vec{a}|^2\right]. \qquad (3.16)$$

This is a flat tilted surface that is defocused from the GIP by $2W_{220M}\,|\vec{a}|^2$.

CHAPTER 4

THE WEDGE

When the angle between the faces of a thin refractive prism is small, it is customary to call it a wedge.

We can consider the wedge being derived from a plane-parallel plate by having the surfaces tilted by the amount $\pm\vec{\alpha}/2$, where $\vec{\alpha}$ is the vertex angle of the wedge. The wedge will have a plane of symmetry that is the plane bisecting the vertex angle of the wedge as shown in Fig. 4.1. Therefore when we refer to a tilted wedge, the tilt will be the tilt of this plane with respect to the reference axis.

As was for the plane-parallel plate, the wedge will be assumed to be located in a system space where the image and pupil are at a finite distance. Again, the reference axis will be the optical axis of the system.

First-Order Properties

If we place a wedge in the system and tilt it, the surfaces of the wedge will be tilted with respect to the reference axis by the angles $\vec{\beta} \pm \vec{\alpha}/2$ as shown in Fig. 4.1.

Applying Eq. 2.3 to both surfaces, we can obtain the relative image displacement by the tilted wedge

$$\vec{\delta}Q' = \vec{\delta}Q - \frac{\Delta(n)un}{n'\mathscr{H}C}\vec{\beta}t + \frac{\Delta(n)u}{\mathscr{H}C}\vec{\alpha}\ell - \frac{\Delta(n)^2u}{n'\mathscr{H}C}\frac{\vec{\alpha}}{2}t \ . \qquad (4.1)$$

Here $\vec{\beta}$ is the tilt of the wedge, $\vec{\alpha}$ is the vertex angle, t is the thickness of the wedge along the reference axis, and ℓ is the distance from the plane bisecting the vertex angle of the wedge to the object plane as shown in Fig. 4.1.

Comparing this expression with Eq. 3.1 for the plane-parallel plate, we see that here we have two additional terms contributed by the wedge, such that if we set $\vec{\alpha} = 0$, the expression reduces to the expression for the plane-parallel plate. For the wedge, the relative image displacement depends on the position of the wedge in the system, i.e., if we move the wedge, the center of the image field will also move.

The same argument applies to the pupils. The relative exit pupil displacement is given by

$$\vec{\delta}E' = \vec{\delta}E + \frac{\Delta(n)\bar{u}n}{n'\mathscr{H}C}\vec{\beta}t - \frac{\Delta(n)\bar{u}}{\mathscr{H}C}\vec{\alpha}\ell + \frac{\Delta(n)^2\bar{u}}{n'\mathscr{H}C}(\frac{\vec{\alpha}}{2})t \qquad (4.2)$$

Here ℓ is the distance from the plane bisecting the vertex angle of the wedge to the pupil.

The paraxial ray height $\vec{\bar{y}}^*$ at the surface and the paraxial ray angle $\vec{\bar{u}}^*$ preceding the surface for the OAR can be found using Eqs. 2.5 and 2.6.

Applying Eq. 2.7 for both surfaces of the wedge, we can obtain the expression for the Gaussian image plane tilt

$$\vec{\theta}' = \vec{\theta} + \frac{\vec{\alpha}\Delta(n)}{n'} , \tag{4.3}$$

where $\vec{\theta}$ is the tilt angle of the object plane as shown in Fig. 4.2. As we can see from Eq. 4.3, the tilt of the Gaussian image plane does not depend on the tilt of the wedge; it depends only on the vertex angle of the wedge and its refractive index.

Since the wedge surfaces are not parallel, the wedge does not have a single local axis. Each surface will have the center of aberration contribution displaced from the reference axis at a different point in the image plane. The aberration displacement vector for each surface can be found using Eqs. 2.8 or 2.11.

A unique property of the wedge is that the separation of the aberration centers for the wedge surfaces is constant and given by,

$$\vec{a}_2 - \vec{a}_1 = (n'\vec{\alpha})/(n\bar{u}) , \tag{4.4}$$

which is independent of tilt. When we change the tilt of the wedge, the aberration centers move as a pair with constant separation. Also, we can see that there is a particular tilt of the wedge such that the aberration centers are displaced symmetrically about the center of the image field. In that case, the OAR goes symmetrically through the wedge, i.e., the angle of incidence of the OAR on the surface bisecting the vertex angle of the wedge is zero. This is shown in Fig. 4.3.

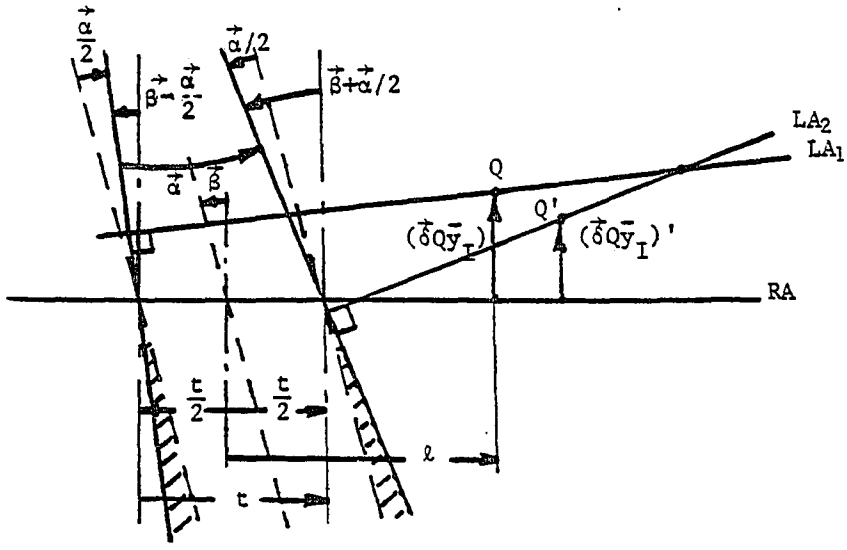

Fig. 4.1. Image field displacement by a tilted wedge.

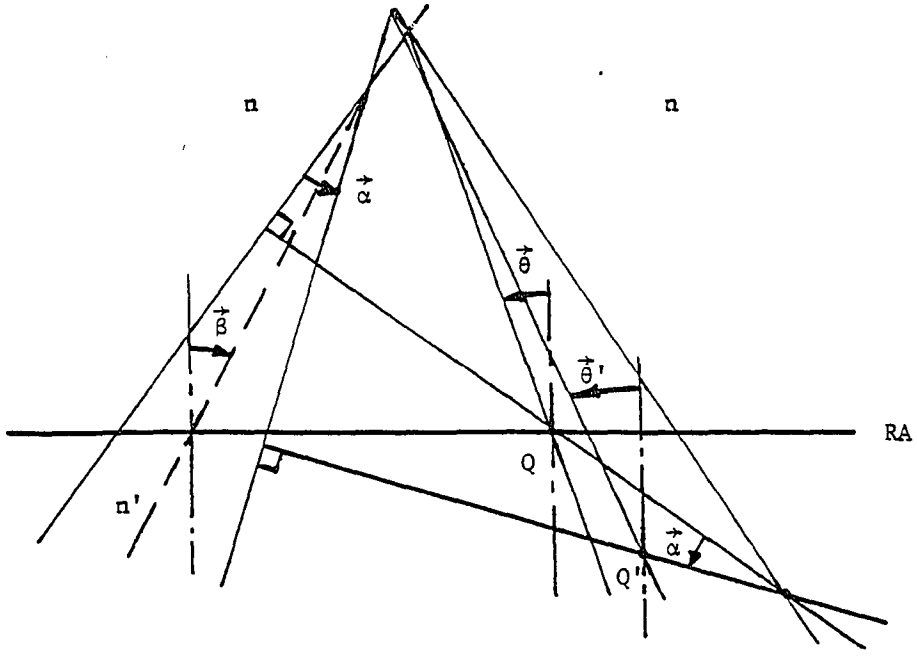

Fig. 4.2. Tilt of the Gaussian image plane by a wedge.

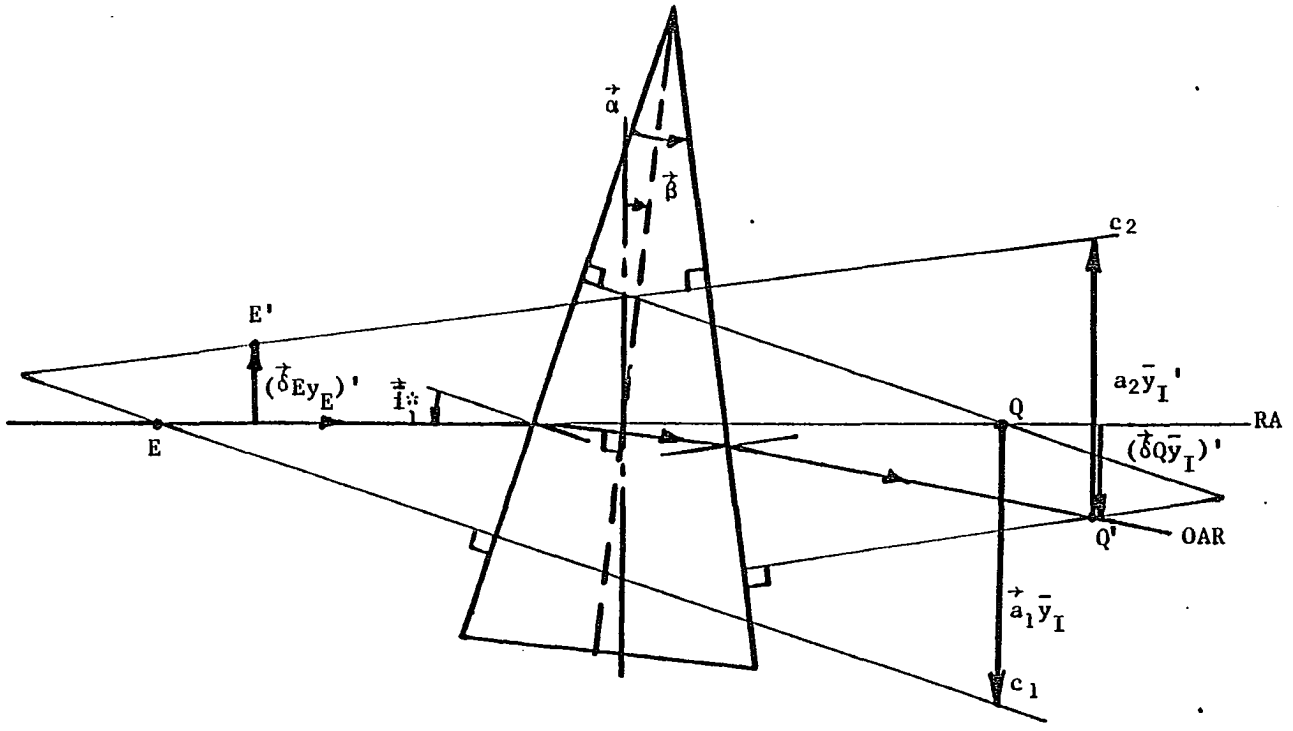

Fig. 4.3. Aberration centers of the wedge.

C_1 and C_2 are the centers of aberration fields for the first and the second surface.

Third-Order Aberration Fields

Since the aberration center displacement vectors for the surfaces of the wedge are not equal to each other, the aberration fields of the wedge placed in the system can be described by the equations given in Chapter 2. The coma field will be linear and shifted in the image plane, astigmatism will be binodal with a quadratic medial focal surface shifted and defocused from the Gaussian image plane and distortion will have three third-order nodes.

If we look at the expressions for the perturbation vectors for each type of aberration, we can see that for the wedge,

$$\vec{a}_{131} = \vec{a}_{220M} = \vec{a}_{222} = \vec{a}_{311} \ , \tag{4.5}$$

and

$$\vec{b}^{2}_{222} = \vec{b}^{2}_{311} \ , \tag{4.6}$$

i.e., the coma node, the center of symmetry of the astigmatism, and the central distortion node all lie at the same point in the field. The nodes of binodal astigmatism and the two other nodes of distortion will also coincide.

Since the aberrations for each surface of the wedge are not equal and opposite in sign, the center of symmetry for each type of aberration will lie on the line connecting two aberration field centers but will not be between them as shown in Fig. 4.4.

Consider two special orientations for the single wedge.

1. The center of symmetry of the aberrations (including the node for coma) is at the center of the image field. The condition for that is

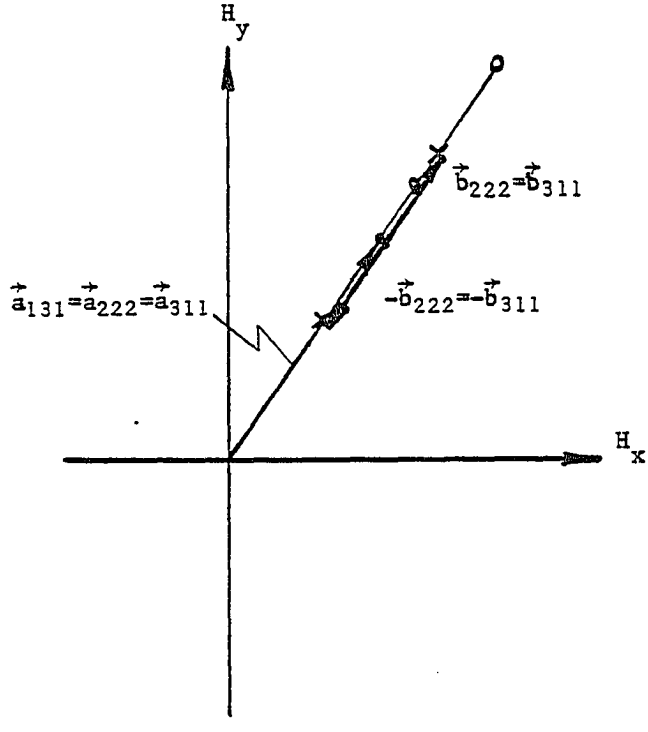

Fig. 4.4. Aberration fields of the wedge.

• denotes the center of the coma field, the center of symmetry for astigmatism and one of the distortion nodes. x denotes the astigmatic and two other distortion nodes, and o denotes the aberration center for each surface of the wedge.

$$\vec{A}_{131} = \vec{A}_{222} = 0, \tag{4.7}$$

which is obtained when

$$\frac{\vec{a}_1}{\vec{a}_2} = \frac{y_2}{y_1}, \tag{4.8}$$

where y_1 and y_2 are marginal ray heights on the surfaces of the wedge.

From this condition, we can obtain the expression for the tilt angle of the wedge which will place the center of symmetry for all aberrations in the center of the image field:

$$\vec{\beta} = -n\vec{\alpha}\left[1 + n\left(\frac{\ell}{t} + \frac{1}{2}\right)\right] + \frac{\vec{\alpha}}{2} + \vec{u}^*. \tag{4.9}$$

Here n is the refractive index of the wedge (the wedge is assumed to be in the air).

2. One of the nodes of the binodal astigmatism (and distortion) is at the center of the image field. The condition for that is:

$$\vec{B}^2_{222} = 0 . \tag{4.10}$$

The condition for the aberration displacement vectors is

$$\frac{\vec{a}_1^2}{\vec{a}_2^2} = \frac{y_2}{y_1}, \tag{4.11}$$

and the tilt angles of the wedge are

$$\vec{\beta} = -n^2\vec{\alpha}\left(\frac{\ell}{t} + \frac{1}{2}\right)\left[1 + \frac{t}{n(\ell+t/2)} \pm \sqrt{1 + \frac{t}{n(\ell+t/2)}}\right]$$

$$+ \frac{\vec{\alpha}}{2} + \vec{u}^* . \tag{4.12}$$

Equations 4.9 and 4.12 indicate an interesting property of the wedge. If

we move the wedge in such a way that the ratio t/ℓ stays constant, the node of the coma field (or the astigmatic field) will stay at the center of the image field ($\vec{\beta}$ does not change), as well as the distance between the nodes, but the magnitude of all aberrations will change, since this motion of the wedge will change its thickness.

It can be seen from Fig. 4.5 that if we connect the vertex of the wedge A with the center of the object for the wedge Q and move it in such a way that the dihedral line of the wedge slides along the line AQ, the ratio t/ℓ will be constant. We should point out here that with the wedge, the designer has more variables with which to control the aberrations than in the case with the tilted plane-parallel plate.

For example, we can vary the separation of the nodes by moving the wedge along the reference axis keeping the thickness and tilt angle fixed. The magnitude of the total aberrations will not change, since the thickness does not change. On the other hand, we can move the wedge transversely keeping the tilt and distance to the object the same, thereby varying the aberrations of the wedge as well as the node separations.

Another very useful way to look at the wedge is as a plane-parallel plate with two thin ($t \neq 0$) wedges added to it (one in front, the other in back) as shown in Fig. 4.1. The vertex angles of these thin wedges are $\pm\vec{\alpha}/2$ and the aberration displacement vectors for the surfaces will be,

$$\vec{a}_1 = \vec{a}_p - \vec{a}_{w,1}$$

$$\vec{a}_2 = \vec{a}_p + \vec{a}_{w,2} \tag{4.13}$$

where $\vec{a}_{w,1} = \dfrac{\vec{\alpha} + \vec{u}_1^*}{2u_1}$, $\vec{a}_{w,2} = \dfrac{\vec{\alpha} - \vec{u}^*_2}{2u_2}$.

Once we know the effect of the tilted plane-parallel plate on the aberrations, we can simply add the effect of these two wedges. The effect of adding them is to move the center of the image field to a new point in the field and split the center of the aberrations due to the plane-parallel plate on two surface centers for the wedges $-\vec{a}_{w,1}$ and $\vec{a}_{w,2}$. This is illustrated in Fig. 4.6 where the tilt of the wedge is not coplanar with the wedge angle $\vec{\alpha}$.

Using this approach, it is easy to find the centers of the aberration fields for the wedge surfaces in this non-coplanar case. Also, we should point out here that when we tilt the wedge, we change the plate contribution while the wedge contribution remains the same. If we rotate the wedge keeping $\vec{\beta}$ constant, the tips of the vectors $\pm\vec{a}_{w,1,2}$ and $\vec{\delta}Q'_w$ will describe circles around the centers of the image field and aberration fields due to the plane-parallel plate.

As for the plate, there are a few interesting special cases involving wedges.

Case I

The wedge is placed in the system where the aberrations of that system and the plane-parallel plate of the same thickness (the thickness of the wedge along the reference axis) are corrected. We can tilt (or

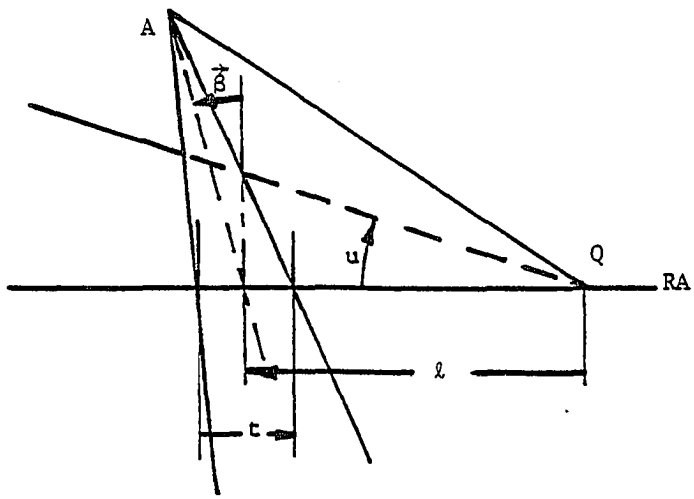

Fig. 4.5. The line AQ along which the motion of the dihedral edge will keep the nodes of the aberration fields stationary.

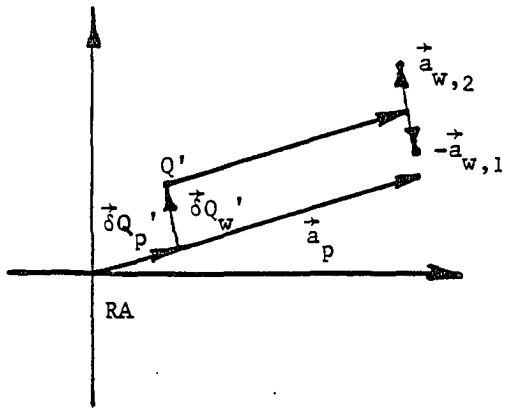

Fig. 4.6. Image and aberration field displacements from a plane-parallel plate with thin wedges added to it.

move) the wedge to find a position where the center of symmetry of all aberration fields falls at the center of the image field. Then, since the center of the system aberrations is at the center of the image field, and also since the aberrations of the system and the equivalent plane-parallel plate are equal and opposite in sign, the coma fields will cancel each other and coma will be zero across the entire field.

The behavior of astigmatism is similar to Case IV of Chapter 3. The binodal astigmatism due to the wedge is added to the conventional quadratic astigmatism of the system. In this case, the total astigmatism is constant. The astigmatism with respect to the medial focal surface is given by

$$W = \frac{1}{2}(W_{222}\vec{b}^2_{222})\cdot\vec{\rho}^2 \tag{4.14}$$

where W_{222} is the aberration coefficient of the equivalent plane-parallel plate.

$$\vec{b}^2_{222} = \frac{W_{222,1}\,\vec{a}^2_1 + W_{222,2}\,\vec{a}^2_2}{W_{222}} \,. \tag{4.15}$$

The subscript following the comma indicates the surface number. The orientation of the line foci is governed by the vector $\vec{b}^2_{222}$.

The medial focal surface is a flat surface defocused from the GIP. The amount of defocus can be found as described in Chapter 2.

Case II

Two wedges are placed in an otherwise corrected system. The wedges are identical and tilted in the same plane as shown in Fig. 4.7.

We know that we can tilt the first wedge and find an angle such that the coma node will be at the center of the image field with the astigmatic nodes located symmetrically with respect to it. For the second wedge, we can find the location of the wedge where $t_2/\ell_2 = t_1/\ell_1$ (see Fig. 4.7), where t_1 and t_2 in this case are the thicknesses of the wedges along the OAR (not the reference axis as was before).

Then we can tilt the second wedge to superimpose its nodes on the nodes of the first wedge as shown in Fig. 4.8. This angle will be the same angle as the first wedge with respect to the OAR. Since the ratio of the wedge thickness to the distance from the wedge to the object along the reference axis is the same for both wedges, the distances between the astigmatic nodes of both wedges will be equal.

The Gaussian image plane is not tilted with respect to the reference axis because the vertex angles of both wedges are equal in magnitude and opposite in sign. The center of the image field is displaced from the reference axis. The resulting coma field will be linear with the node at the center of the image field. Its magnitude will be the sum of the magnitudes of the component fields. The expression for coma is given by

$$W = (W_{131,1} + W_{131,2})(\vec{H}\cdot\vec{\rho})(\vec{\rho}\cdot\vec{\rho}) \ , \qquad (4.16)$$

where the subscript following the comma identifies the wedge.

The astigmatism will be binodal with the nodes located at the node points of the component fields and symmetrical with respect to the coma node and the center of the image field. The astigmatism with

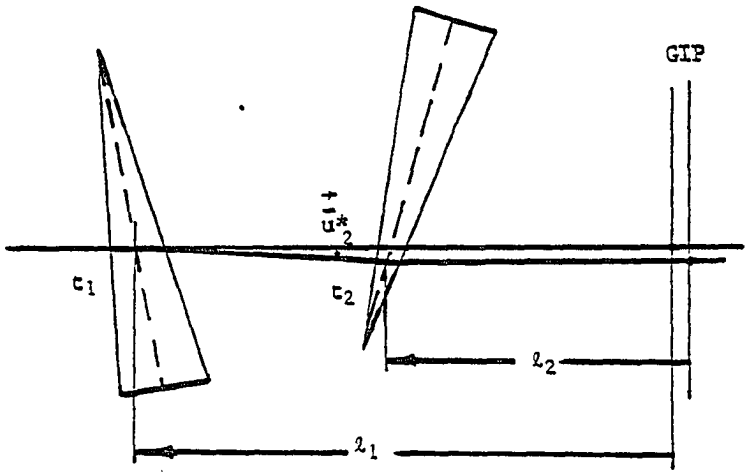

Fig. 4.7. Case II. Wedges are tilted in the same plane.

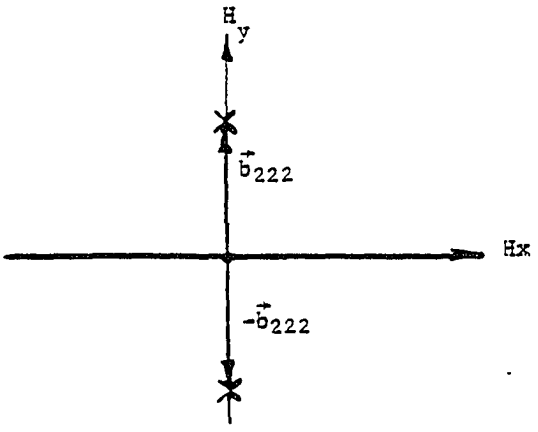

Fig. 4.8. Wedges are tilted in the same plane. The coma nodes are at the center of the image field.

• denotes the coma nodes, x denotes the astigmatic nodes.

respect to the medial surface is given by

$$W = \frac{1}{2}\,(W_{222,1} + W_{222,2})\left[\vec{H}^2 - \vec{b}^2_{222}\right]\cdot\vec{\rho}^2\ , \tag{4.17}$$

where the subscript following the comma identifies the wedge as above and $\vec{b}^2_{222}$ is the perturbation vector for either of the wedges.

We can tilt the wedges by another pair of angles (see Eq. 4.12) and place one of the astigmatic nodes for both wedges at the center of the image field as shown in Fig. 4.9.

The resulting astigmatic field would then be a normal quadratic field if the magnitudes of the component fields were the same. If the wedges are placed in the system close to each other so that the magnitudes of the component fields differ by a small amount, the resulting astigmatism will be binodal with one of the nodes at the center of the image field and the other node being close to it.

The coma will not be zero at the center of the image field due to the difference in magnitudes of the component fields, but again, it will be small at the center of the image field since the node will be very close to it, assuming that the wedges are placed close to each other.

Case III

Two wedges are placed in a system with no aberrations. The wedges are identical and cross-tilted as shown in Fig. 4.10. Here we will keep the ratio of the wedge thickness to the distance from it to the object the same for both wedges. The center of the image field will

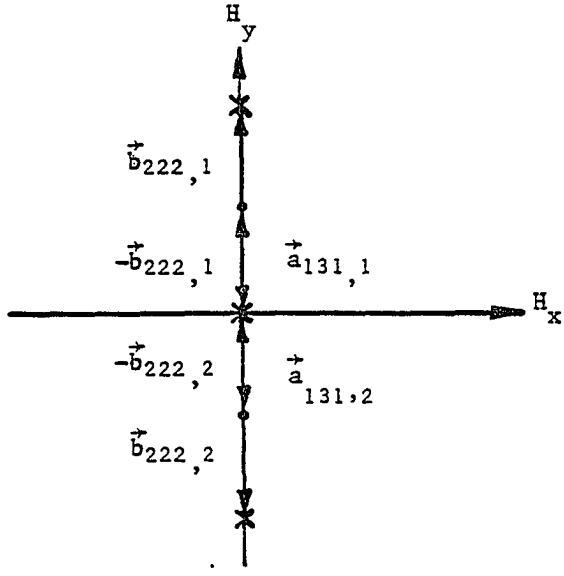

Fig. 4.9. Wedges are tilted in the same plane. One of the astigmatic nodes of both wedges is at the center of the image field.

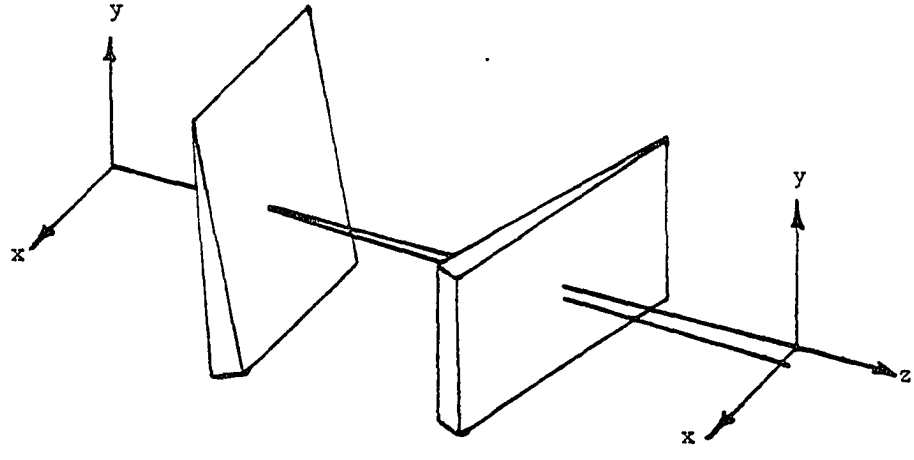

Fig. 4.10. Cross-tilted wedges of Case III.

be also displaced in this case. The Gaussian image plane will be tilted with respect to the reference axis, because now the vertex angles of the wedges are not coplanar.

If we locate the coma nodes of both wedges at the center of the image field and the astigmatic nodes symmetrical with respect to it as shown in Fig. 4.11, then due to the symmetry of the coma, the resulting coma field will be the same as in Case II (ordinary linear coma with the node at the center of the field). This is given by Eq. 4.16.

The astigmatism will be binodal again due to the difference in magnitudes of each component field. If two wedges are placed close to each other so that the difference in magnitudes of the astigmatic component fields is small, then the distance between the nodes of the resulting binodal astigmatism is very small, and they almost degenerate into one node at the center of the image field.

The expression for the binodal astigmatism with respect to the medial surface can be obtained using equations from Chapter 2 and calculating the perturbation vectors for the system surface by surface. This expression is

$$W = \frac{1}{2}(W_{222,1} + W_{222,2})\left[\vec{H}^2 - \vec{b}^2_{222}\,\frac{W_{222,1} - W_{222,2}}{W_{222,1} + W_{222,2}}\right]\cdot\vec{\rho}^2 \qquad (4.18)$$

Here the subscript after the comma identifies the wedges, and $\vec{b}^2_{222}$ is the perturbation vector for the astimgatism of either of the wedges.

The nodes will be located at

$$\vec{H} = \pm \vec{b}_{222} \sqrt{\frac{W_{222,1} - W_{222,2}}{W_{222,1} + W_{222,2}}} \quad . \tag{4.19}$$

If we locate one of the astigmatic nodes for each wedge at the center of the image field by tilting the wedge by the angle given by Eq. 4.12 as shown in Fig. 4.12, the resulting astigmatic field will be binodal with one of the nodes at the center of the image field and the other in the vicinity of point P if the wedges are close to each other.

The resulting coma field is linear with the node located on the line connecting the two component field nodes and almost half way between them because the magnitudes of the component fields differ by small amount.

The expression for the resulting aberration fields are easily obtained using the equations of Chapter 2.

Now it is easy to see the effect of placing two wedges in a system where the aberrations would balance the aberrations of two equivalent plane-parallel plates squared on the axis of the system.

Case IV

The wedges are tilted in the same plane. At first we tilt the wedges to place the coma nodes at the center of the image field. We now must add to the aberration fields of Case II the aberrations of the system, which are also centered in the image field.

It is easy to see that coma will be zero across the entire field, since the aberrations of the system are equal to the sum of the

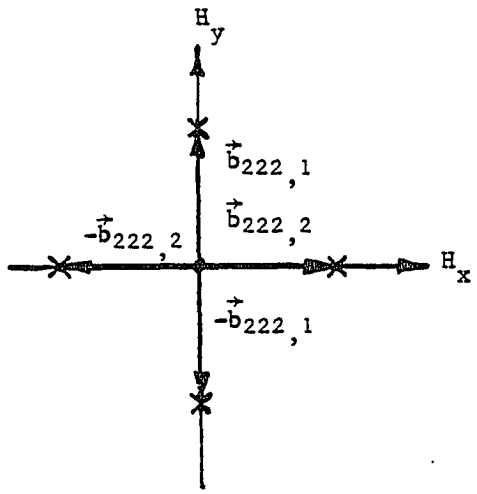

Fig. 4.11. Wedges are cross-tilted. The coma nodes are at the center of the image field.

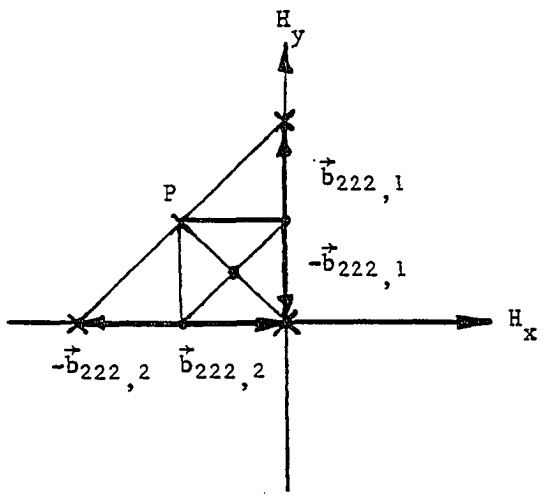

Fig. 4.12. Wedges are cross-tilted. One of the astigmatic nodes of both wedges is at the center of the image field.

aberrations of the equivalent plates and opposite in sign. Astigmatism will be constant in magnitude and orientation across the field and is given by

$$W = \left[-\frac{1}{2} \left(W_{222,1} + W_{222,2} \right) \vec{b}_{222}^{2} \right] \cdot \vec{\rho}^{2} \ , \tag{4.20}$$

as obtained from Eq. 4.17.

If the arrangement of the wedges is as shown in Fig. 4.9, then the astigmatism will be linear with the node at the center of the image field and the magnitude being small if the difference between the magnitudes of the component fields is small.

Coma will be constant across the field with a small magnitude if we place the wedges close to each other.

Case V

The wedges are cross-tilted. In the first case, we have coma equal to zero across the field for the same reason as before. Astigmatism again is constant and given by

$$W = \left[-\frac{1}{2} \left(W_{222,1} - W_{222,2} \right) \vec{b}_{222}^{2} \right] \cdot \vec{\rho}^{2} \ . \tag{4.21}$$

Here we will have small constant astigmatism if we place the wedges close to each other. Therefore we can say that if we have a system with a plane-parallel plate where the total aberrations are corrected, we can split that plate into two pieces, make wedges out of them, and then tilt and place the wedges in the manner described above, the aberrations will stay practically corrected.

If the arrangements of the wedges is as shown in Fig. 4.12, coma is constant across the field and astigmatism is linear with the node at the center of the image field.

CHAPTER 5

THE MIRROR

A curved mirror has power and therefore can be treated as a system by itself.

A spherical mirror does not have an axis; any line passing through the center of curvature can be treated as an axis. For a single spherical mirror acting as an image-forming system, we can describe the first- and third-order properties with respect to any line taken as a reference axis.

The first-order properties of a spherical refracting surface were investigated in detail in Chapter 2. For the spherical mirror, the same equations can be used if we let $n' = -n$.

If we consider the mirror in air ($n = 1$), the expression for the relative image displacement (Eq. 2.2) becomes

$$\vec{\delta}Q' = \vec{\delta}Q - \frac{2y}{\mathscr{K}}\vec{\beta}_0 \ , \tag{5.1}$$

and the expression for relative pupil displacement (Eq. 2.4) becomes

$$\vec{\delta}E' = \vec{\delta}E + \frac{2\bar{y}}{\mathscr{K}}\vec{\beta}_0 \ . \tag{5.2}$$

The tilt of the Gaussian image plane for the spherical mirror can be found as described in Chapter 2.

As we already know, the center of aberrations for a spherical surface is along the line connecting the center of the pupil with its center of curvature as shown in Fig. 2.4. As we can see from this

figure, the location of the aberration center for a surface depends on the position of the pupil.

For a spherical surface, we should consider a special case, when the pupil is at the center of curvature ($\bar{i} = 0$).

In a centered system, the only aberration introduced by this surface will be spherical aberration. If the pupil center is displaced from the center of curvature of the surface, as shown in Fig. 5.1, other aberrations, uniform over the field, will be generated.

The relative displacement of the center of curvature from the pupil center is given by

$$\vec{a} = \frac{\vec{\delta}C - \vec{\delta}E}{y_E} , \tag{5.3}$$

where y_E is the pupil radius. In this case, the aberration center for this surface lies at infinity and the aberration contribution due to this surface is

$$\begin{aligned} W &= W_{040}[(\vec{\rho} - \vec{a})\cdot(\vec{\rho} - \vec{a})][(\vec{\rho} - \vec{a})\cdot(\vec{\rho} - \vec{a})] \\ &= W_{040}(\vec{\rho}\cdot\vec{\rho})(\vec{\rho}\cdot\vec{\rho}) - W_{040}(\vec{\rho}\cdot\vec{a})(\vec{\rho}\cdot\vec{\rho}) \\ &\quad + 4W_{040}(\vec{\rho}\cdot\vec{a})^2 + 2W_{040}(\vec{a}\cdot\vec{a})(\vec{\rho}\cdot\vec{\rho}) \\ &\quad - 2W_{040}(\vec{a}\cdot\vec{a})(\vec{\rho}\cdot\vec{a}) + W_{040}(\vec{a}\cdot\vec{a})^2 . \end{aligned} \tag{5.4}$$

The first term is just the ordinary spherical aberration term. Considering the aperture dependence of the following terms, we can see that the second, third, fourth, and fifth terms describe constant coma, astigmatism, field curvature, and distortion respectively. The last term is piston error.

Third-Order Aberration Fields

For a single spherical mirror, aberrations can be described as ordinary aberrations always centered on the line passing through the pupil center and the center of curvature. Since a single spherical mirror can be part of a larger system with a defined reference axis, we can describe its aberrations with respect to the reference axis as follows.

If $\vec{a}$ is the aberration displacement vector in the image plane, coma, astigmatism, and distortion introduced by this mirror do not change, instead they are simply shifted in the image plane to the point located by the vector $\vec{a}$. The medial focal surface is a quadratic surface, the vertex of which is displaced in the Gaussian image plane by the vector $\vec{a}$. There is no longitudinal shift. The effect of a stop shift in a tilted and decentered spherical mirror is to change the magnitude and direction of the aberration displacement vector. We should point out here that the magnitude of the aberrations (except spherical aberration) will also change.

Once we know what the aberrations are for a single tilted and decentered spherical mirror, we can determine the aberrations of two-tilted and decentered spherical mirrors.

The system of two-tilted and decentered spherical mirrors can be treated as a system centered on the line passing through both centers of curvature with a decentered pupil or as a system perturbed with respect

to a reference axis.

In the latter case, generally, the center of the resulting image field will be displaced from the reference axis. The centers of the aberration fields for each mirror will be displaced from the center of the image field.

The resulting spherical aberration will not change, since, as we know, spherical aberration is not affected by tilts and decenters.

The coma field will be a linear coma field shifted in the image plane; astimgatism will be binodal, and distortion will have three third-order nodes. The location of the nodes will depend on the magnitude and sign of the component fields, but in general, there will not be any symmetry.

Special Cases

I. The pupil is centered on the line connecting the centers of curvature of the two mirrors. In this case, the system is simply a centered system, and the resulting aberrations are ordinary aberration fields centered on this line.

II. Two spherical mirrors are cross-tilted. Here we will examine the case of two cross-tilted spherical mirrors arranged as shown in Fig. 5.2. The system is obtained as follows. Consider two concave spherical mirrors with common center of curvature at point Q'. Let the line O_1, O_2 passing through point Q' be the reference axis. We can tilt the first mirror about point O_1 by an angle $\vec{\beta}_1$. The second mirror is

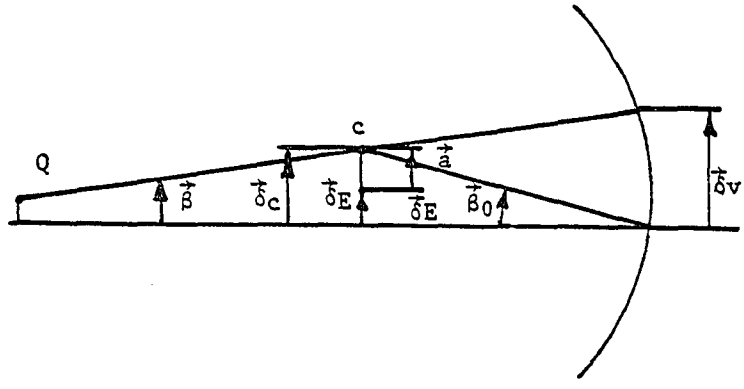

Fig. 5.1. Special case when the pupil is laterally displaced from the center of curvature of the spherical surface.

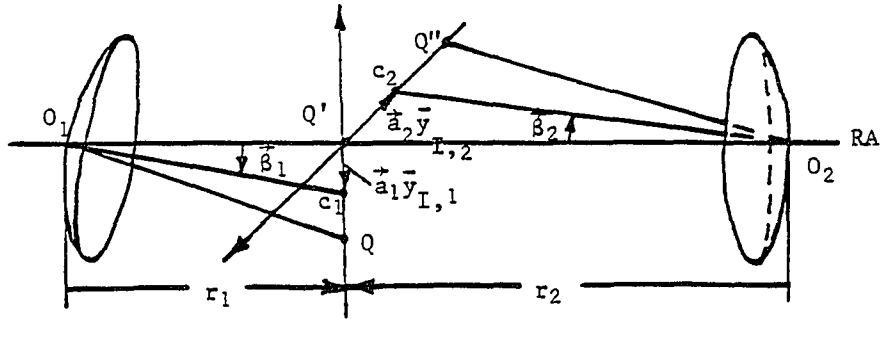

Fig. 5.2. Two spherical mirrors are cross-tilted.

tilted about point O_2 by an angle $\vec{\beta}_2$ in the orthogonal direction. The object plane for the first mirror is chosen to be the plane containing both centers of curvature and perpendicular to O_1O_2. If we choose the center of the object field for the first mirror to be at point Q, so that its image lies at point Q' (which is the object for the second mirror), then third-order spherical aberration and coma of each mirror will be zero.

The center of the astigmatic field for each mirror will be displaced from the center of the image field. The amount of this displacement can be found as follows:

$$\begin{aligned} \vec{a}_1\bar{y}_{I_1}' &= \vec{\beta}_1 r_1 \ , \\ \vec{a}_2\bar{y}_{I_2} &= \vec{\beta}_2 r_2 \ , \end{aligned} \tag{5.5}$$

where $\vec{\beta}_1$ and $\vec{\beta}_2$ are the tilt angles of the mirrors, r_1 and r_2 are their radii of curvature, $\bar{y}_{I_1}' = \bar{y}_{I_2}$ is the image radius from the first mirror and object radius for the second one.

As can be seen from Fig. 5.2, the location of the pupil does not change the aberration center displacement vectors, it changes only the magnitude of distortion due to each mirror.

The resulting aberrations will be as follows: spherical aberration and coma will be zero, and astigmatism will be binodal as shown in Fig. 5.3.

The condition for one of the nodes to be at the center of the image fields is given by

$$W_{222,1}\vec{a}_1^{\,2} + W_{222,2}\vec{a}_2^{\,2} = 0 \ , \tag{5.6}$$

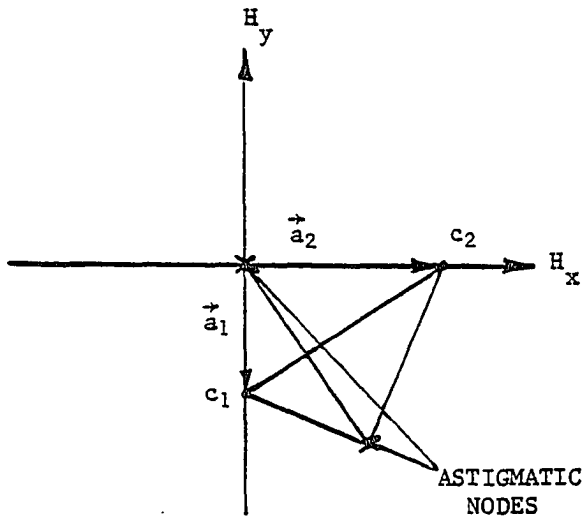

Fig. 5.3. Binodal astigmatism of two cross-tilted spherical mirrors.

C_1 and C_2 are the astigmatic field centers of the first and second mirrors.

where $W_{222,1}$ and $W_{222,2}$ are the wave aberration coefficients of each mirror and are given by

$$W_{222i} = \frac{1}{2} \varkappa c^2 \phi_i, \text{ and } i = 1,2. \tag{5.7}$$

Here ϕ is the power of the mirror. Combining Eqs. 5.5, 5.6, and 5.7, we obtain

$$\left[\frac{\vec{\beta}_1}{\vec{\beta}_2}\right]^2 = \frac{\phi_2}{\phi_1} . \tag{5.8}$$

Using Eq. 5.8, it is easy to find the tilt of the second mirror (if the tilt of the first mirror is given) to correct astigmatism on axis.

An Aspheric Mirror.

When an aspheric is added to a surface, all first-order properties of the surface remain unchanged, since aspherizing the surface affects only fourth and higher degree terms. There is also no change in the Petzval term. We know that if the aperture stop is centered on the aspheric surface the only effect of the aspherizing is to change spherical aberration. If the aspherized surface is not at or conjugate to the aperture stop the aspherizing will also introduce coma, astigmatism, and distortion.

From Chapter 2, we already know that the aberration center of the aspheric contribution will be displaced from the center of the image field and in general from the aberration center of the base sphere. We

also know that the center of the aberration contribution due to the aspheric is along the line connecting the vertex of the aspheric cap with the center of the pupil as shown in Fig. 5.4.

The relative displacement of the aberration field due to the aspheric in the image plane is given by Eq. 2.12. For an aspheric mirror, the effect of tilt and decentration is the displacement of the aspheric cap vertex $\vec{\delta}V_A$ and the center of curvature of the surface $\vec{\delta}_C$.

A special case for the aspheric surface is when the pupil is at the surface ($\bar{y} = 0$). In this case the center of the aberration field due to the aspheric is at infinity. In the centered system this aspheric will generate only spherical aberration. If the vertex of the aspheric cap is displaced from the center of the pupil, aberrations uniform over the field will be generated.

The aberrations generated by this surface can be obtained using Eq. 5.4, where instead of vector $\vec{a}$ we should substitute $\vec{a}_A$ which can be found as

$$\vec{a}_A = \frac{\vec{\delta}V_A - \vec{\delta}E}{y_E} . \tag{5.9}$$

Often when the aperture stop is at the aspheric surface (for example, in a reflecting telescope) and this surface is tilted and decentered, the aspheric cap still remains centered relative to the aperture stop. Therefore the only effect of tilt and decenter in this case is to shift the aberration center due to the base sphere in the image plane to the point located by the vector $\vec{a}$ (as in the case of a

single spherical mirror).

There is a special case when the aspheric cap is intentionally decentered with respect to the aperture stop, namely the case of an off-axis aspheric, such as an off-axis parabola.

In this case we can find $\vec{a}_A$ using Eq. 5.9 where either $\vec{\delta}_A$ or $\vec{\delta}_E$ will be zero, depending on the choice of reference axis. This case is illustrated in Fig. 5.5 where the reference axis is the line passing through the center of curvature of a surface and the vertex of the aspheric cap. The center of the aberration field due to the base sphere is along the line connecting the pupil center E with the center of curvature. The aberration center due to the aspheric is at infinity and, in addition to the base sphere, the aspheric will generate other aberrations uniform over the field as given by Eq. 5.4.

In the general case where the stop is not at or conjugate to the aspheric surface, the resulting aberration fields can be found using equations given in Chapter 2.

The aspheric surface can be treated as a system with two surfaces, each surface producing its own displacement of the aberration field center in the image plane.

We should point out here that in the general case, the resulting aberration fields will be as follows. Coma will be the usual linear coma field displaced from the center of the image field. Astigmatism will be binodal and distortion will have three third-order nodes.

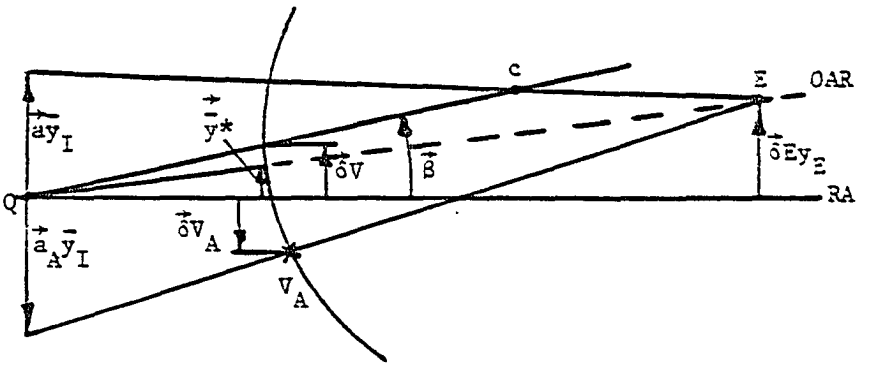

Fig. 5.4. The center of the aberrations due to the aspheric.

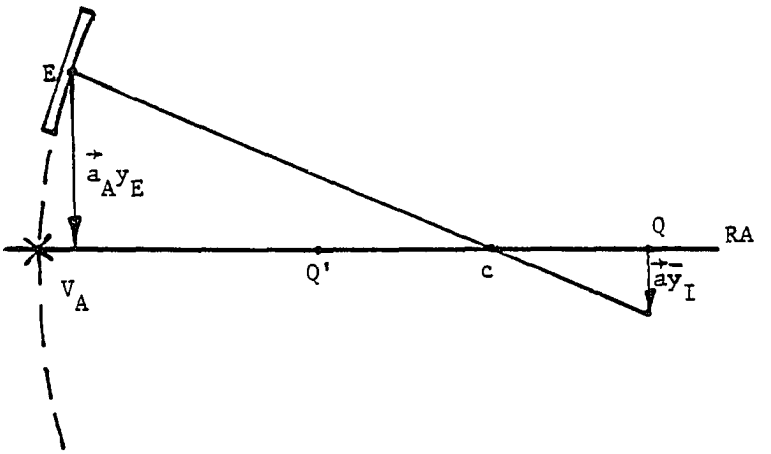

Fig. 5.5. Off-axis aspheric.

Once we know the aberrations at a tilted and decentered single aspheric surface, we can examine a few interesting special cases of systems containing two mirrors.

Special Cases

I. The classical Cassegrain telescope. In this system, both mirros are aspherics and the stop is at the primary mirror.

The effect of misalignment in such a telescope is the introduction of coma and astigmatism on axis. We can show that by tilting the secondary mirror, coma can be removed on axis, but it does not mean that the telescope has been aligned since binodal astigmatism may still be present in the system. If both mirrors in the telescope are tilted and decentered, it is convenient to choose as a reference axis the axis of the primary mirror (that is the line passing through the center of curvature of the mirror and the vertex of the aspheric). The stop will be centered on this axis. The only tilts and decenters with respect to this axis will be tilt and decenter of the secondary mirror.

If we assume the object center to be along the reference axis, then the center of the image will be displaced with respect to the reference axis. The center of the aberration field due to the primary mirror will not be displaced from the center of the image field. For the secondary mirror, the center of the aberration fields due to the base sphere and the aspheric cap will be displaced from the center of the image field and can be found as described before (Eqs. 2.8 and 2.12).

Third-order spherical aberration in a classical Cassegrain design is corrected and it will not be affected by misalignment. Coma will be ordinary linear coma shifted in the image plane. Astimgatism will be binodal, and distortion will have three third-order nodes.

By tilting and decentering the secondary mirror, we can make coma zero at the center of the field. The condition for this is that $\vec{A}_{131} = 0$, from which it follows that

$$\frac{\vec{a}}{\vec{a}_A} = - \frac{W_{131A}}{W_{131}} , \tag{5.10}$$

and

$$\frac{\vec{\delta c}}{\vec{\delta V}_A} = - (W_{131A}\, \bar{I}_2)/(W_{131}\bar{y}_2 c_2) = \text{constant} \tag{5.11}$$

where W_{131A} and W_{131} are the wave aberration coefficients for the aspheric and the base sphere of the secondary mirror respectively.

Equation 5.11 implies that there is a pivot point for the secondary mirror about which we can rotate the secondary mirror and coma will remain zero at the center of the field. The pivot point can be found as the intersection point of a line connecting the center of curvature to the vertex of the aspheric, and the reference axis as shown in Fig. 5.6.

In general, astigmatism of the system will be binodal, and not symmetrical with respect to the center of the field. The condition for one of the astimgatic nodes to be at the center of the field is

different from the condition for zero coma. It is $\vec{B}_{222} = 0$ and

$$\frac{\vec{a}^2}{\vec{a}^2_A} = -\frac{W_{222A}}{W_{222}} , \tag{5.12}$$

where W_{222A} and W_{222} are the wave aberration coefficients for the aspheric and the base sphere of the secondary mirror. This means that, generally, we cannot have both coma and astigmatism zero at the center of the field of a misaligned system, unless both Eqs. 5.10 and 5.12 are satisfied.

The tilt of the image plane with respect to the reference axis in a misaligned classical Cassegrain telescope can be found using Eq. 2.7.

The system is aligned only if both coma and astigmatism are zero at the center of the field and astigmatism is the usual centered type, which is quadratic with the field.

The distortion field of the misaligned system will be non-symmetric with three third-order nodes.

II. The Ritchey-Chretien telescope. The difference between the Ritchey-Chretien and the classical Cassegrain design is that for the former, with different aspherics on the mirrors, spherical aberration and coma are both corrected.

Since coma is corrected in the aligned system, the effect of misalignment is the introduction of coma which is constant in both magnitude and orientation across the field.

Again we can tilt the secondary mirror to make coma zero across the field and we can also find the pivot point about which we can rotate the secondary mirror, keeping coma zero across the field. For this system, the pivot point will be at a slightly different location on the axis, since the wave aberration coefficients of the secondary mirror are different from those of a classical Cassegrain design.

Since coma will be zero at every point in the field, we can choose the center of the image field to be at one of the nodes of the binodal astigmatism.

To align the system, it is not enough just to make coma zero across the field. If the system is not aligned, astigmatism will be binodal, and the image plane tilted. Therefore during the alignment, it is advisable to examine either the astigmatism of the system or the image plane tilt.

III. Unobscured aperture telescope. Using the insights developed earlier, we can demonstrate the approach to the design of an unobscured aperture telescope.

The system will be based on the classical Cassegrain design. We choose the reference axis to be the axis of the system before the mirrors are tilted and decentered and tilt both mirrors as shown in Fig. 5.7.

Since the stop is at the primary mirror, the aspheric of the primary does not generate any field aberrations.

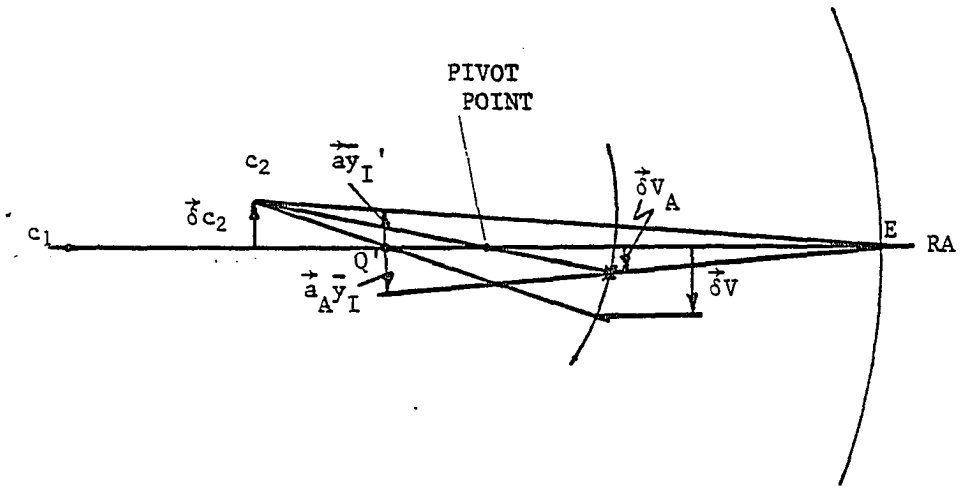

Fig. 5.6. The pivot point for classical Cassegrain or Ritchey-Chretien design telescopes.

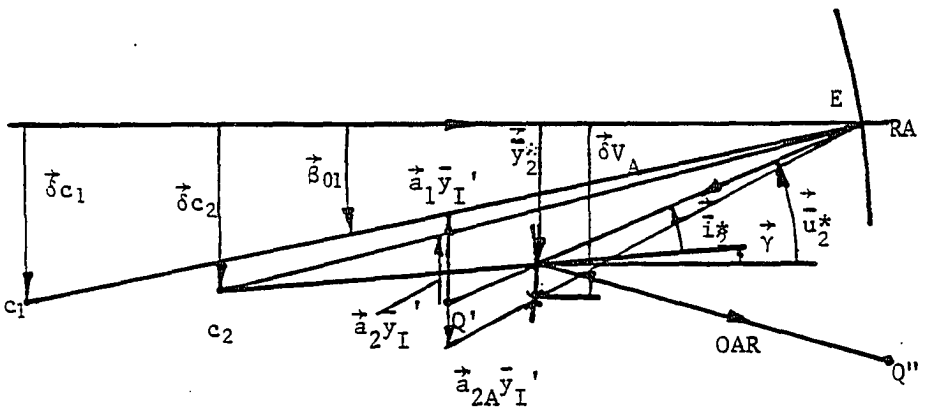

Fig. 5.7. Unobscured telescopic system based on classical Cassegrain or Ritchey-Chretien design.

The aberration fields due to the base sphere of the primary will be displaced in the image plane by the vector $\vec{a}_1$.

Both the base sphere and aspheric of the secondary mirror will contribute to aberrations. Their aberration fields will be also be displaced in the image field by the vectors $\vec{a}_2$ and $\vec{a}_{2A}$ due to the base sphere of the secondary mirror and its aspheric cap respectively.

If we want both coma and astigmatism to be zero at the center of the image field, we should satisfy the conditions,

$$W_{131,1}\vec{a} + W_{131,2}\vec{a}_2 + W_{131,2A}\vec{a}_{2A} = 0 \tag{5.13}$$

$$W_{222,1}\vec{a}_1^{\,2} + W_{222,2}\vec{a}_2^{\,2} + W_{222,2A}\vec{a}_{2A}^{\,2} = 0 \ , \tag{5.14}$$

where subscripts following commas identify the mirrors.

Here we have two equations with three unknowns. However, we can eliminate one of the unknowns by expressing it as a function of the other two by using the first equation and substituting this expression into the second equation.

The solution for the ratio of the two aberration displacement vectors due to the tilted mirrors is given by

$$\frac{\vec{a}}{\vec{a}_{2A}} = \frac{-W_{131,1}W_{131,2A}W_{222,2}}{W_{222,2}W_{131,1}^2 + W_{131,2}^2W_{222,1}}$$

$$\pm \frac{W_{131,2}[-(W_{131,2A}^2W_{222,2}W_{222,1}+W_{131,1}^2W_{222,2}W_{222,2A}+W_{131,2}^2W_{222,1}W_{222,2A})]^{1/2}}{W_{222,2}W_{131,1}^2+W_{131,2}^2W_{222,1}} \tag{5.15}$$

If we define

$$A = \frac{-W_{131,1}W_{131,2A}W_{222,2}}{W_{222,1}W_{131,2}^2 + W_{131,1}^2W_{222,2}} \tag{5.16}$$

and

$$B = \frac{W_{131,2}[-(W_{131,2A}^2W_{222,2}W_{222,1}+W_{131,1}^2W_{222,2}W_{222,2A}+W_{131,2}^2W_{222,1}W_{222,2A})]^{1/2}}{W_{222,2}W_{131,1}^2+W_{131,2}^2W_{222,1}} \tag{5.17}$$

then we can rewrite Eq. 5.15 as

$$\frac{\vec{a}_1}{\vec{a}_{2A}} = A \pm B \, . \tag{5.18}$$

Using Eqs. 2.8 and 2.12 we can write

$$\vec{a}_2 = -\vec{\bar{i}}_2^*/\bar{i}_2 \, , \tag{5.19}$$

$$\vec{a}_{2A} = (\delta\vec{V}_{2A} - \vec{\bar{y}}_2^*)/\bar{y}_2 \, , \tag{5.20}$$

and

$$\vec{a}_1 = (\vec{\beta}_{01})/\bar{u}_1 \, . \tag{5.21}$$

From Fig. 5.7 we can see that

$$\vec{\bar{y}}_2^* = \vec{\bar{u}}_2^* t \tag{5.22}$$

and

$$\vec{\bar{i}}_2^* = \vec{\bar{u}}_2^* - \vec{\gamma} \, , \tag{5.23}$$

where t is the distance between the primary and secondary mirrors and $\vec{\gamma}$ is the tilt angle of the secondary mirror with respect to the reference axis about the point of intersection of the OAR with the secondary mirror.

From Fig. 5.7 we can see that for this configuration,

$$\vec{\bar{u}}_2^* = 2\,\vec{\beta}_{01} \, , \tag{5.24}$$

where $\vec{\beta}_{01}$ is the tilt angle of the primary mirror with respect to the reference axis as shown in Fig. 5.7.

Combining Eqs. 5.18 through 5.24 we obtain

$$\vec{\delta}V_{2A} = \vec{\beta}_{01}\bar{y}_2/(A\pm B)\bar{u}_1 + 2\vec{\beta}_{01}t \ . \tag{5.25}$$

The design procedure may be as follows. We can choose the tilt of the primary mirror $\vec{\beta}_{01}$, such that the secondary mirror will not obscure the light coming to the primary mirror. Then using Eq. 5.25 we can find the decenter $\vec{\delta}V_{2A}$ for the secondary mirror (Eq. 5.25 provides two solutions). To find the tilt of the secondary mirror, we have to solve Eq. 5.13 for $\vec{\gamma}$.

The solution is

$$\vec{\gamma} = -\left[C(\vec{\delta}V_{2A} - 2\vec{\beta}_{01}t)\bar{i}_2/\bar{y}_2 + D\vec{\beta}_{01}\bar{i}_2/\bar{u}_1\right] + 2\vec{\beta}_{01}, \tag{5.26}$$

where

$$C = \frac{W_{131,2A}}{W_{131,2}} \tag{5.27}$$

and

$$D = \frac{W_{131,1}}{W_{131,2}} \ . \tag{5.28}$$

For the Ritchey-Chretien design, Eq. 5.13 will indicate the condition for coma being zero across the entire field. Then we can simply choose one of the nodes of binodal astigmatism to be the center of the image field.

CHAPTER 6

THIN LENS

We know that a single spherical surface does not have an axis, but a system of two spherical surfaces together do have an axis which is the line passing through the centers of curvature, unless, of course, the centers coincide.

In the case of a non-trivial thin lens, where the surfaces are in contact, the centers do not coincide and the thin lens must necessarily have an axis. In addition the thin lens has a vertex which is the intersection of the axis with the lens itself.

Also, a thin lens can be treated as a system by itself, rather than only as a component.

First we will examine a thin lens which is tilted and decentered with respect to a reference axis.

Using the equations of Chapter 2 for each surface of the lens, we obtain the expression for the relative displacement of the image field

$$\vec{\delta}Q' = \vec{\delta}Q + \frac{y\phi}{\mathcal{H}}\vec{\delta}V = \vec{\delta}Q + \left(\frac{1}{m} - 1\right)\vec{\delta}V/\bar{Y}_I \ . \tag{6.1}$$

Here ϕ is the power of the lens, y is the marginal ray height on the lens, $\mathcal{H}$ is the Lagrange invariant, m is the magnification of the lens, and $\vec{\delta}V$ is the vertex displacement as shown in Fig. 6.1.

As can be seen from this expression, the relative displacement of the center of the image field does not depend on the tilt of a thin lens. It follows directly from the fact that the nodal points of the lens coincide at the lens.

The Gaussian image plane tilt of a thin lens with respect to the reference axis can be found using Eq. 2.7. Here we should point out that it depends only on the lens tilt, not on the lens decenter.

In a thin lens each surface will produce a displacement of its aberration center in the image field and we already know how to find this displacement for a spherical (or aspheric) surface.

For a thin lens these displacements are shown in Fig. 6.2. The resulting third-order aberration fields are as follows. Spherical aberration is unchanged. Coma is the usual linear coma shifted from the center of the image field, astigmatism is binodal, and distortion has three third-order nodes.

Both tilt and decenter of a lens will affect the location of the nodes with respect to the center of the image field.

For a thin lens, as for the mirror described above, the magnitude of the aberration displacement vectors and therefore the location of the nodes depends on the location of the stop.

We will consider two special cases.

I. The center of the stop is on the axis of the thin lens. Then the aberration centers for both surfaces will also be on this axis and the aberration fields become the usual fields centered on the local axis

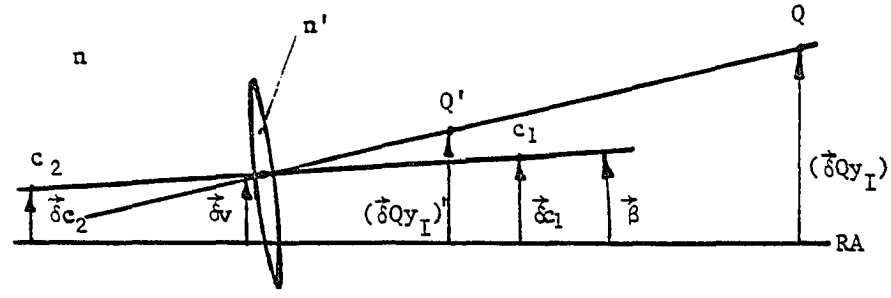

Fig. 6.1. Displacement of the image in tilted and decentered thin lens.

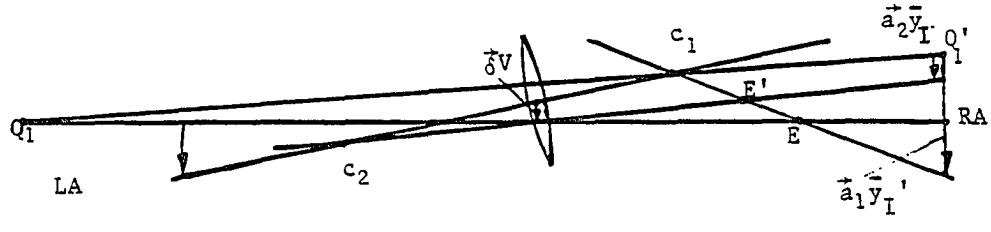

Fig. 6.2. Aberration center displacement vectors for each surface of the thin lens.

E' and Q' are the images of E and Q after the first surface of the lens.

of the lens. In fact, we cannot really say that the lens is tilted and decentered. We can simply say that the center of the image field just has been shifted.

II. The stop is at or conjugate with the plane containing the center of curvature of one of the lens surfaces and displaced from it.

The aberration center of this surface is then at infinity and the aberrations generated by this surface will be constant with the field as described in Chapter 5.

The resulting aberration fields will be the usual aberration fields shifted in the image plane to the point located by the aberration center displacement vector of the other surface.

There is another way to describe the aberrations of a tilted and decentered thin lens.

Since the lens has an axis, it can be considered as a centered system for which aberration coefficients can be easily calculated. The the effect of the tilt and decentration for a thin lens is the displacement of the pupil with respect to the lens axis, which is the reference axis of the system.

Aberrations of a system with eccentric pupil are described in the Appendix.

We know that aberrations of a thin lens depend on the lens shape factor. Treating the thin lens as a centered system with eccentric pupil we can examine the dependence of the lens aberrations on the shape factor.

Coma of a tilted and decentered thin lens is given by (Eq. A.4)

$$W = W_{131}\left[(\vec{H} - \vec{k}_{131}) \cdot \vec{\rho}\right](\vec{\rho} \cdot \vec{\rho}) \tag{6.2}$$

where

$$\vec{k}_{131} = \left(\frac{4W_{040}}{W_{131}}\right)\vec{c} \ , \tag{6.3}$$

W_{040}, W_{131} are the wave aberration coefficients of the thin lens, and $\vec{c}$ is displacement vector of the center of the pupil.

The wave aberration coefficients of a thin lens can be expressed as follows

$$W_{040} = \frac{1}{32}y^4\phi^3\sigma_I \ , \tag{6.4}$$

$$W_{131} = \frac{1}{4}\mathcal{H}\, y^2\phi^2(\sigma_{II} + S\sigma_I) \ , \tag{6.5}$$

$$W_{222} = \frac{1}{2}\mathcal{H}^2\phi(\sigma_{III} + 2S\sigma_{II} + S^2\sigma_I) \ , \tag{6.6}$$

where y is the marginal ray height at the principle planes, ϕ is the lens power, S is the stop shift factor, and σ_I, σ_{II}, and σ_{III} are the structural aberration coefficients. For a thin lens (stop at the lens) they are given by

$$\sigma_I = AX^2 - BXY + CY^2 + D \tag{6.7}$$

$$\sigma_{II} = EX - FY \tag{6.8}$$

$$\sigma_{III} = 1 \tag{6.9}$$

Here X is the shape factor and Y is the magnification factor. They can be expressed as

$$X = \frac{c_1 + c_2}{c_1 - c_2} \tag{6.10}$$

$$Y = \frac{1 + m}{1 - m} \tag{6.11}$$

and

$$A = \frac{n + 2}{n(n-1)^2} , \tag{6.12}$$

$$B = \frac{4(n + 1)}{n(n-1)} , \tag{6.13}$$

$$C = \frac{3n + 2}{n} , \tag{6.14}$$

$$D = \frac{n^2}{(n-1)^2} , \tag{6.15}$$

$$E = \frac{n + 1}{n(n - 1)} , \tag{6.16}$$

$$F = \frac{2n + 1}{n} , \tag{6.17}$$

where c_1 and c_2 are the curvatures of the first and second surfaces of the lens, m is the lens magnification, and n is its index of refraction.

Using Eqs. 6.3, 6.4, and 6.5, we obtain

$$\vec{k}_{131} = \frac{y^2\phi}{2\mathcal{H}} \frac{\sigma_I}{\sigma_{II}} \vec{c} \tag{6.18}$$

with S = 0 (stop at the lens).

Astigmatism with respect to the medial surface is given by (Eq. A.13)

$$W = \frac{1}{2} W_{222} \left[(\vec{H} - \vec{k}_{222})^2 - \vec{\ell}^2_{222} \right] \cdot \vec{\rho}^2 \tag{6.19}$$

where

$$\vec{k}_{222} = \frac{W_{131}}{W_{222}} \vec{c} , \tag{6.20}$$

$$\vec{\ell}^2_{222} = \left(\frac{W^2_{131} - 8W_{040} W_{222}}{W^2_{222}} \right) \vec{c}^2 , \tag{6.21}$$

and W_{222} is the wave aberration coefficient of the thin lens.

Combining Eqs. 6.4, 6.5, 6.5, 6.20, and 6.21, we obtain (stop at the lens)

$$\vec{k}_{222} = \frac{y^2\phi}{2\mathcal{H}}\vec{c}\sigma_{II} \tag{6.22}$$

$$\vec{\ell}^2_{222} = \frac{y^4\phi^2}{4\mathcal{H}^2}\vec{c}^2(\sigma_{II}^2 - 2\sigma_I) \tag{6.23}$$

In Eqs. 6.18, 6.22, and 6.23, only the structural aberration coefficients depend on the lens shape factor. This dependence is illustrated in Fig. 6.3 where magnification factor Y was chosen to be zero for simplicity.

From this figure we can see that if X = 0, the coma node is at infinity, i.e., coma is constant. Astigmatism is binodal with the nodes located symmetrically with respect to the center of the image field.

Also it can be seen from Fig. 6.3 that if $X = \pm n^2$ (intersection points for the line and two branches of the hyperbola), then $\sigma_I = \sigma_{II}^2$. In this case $\vec{k}_{131} = \vec{k}_{222}$ and $|\vec{\ell}_{222}| = |\vec{k}_{222}|$, i.e., the node for coma lies at the center of symmetry of binodal astigmatism as shown in Fig. 6.4. Since the magnitude of the vector $\vec{\ell}^2_{222}$ is negative, the nodes of binodal astigmatism lie on the line orthogonal to the pupil displacement vector $\vec{c}$.

We know that the structural aberration coefficients for coma and astigmatism of a thin lens depend on the longitudinal stop shift (that is, a shift along the reference axis), we can move the stop to the location at which coma for the thin lens with pupil centered on the lens

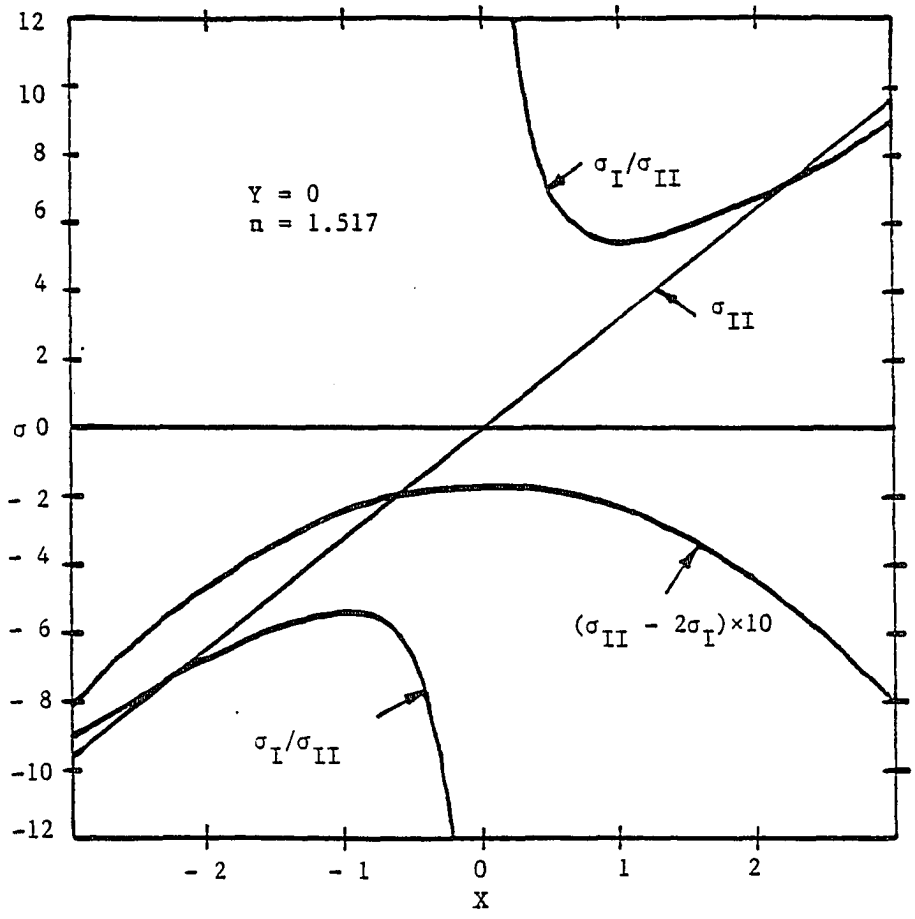

Fig. 6.3. Dependence of perturbation vectors for coma and astigmatism on the lens shape factor (stop at the lens).

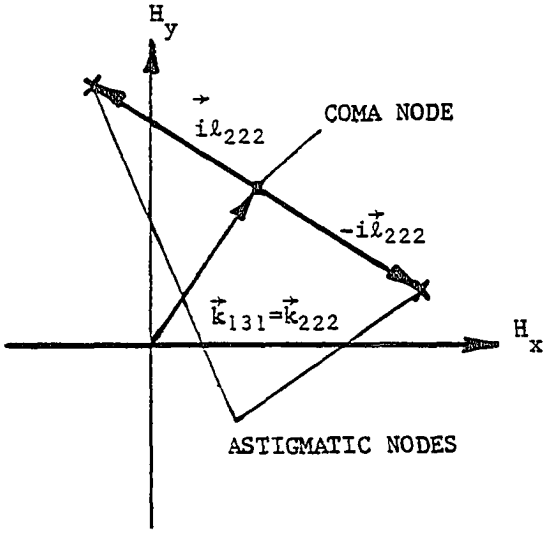

Fig. 6.4. The nodes for coma and astigmatism of a thin lens with shape factor $X = \pm n^2$ (stop at the lens).

axis will be zero and examine a few special cases.

Case I. For a thin lens with a centered pupil, coma is corrected. From Eq. 6.5, we can find the location of the stop for zero coma. It is given by

$$S = - \frac{\sigma_{II}}{\sigma_I} \tag{6.24}$$

and

$$\phi s = - \frac{2\sigma_{II}}{\sigma_{II} - \sigma_I} , \tag{6.25}$$

where s is the distance of the entrance pupil from the front principle plane.

Then the structural aberration coefficients (after the stop shift) become

$$\sigma_I' = \sigma_I$$

$$\sigma_{II}' = 0$$

$$\sigma_{III}' = 1 - \frac{\sigma_{II}^2}{\sigma_I} . \tag{6.26}$$

Coma is constant across the field and can be obtained using Eq. A.4 as

$$W = (-\vec{K}_{131} \cdot \vec{\rho})(\vec{\rho} \cdot \vec{\rho}) , \tag{6.27}$$

where

$$\vec{K}_{131} = 4W_{040}\vec{c} = \frac{1}{8}y'\phi^3\vec{\sigma}_I . \tag{6.28}$$

Astigmatism is binodal and given by (A.13)

$$W = \frac{1}{2}W_{222}(\vec{H}^2 - \vec{t}_{222}^2) \cdot \vec{\rho}^2 \tag{6.29}$$

where $\vec{k}_{222} = 0$ and

$$\vec{\ell}^2_{222} = -\frac{8W_{040}\vec{c}^2}{W_{222}} = -\frac{y'\phi^2}{2n'}\vec{c}^2\frac{\sigma_I'}{\sigma_{III}'} \tag{6.30}$$

Figure 6.5 illustrates the dependence of astigmatism, the stop shift parameter, and the perturbation vectors of a thin lens on its shape factor. As can be seen from this figure $\sigma'_{III} = 0$ at two points, when $X = \pm n^2$, and the nodes of binodal astigmatism will move to infinity, resulting in constant astigmatism.

Case II. For a thin lens with the centered pupil coma and astigmatism are corrected (as above).

In this case $\sigma'_{II} = \sigma'_{III} = 0$ when $X = \pm n^2$. Coma is constant as before and given by Eq. 6.27. Astigmatism also becomes constant and can be obtained using Eq. A.13 as

$$W = \vec{L}^2_{222} \cdot \vec{\rho}^2 , \tag{6.31}$$

where

$$\vec{L}^2_{222} = 4W_{040}\vec{c}^2 = \frac{1}{8}y'\phi^3\vec{c}^2\sigma_I \tag{6.32}$$

As we can see from Eqs. 6.28 and 6.32, the magnitude of constant coma and astigmatism depend on the magnitude of spherical aberration. In this case,

$$\sigma_I = \frac{n^2(n+1)^2}{(n-1)^2} \tag{6.33}$$

and

$$\phi s = -\frac{2(n^2-1)}{(n^2-1) \mp (n+1)^2 n} . \tag{6.34}$$

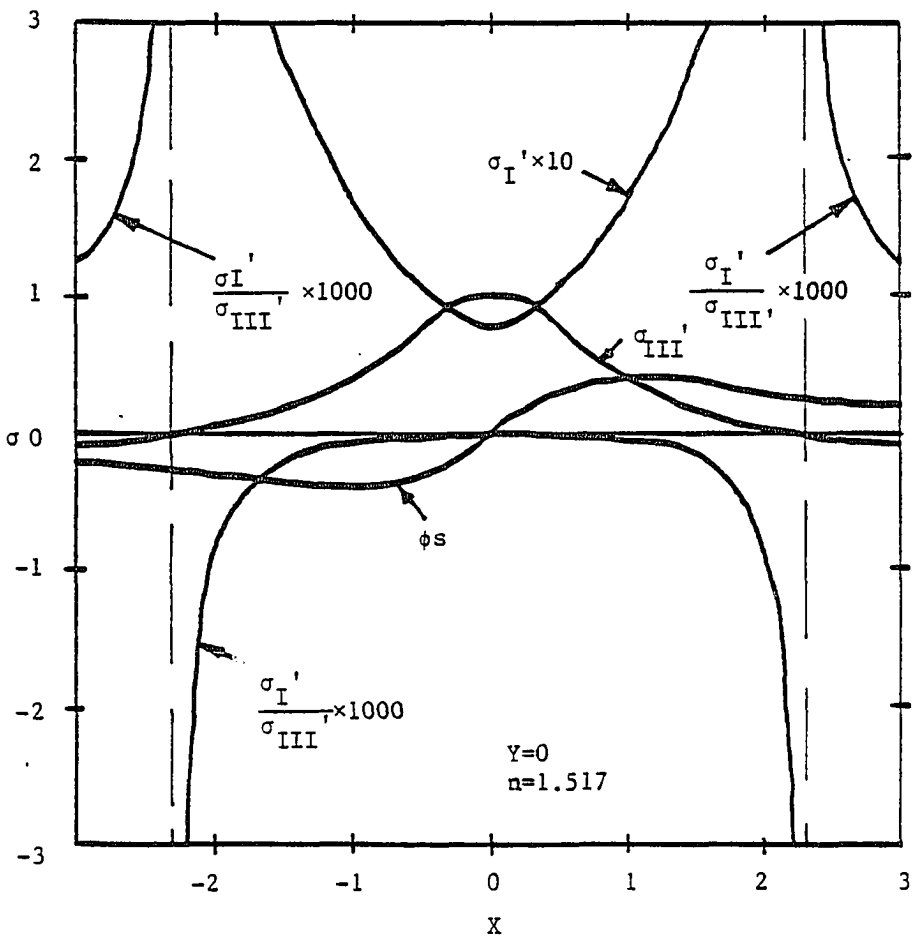

Fig. 6.5. Special case. Stop is shifted to correct coma.

CHAPTER 7

COMPARISON OF EXAMPLES WITH REAL RAY TRACES

In this chapter, we present several examples showing the use of the theory developed above. A few special cases from the previous chapters were taken, the systems were designed, and then checked with a real ray trace program.

The program used for these examples was Super-Oslo, run on an HP9816 computer. An unusual representation of a vector was chosen for these examples. As in most design programs, an absolute coordinate system with its y-axis (vertical) in the meridianal plane of the aligned system was chosen. In this coordinate system a vector was represented as $\vec{a} = ae^{i\theta}$. This is illustrated in Fig. 7.1.

Example I. The system chosen as a first example consisted of two plane-parallel plates placed in a system that had the following specifications: $u = -0.125$, $\bar{u} = 0.1$, and f-number = F/4. The thickness of the plates was 20 mm and their glass BK7. The plates were tilted in the same plane in opposite directions by an angle of 10°. Also, the aberrations of the system and the plates were balanced before the plates were tilted.

From Chapter 3 we know that spherical aberration is not affected by tilt. Coma should be zero across the entire field and astigmatism should be constant.

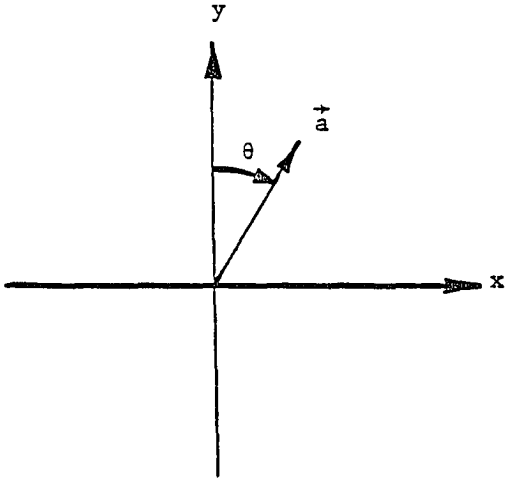

Fig. 7.1. Vector representation in the examples.

We calculated the aberration center displacement vector for each plate: $\vec{a}_1 = (\vec{\beta}_1)/\bar{u} = 1.7633e^{i0°}$ and $\vec{a}_2 = (\vec{\beta}_2)/\bar{u} = 1.763e^{i180°}$. Astigmatism with respect to the medial surface is given by (see Eq. 2.34)

$$W = \frac{1}{2}\vec{B}^2_{222}\cdot\vec{\rho}^2 , \tag{7.1}$$

where

$$\vec{B}^2_{222} = (W_{222,1} + W_{222,2})\vec{a}^2 \tag{7.2}$$

and $\vec{a}_1^2 = \vec{a}_2^2 = \vec{a}^2$.

The wave aberration coefficient for each plane-parallel plate is given by

$$W_{222} = -\frac{1}{2}\bar{u}^2 u^2 \frac{n^2 - 1}{n^3}t . \tag{7.3}$$

We calculated the magnitude of astigmatism with respect to the medial surface using Eqs. 7.1, 7.2, and 7.3. We found it to be 1.81 μm ($\rho = 1$). Then the transverse ray aberration at the Gaussian image plane (where $\rho = 1$) should be 58 μm.

To check the theory, we set the system up in the computer. The system is shown in Fig. 7.2 and the specifications of this system are given in Table 7.1. As can be seen from Fig. 7.2, when plates are not tilted, we have a perfect image.

Fig. 7.3 shows the ray fans and spot diagrams of the system with two tilted plane-parallel plates. As can be seen from this figure, astigmatism is constant with the magnitude about 60 μm. There is no coma.

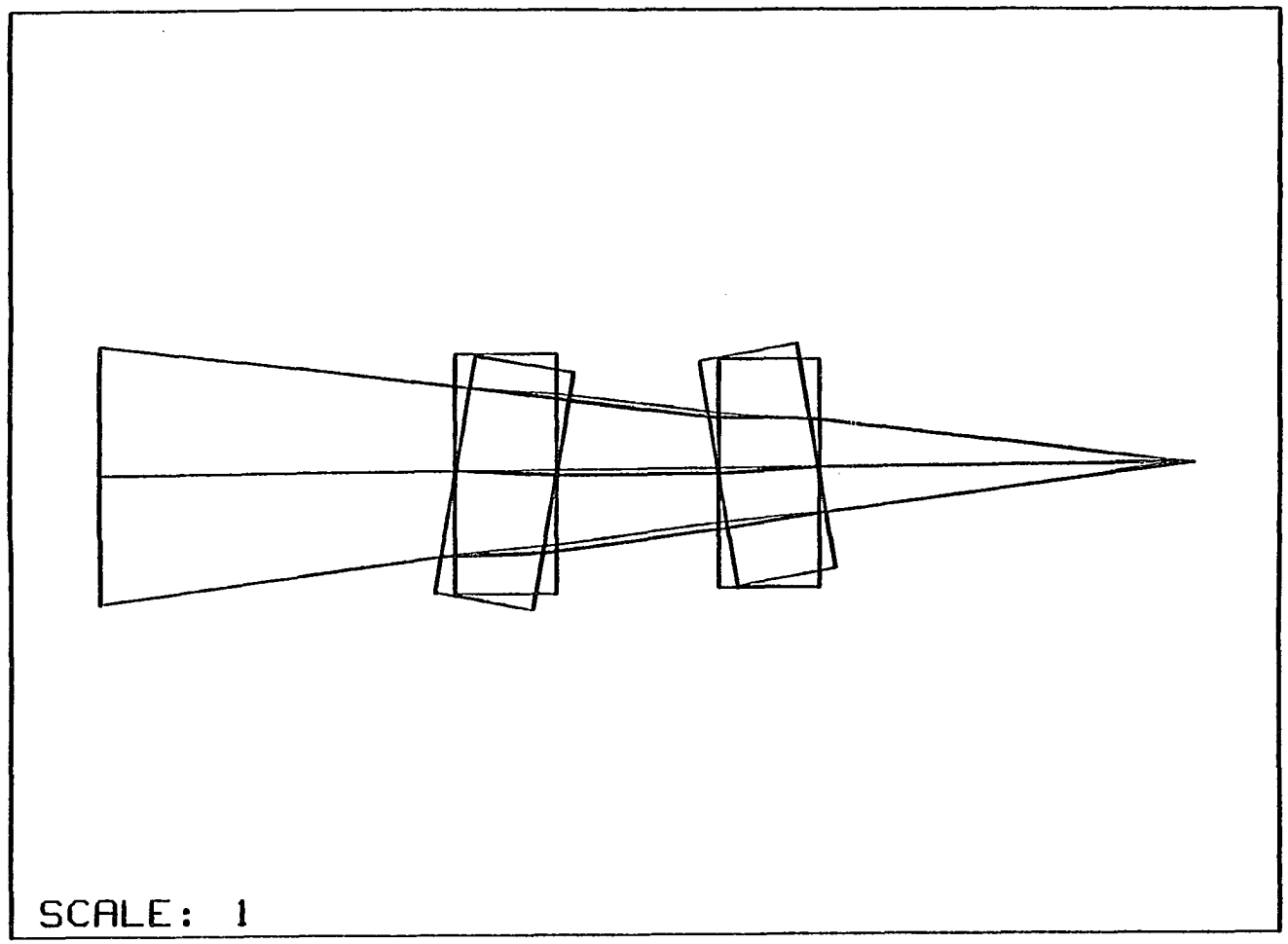

Fig. 7.2. Example I. Two plates are tilted in the same plane.

Table 7.1. Specifications of the system used in Example I.

*RTG
PLATES_EXAMPLE

SRF	RADIUS	THICKNESS	GLASS	NOTE
1	--	128.185658	AIR	
2	--	-20.000000	BK7	
3	--	-31.814346	AIR	
4	--	-20.000000	BK7	
5	--	-70.000000	AIR	
6	--	1.00000E-07	BK7	
7	--	70.000000	AIR	
8	--	20.000000	BK7	SPECIAL
9	--	31.814346	AIR	SPECIAL
10	--	20.000000	BK7	SPECIAL
11	--	71.814346	AIR	SPECIAL
12	--	--	AIR	SPECIAL

*SPECIAL DATA

SRF	TYPE	VALUE
8	DT	1.000000
8	TLA	-10.000000
9	DT	1.000000
9	DCY	3.526540
10	DT	1.000000
10	DCY	5.609728
10	TLA	20.000000
11	DT	1.000000
11	DCY	-3.526540
12	DT	1.000000
12	TLA	-10.000000

*GENERAL DATA

EPR	OBY	THO	FMODE	IMAGE	DESIGNER
25.000001	20.000000	-200.000008	FOC	12	TD
UNITS	OBX	CVO	AMODE	ASTOP	REVCODE
1.000000	--	--	UNC	6	HP16BUAZ1

*PARAXIAL CONSTANTS

EFL	FNB	GIH	PIV	PTZRAD	TMAG
-1.12590E+18	4.000000	20.000000	-2.500000	--	1.000000

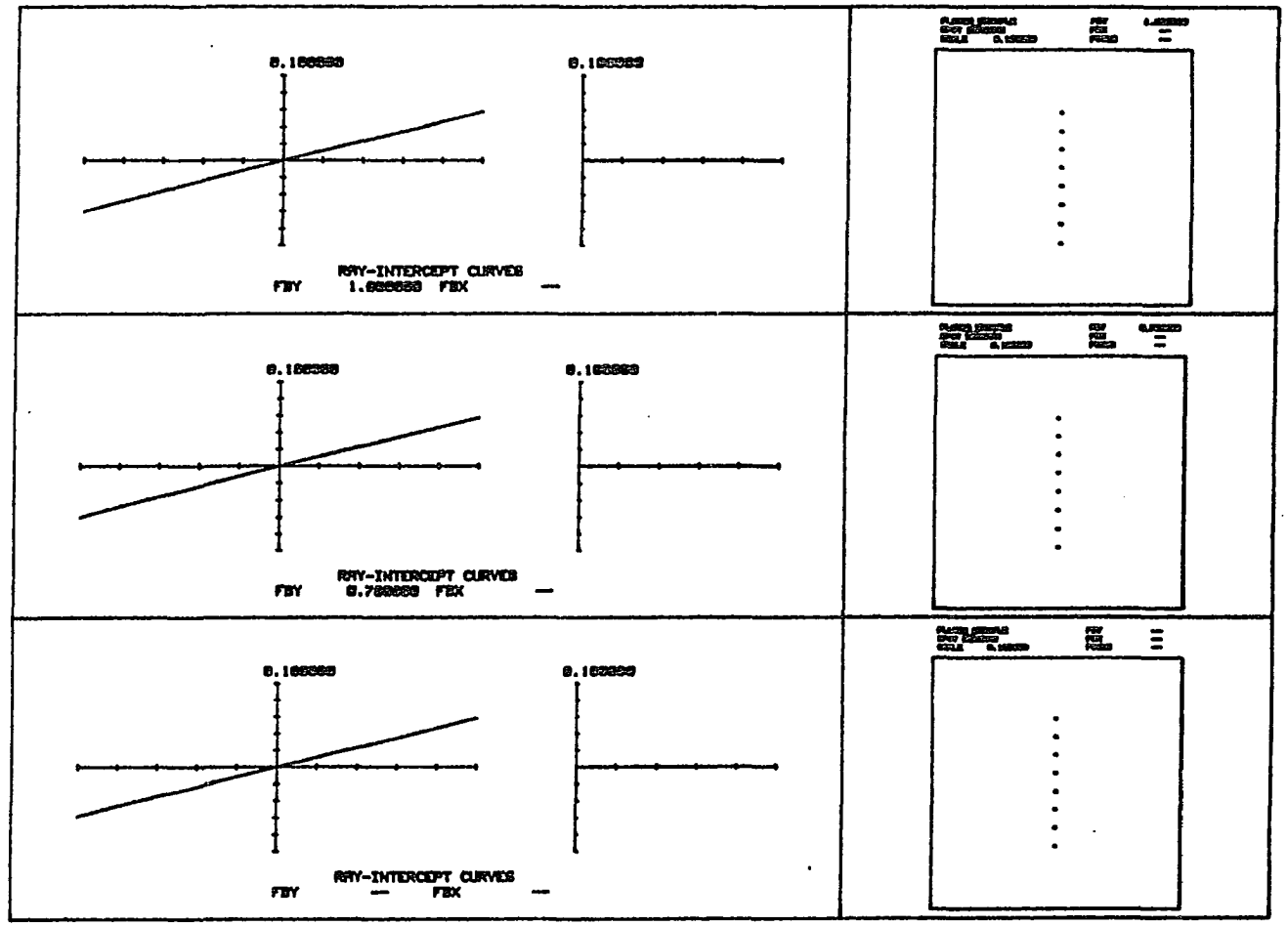

Fig. 7.3. Ray fans and spot diagrams for the system of Example I.

Example II. In the second example, the same system was used, but the plates were cross-tilted with tilt angles of 10°. The aberration center displacement vectors in this case were $\vec{a}_1 = 1.7633e^{i180°}$ and $\vec{a}_2 = 1.7633e^{-i90°}$. Again, spherical aberration is not affected. Coma should be constant and astigmatism should be linear with the node at the center of the field. Coma is given by (see Eq. 2.18)

$$W = \left[-\vec{A}_{131}\cdot\vec{\rho}\right](\vec{\rho}\cdot\vec{\rho}) \ , \tag{7.4}$$

where

$$\vec{A}_{131} = W_{131,1}\vec{a}_1 + W_{131,2}\vec{a}_2$$
$$= 1.405e^{-i135°} \ \mu m. \tag{7.5}$$

The wave aberration coefficient for each plate is given by

$$W = -\frac{1}{2}\,\bar{u}u^2\left(\frac{n^2-1}{n^3}\right)t \ . \tag{7.6}$$

Using Eqs. 7.4, 7.5, and 7.6, we calculated the magnitude and direction of coma. With $\rho = 1$, the magnitude of coma was 1.405 μm, and its direction was −135°. The transverse ray aberration for coma at $\rho = 1$ should be 33.72 μm. The linear astigmatism with respect to the medial focal surface is given by (see 2.33)

$$W = \frac{1}{2}\left[-2\vec{H}\vec{A}_{222}\right]\cdot\vec{\rho}^2 \ , \tag{7.7}$$

where

$$\vec{A}_{222} = W_{222}(\vec{a}_1 + \vec{a}_2) \ . \tag{7.8}$$

Using Eqs. 7.8, 7.7, and 7.3, we calculated the magnitude of astigmatism with respect to the medial focal surface at $H = 1$ and $\rho = 1$. It was

1.45 μm. Then the transverse ray aberration in the Gaussian image plane should be 23.24 μm. Table 7.2 shows the specification of the system with two cross-tilted plates. The ray fans and spot diagrams for the system with two cross-tilted plates are shown in Fig. 7.4.

As we can see from this figure, on axis we have pure coma oriented −135° from the y-axis. For points off-axis, the magnitude and orientation of coma is the same but the amount of astigmatism increases as we move farther from the center of the field. The effect of linear astigmatism added to coma can be well seen in the spot diagrams.

The magnitude of coma as it is taken from the ray fans is about 32 μm and astigmatism at full field is about 20 μm (after defocus has been subtracted).

Figure 7.5 shows the field curves of the linear astigmatism. We can see that indeed the node is located at the center of the field.

Example III. In this example, we examined Case IV of Chapter 4, which is the case of the system with two wedges. Here we used the system of the first two examples. The wedges had the same vertex angle which was 2° and they were tilted in the same plane in opposite directions.

We chose the distance from the object point to the plane bisecting the first wedge to be $\ell_1 = 120$ mm and thickness of the first wedge along the OAR $t_1 = 20$ mm. We set $\ell_2 = 75$ mm. Then to have the ratio t/ℓ for the second wedge equal to that of the first one, we calculated the thickness of the second wedge along the OAR $t_2 = 12.5$ mm.

Table 7.2. Specifications of the system used in Example II.

*CTG
PLATES_EXAMPLE

SRF	CURVATURE	THICKNESS	GLASS	NOTE
1	—	128.185658	AIR	
2	—	-20.000000	BK7	
3	—	-31.814346	AIR	
4	—	-20.000000	BK7	
5	—	-70.000000	AIR	
6	—	1.00000E-07	BK7	
7	—	70.000000	AIR	
8	—	—	BK7	SPECIAL
9	—	20.132366	BK7	SPECIAL
10	—	—	AIR	SPECIAL
11	—	31.814346	AIR	SPECIAL
12	—	—	BK7	SPECIAL
13	—	20.132366	BK7	SPECIAL
14	—	—	AIR	SPECIAL
15	—	71.880000	AIR	SPECIAL
16	—	—	AIR	

*SPECIAL DATA

SRF	TYPE	VALUE
8	DT	1.000000
8	TLA	-10.000000
9	DT	1.000000
9	TLA	6.573820
10	DT	1.000000
10	TLA	-6.573820
11	DT	1.000000
11	TLA	10.000000
12	DT	1.000000
12	TLB	10.000000
13	DT	1.000000
13	TLB	-6.573820
14	DT	1.000000
14	TLB	6.573820
15	DT	1.000000
15	TLB	-10.000000

*GENERAL DATA

EPR	OBY	THO	FMODE	IMAGE	DESIGNER
25.000001	20.000000	-200.000008	FOC	16	TED
UNITS	OBX	CVO	AMODE	ASTOP	REVCODE
1.000000	—	—	UNC	6	HP16BUAZ1

*PARAXIAL CONSTANTS

EFL	FNB	GIH	PIV	PTZRAD	TMAG
-1.12590E+18	4.000000	20.000000	-2.500000	—	1.000000

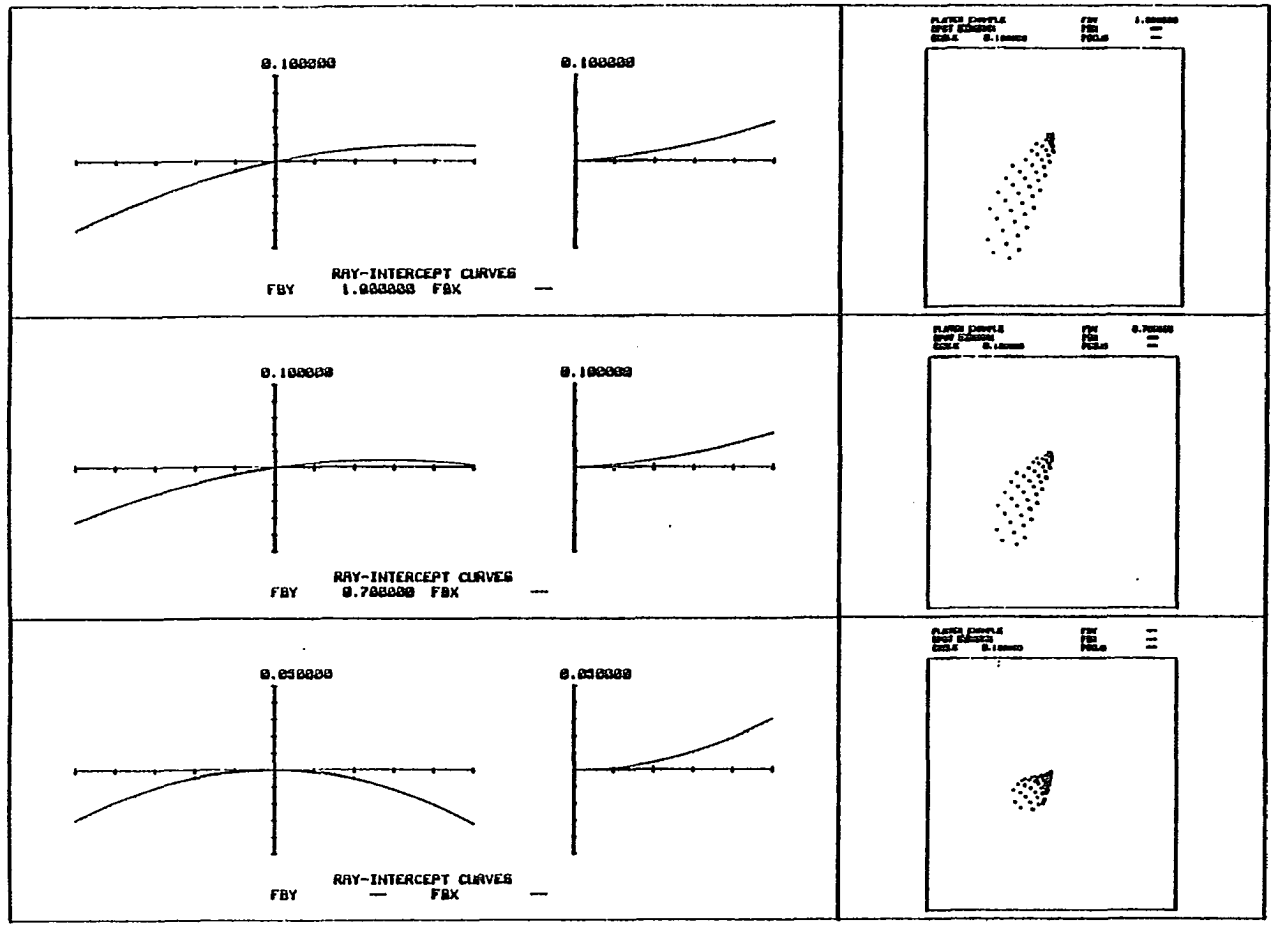

Fig. 7.4. Ray fans and spot diagrams for the system of Example II.

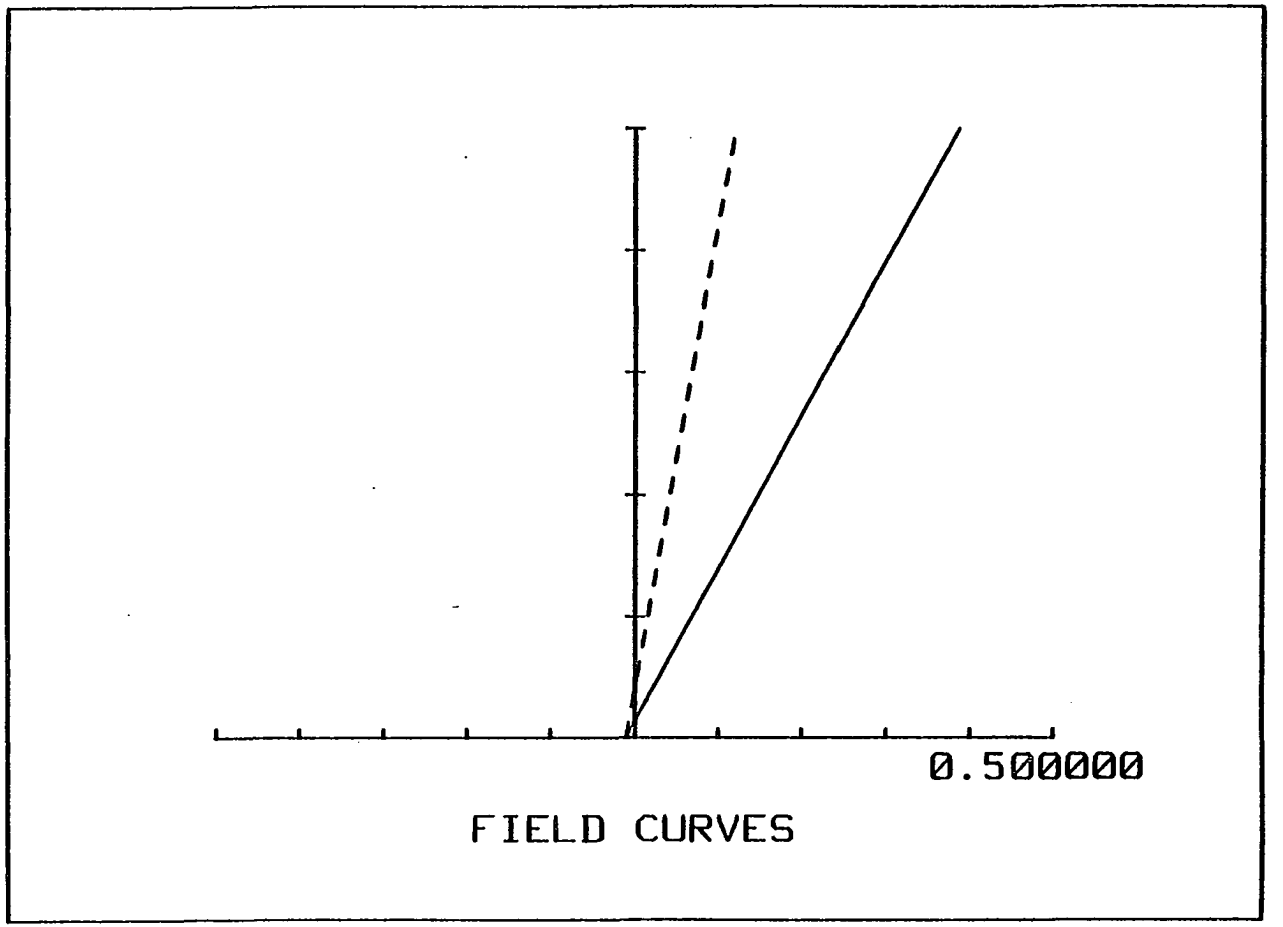

Fig. 7.5. Field curves of the system with two cross-tilted plates.

Using Eq. 4.9, with $\vec{\bar{u}}_1 = 0$, we calculated $\vec{\beta}_1 = 0.487e^{i0°}$. For the second wedge $\vec{\bar{u}}_2 = 0.01805e^{i180°}$, therefore $\vec{\beta}_2 = 0.505e^{i180}$°. If we tilt the wedges by these angles coma should be zero across the entire field.

Astigmatism with respect to the medial surface is given by Eq. 4.20. The aberration center displacement vectors $\vec{a}_1$ and $\vec{a}_2$ for each wedge surface are equal in magnitude and opposite in sign. Squared vectors $\vec{a}_1^2$ and $\vec{a}_2^2$ are equal.

Using Eq. 2.11 and Eq. 4.4, we calculated $\vec{a}_1^2 = 22.02e^{i0°}$ and $\vec{a}_2^2 = 27.27e^{i0°}$. Then, using Eq. 4.15 we calculated $\vec{b}_{222}^2 = -24.505e^{i0°}$ and the magnitude of astigmatism with respect to the medial focal surface should be 13 μm at $\rho = 1$. The transverse ray aberration in the Gaussian image plane should be 420 μm.

Figures 7.6, Table 7.3, and Fig. 7.7 show the system, the system specifications, and the ray fans with corresponding spot diagrams for the system having two tilted wedges. As can be seen from the ray fans, the astigmatism is nearly constant across the field. Small linear astigmatism is present due to the error arising from the fact that the wedges were tilted by large angles (about 26°) to correct the system for coma. Coma is practically zero.

Example IV. As the last example, we examined the case of a misaligned Ritchey-Chretien telescope as described in Chapter 5. The telescope was 2-m aperture and 0.64° full field of view. The f-number of the system was F/9.

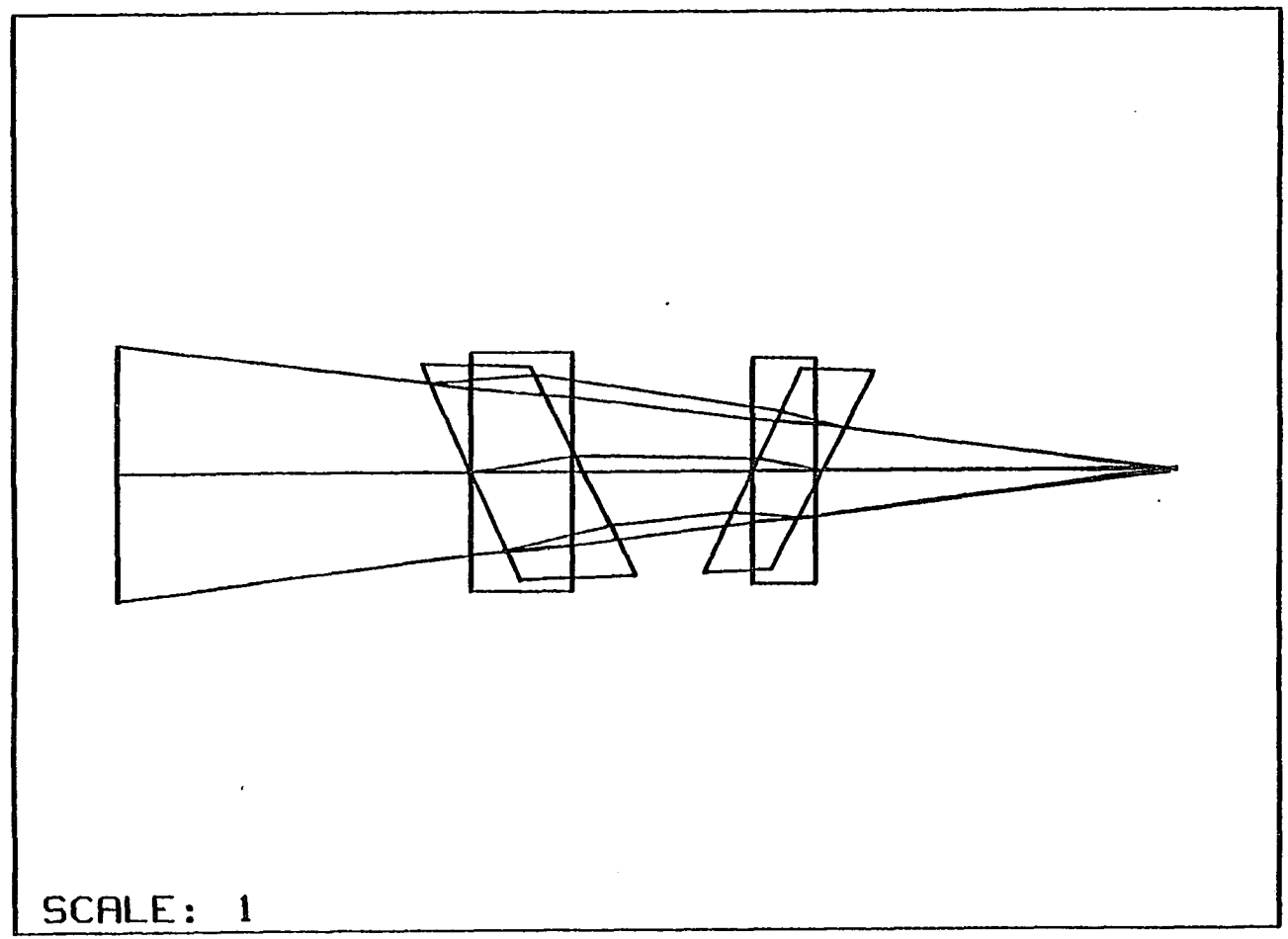

Fig. 7.6. Example III. Two wedges are tilted in the same plane.

Table 7.3. Specifications of the system used in Example III.

```
*RTG
WEDGES_EXAMPLE
SRF        RADIUS      THICKNESS   GLASS     NOTE
1            --       126.991035   AIR
2            --       -12.500000   BK7
3            --       -35.564344   AIR
4            --       -20.000000   BK7
5            --       -70.000000   AIR
6            --      1.00000E-07   BK7
7            --        70.000000   AIR
8            --              --    BK7       SPECIAL
9            --        22.243106   BK7       SPECIAL
10           --              --    AIR       SPECIAL
11           --        33.321238   AIR       SPECIAL
12           --              --    BK7       SPECIAL
13           --        14.027419   BK7       SPECIAL
14           --              --    AIR       SPECIAL
15           --        71.566229   AIR       SPECIAL
16           --              --    AIR

*SPECIAL DATA
SRF  TYPE      VALUE
8    DT         1.000000
8    TLA       24.952790
9    DT         1.000000
9    TLA      -24.952790
10   DT         1.000000
10   TLA       26.952790
11   DT         1.000000
11   TLA      -26.952790
12   DT         1.000000
12   TLA      -25.986698
13   DT         1.000000
13   TLA       25.986698
14   DT         1.000000
14   TLA      -27.986698
15   DT         1.000000
15   TLA       27.983049

*GENERAL DATA
       EPR          OBY          THO        FMODE   IMAGE   DESIGNER
    25.000000    20.000000   -200.000000     FOC      16       TED
      UNITS          OBX          CVO       AMODE   ASTOP   REVCODE
   1.000000           --           --         UNC       6   HP16BUAZ1

*PARAXIAL CONSTANTS
AFOCAL SYSTEM
```

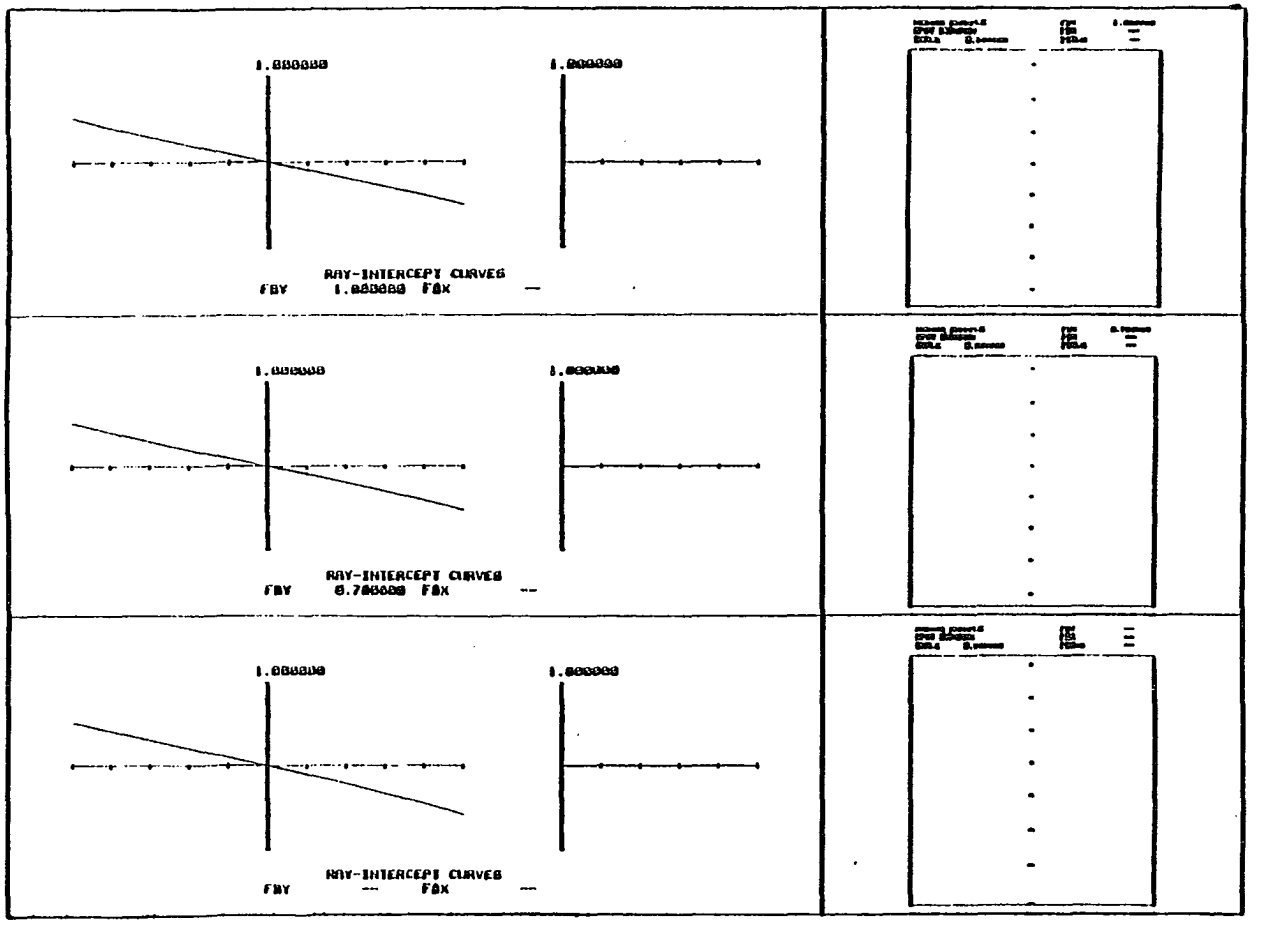

Fig. 7.7. Ray fans and spot diagrams for the system with two wedges.

Figure 7.8, Table 7.4, and Fig. 7.9 show the system configuration, specifications, and the ray fans with corresponding spot diagrams of the system before misalignment.

We found a pivot point for the secondary mirror such that upon rotating the mirror about this point, coma should stay zero across the field.

Using Eq. 5.11 we found that $\vec{\delta}c/\vec{\delta}VA = -2.5139$. In Fig. 7.10 this point corresponds to point P. The distance from the secondary mirror to the pivot point was 1384.454 mm.

With the secondary mirror tilted about point P by an angle of 10 arc min ($\vec{\alpha} = 0.16667e^{i0^\circ}$), we calculated $\vec{\delta}c = -10.1241e^{i0^\circ}$ mm and $\vec{\delta}V_A = 4.0272e^{i0^\circ}$ mm. Knowing the location of the image formed by the primary mirror and the displacement of the center of curvature for the secondary mirror, we obtained $\vec{\beta} = 3.122\times10^{-3}e^{i0^\circ}$.

Using Eq. 2.7 we calculated the tilt of the Gaussian image plane with respect to the reference axis $\vec{\theta}' = 1.249\times10^{-2}e^{i0^\circ}$, then $\theta_0' = \vec{\theta} - \vec{\beta} = 9.365\times10^{-3}e^{i0^\circ}$ and $\vec{\delta}V = 5.062e^{i0}$ mm. Using Eqs. 2.8 and 2.12 we calculated $\vec{a} = 0.19715e^{i180^\circ}$ and $\vec{a}_A = 0.16556e^{i0^\circ}$. After that we calculated the perturbation vectors $\vec{a}^2_{222} = 0.23052e^{i0^\circ}$ and $\vec{b}^2_{222} = -5.7908\times10^{-2}e^{i0^\circ}$. The location of the astigmatic nodes should be at $\vec{H} = \vec{a}_{222} \pm \vec{b}_{222}$. As we calculated, one of the nodes is at $\vec{H}_1 = 0.47116e^{i0^\circ}$ and the other is at $\vec{H}_2 = -0.010123e^{i0^\circ}$.

Table 7.5 shows the specifications of the Ritchey-Chretien telescope with the secondary mirror tilted by an angle of 10 arc min

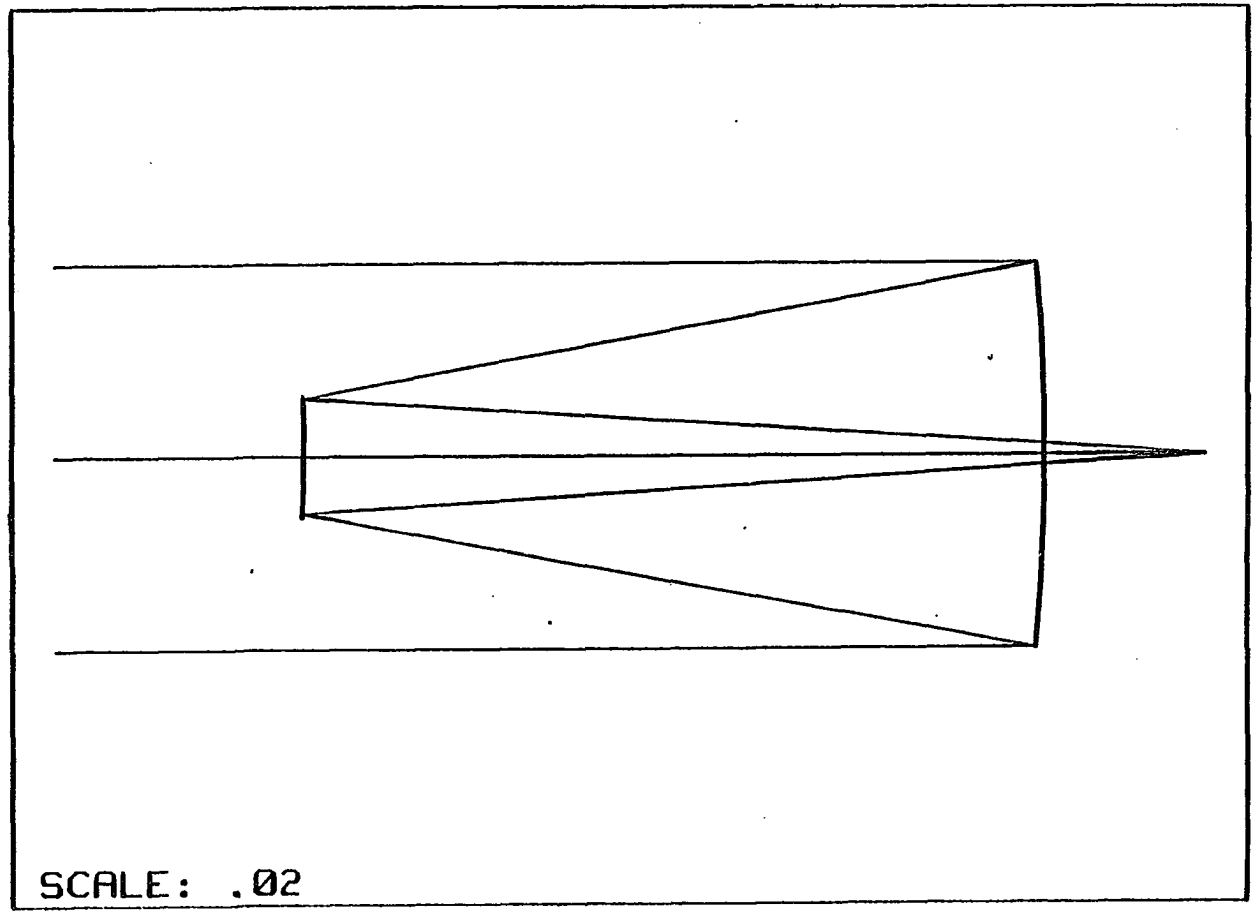

Fig. 7.8. Example IV. Ritchey-Chretien telescope.

Table 7.4. Ritchey-Chretien telescope specifications.

*RTG
RTCH_CHRETIEN

SRF	RADIUS	THICKNESS	GLASS	NOTE
1	--	--	AIR	
2	-1.20000E+04	-4378.378300	REFLECT	ASPHERIC
3	-4864.864800	4864.865700	REFLECT	ASPHERIC
4	--	--	AIR	

*ASPHERIC DATA

SRF	TYPE	VALUE
2	CC	-1.082305
3	CC	-5.027778

*GENERAL DATA

EPR	OBY	THO	FMODE	IMAGE	DESIGNER
1000.000000	-5.55555E+17	1.00000E+20	FOC	4	TED
UNITS	OBX	CVO	AMODE	ASTOP	REVCODE
1.000000	--	--	UNC	1	HP16BUAZ1

*PARAXIAL CONSTANTS

EFL	FNB	GIH	PIV	PTZRAD	TMAG
1.80000E+04	9.000001	100.000000	-5.555555	-4090.908999	-1.80000E-16

*PARAXIAL TRACE

SRF	PY	PU	PI	PYC	PUC	PIC
1	1000.000000	1.00000E-17	1.00000E-17	--	0.005556	0.005556
2	1000.000000	0.166667	-0.083333	--	-0.005556	0.005556
3	270.270283	-0.055556	0.111111	24.324321	0.015556	-0.010556
4	--	-0.055556	-0.055556	100.000000	0.015556	0.015556

*SEIDEL ABERRATIONS

SRF	SA3	CM3	AS3	PZ3	DS3	PA3
1	--	--	--	--	--	--
2	0.095260	0.077160	-0.005144	0.005144	--	--
3	-0.095260	-0.077160	-0.000429	-0.012689	0.000548	-3.47222E-06
SM	-9.18874E-08	-9.73875E-09	-0.005573	-0.007545	0.000548	-3.47222E-06

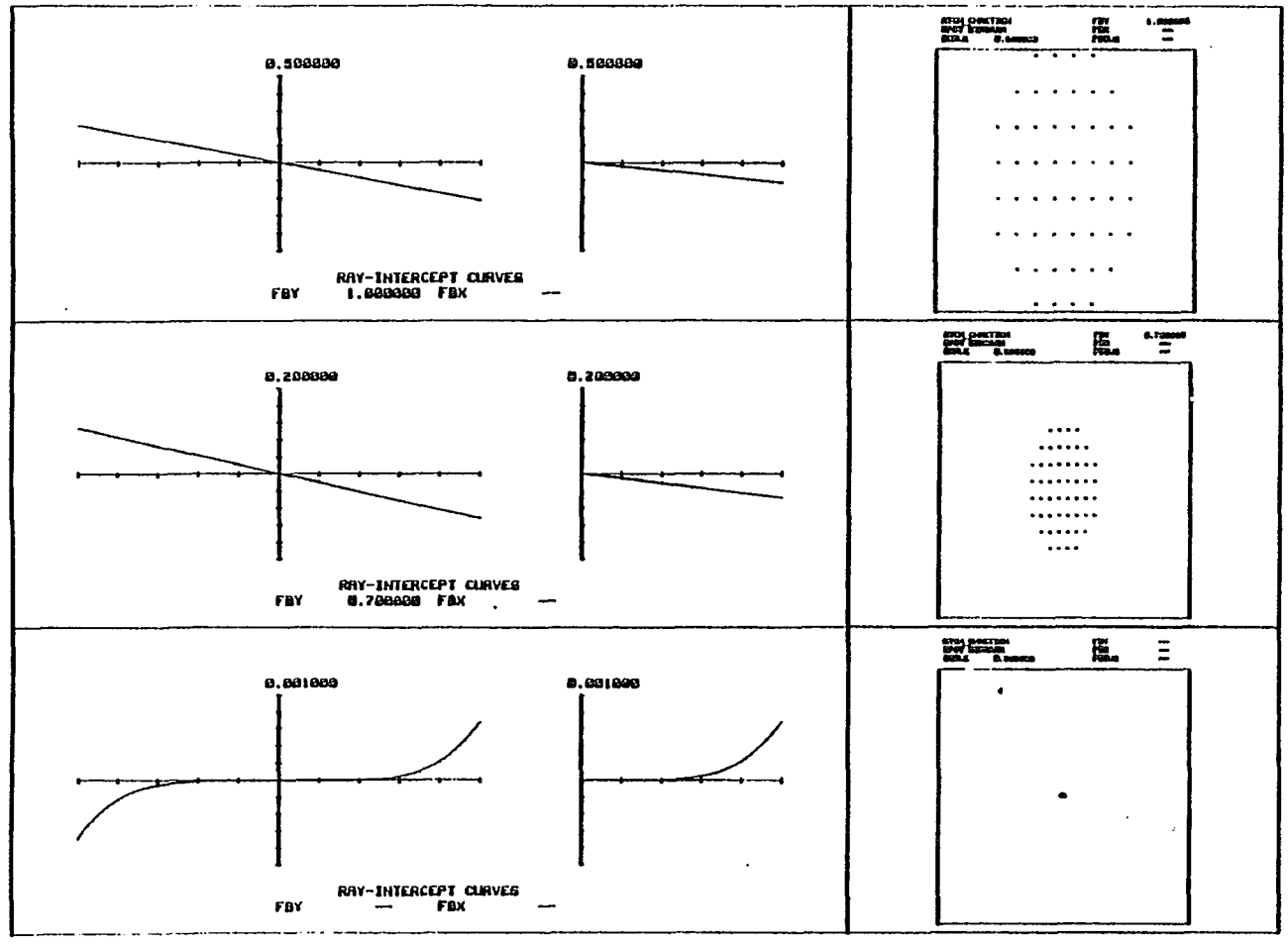

Fig. 7.9. Ray fans and spot diagrams of Ritchey-Chretien telescope before misalignment.

Table 7.5. System specifications of misaligned Ritchey-Chretien telescope.

*RTG
RTCH_CHRETIEN

SRF	RADIUS	THICKNESS	GLASS	NOTE
1	--	--	AIR	
2	-1.20000E+04	-4378.378300	REFLECT	ASPHERIC
3	-4864.864800	--	REFLECT	SPECIAL ASPHERIC
4	--	--	AIR	SPECIAL
5	--	4864.865700	AIR	SPECIAL
6	--	--	AIR	SPECIAL

*ASPHERIC DATA

SRF	TYPE	VALUE
2	CC	-1.082305
3	CC	-5.027778

*SPECIAL DATA

SRF	TYPE	VALUE
3	DT	1.000000
3	DCY	4.027225
3	TLA	0.166667
4	DT	1.000000
4	TLA	-0.166667
5	DT	1.000000
5	DCY	1.034842
5	TLA	0.178854
6	DT	1.000000
6	TLA	0.536546

*GENERAL DATA

EPR	OBY	THO	FMODE	IMAGE	DESIGNER
1000.000000	-5.55555E+17	1.00000E+20	FOC	6	TED
UNITS	OBX	CVO	AMODE	ASTOP	REVCODE
1.000000	--	--	UNC	1	HP16BUAZ1

*PARAXIAL CONSTANTS

EFL	FNB	GIH	PIV	PTZRAD	TMAG
1.80000E+04	9.000001	100.000000	-5.555555	-4090.908999	-1.80000E-16

*PARAXIAL TRACE

SRF	PY	PU	PI	PYC	PUC	PIC
1	1000.000000	1.00000E-17	1.00000E-17	--	0.005556	0.005556
2	1000.000000	0.166667	-0.083333	--	-0.005556	0.005556
3	270.270283	-0.055556	0.111111	24.324321	0.015556	-0.010556
4	270.270283	-0.055556	-0.055556	24.324321	0.015556	0.015556
5	270.270283	-0.055556	-0.055556	24.324321	0.015556	0.015556
6	--	-0.055556	-0.055556	100.000000	0.015556	0.015556

about point P (see Fig. 7.10). The ray fans and corresponding spot diagrams are shown in Fig. 7.11. Fig. 7.12 shows the upper part of the field curves of the misaligned system. The ray fans and spot diagrams were taken at the nodes and half way between them. As can be seen from Fig. 7.11 and 7.12, the nodes are indeed at the locations which were calculated using the theoretical approach. Also, one can clearly see that there is astigmatism half way between the nodes.

We should point out here again that in the case of binodal astigmatism the focal surfaces do not cross each other, they only touch at the node points. Therefore in Fig. 7.12, the solid line and the dashed line should be interchanged in the region between the nodes.

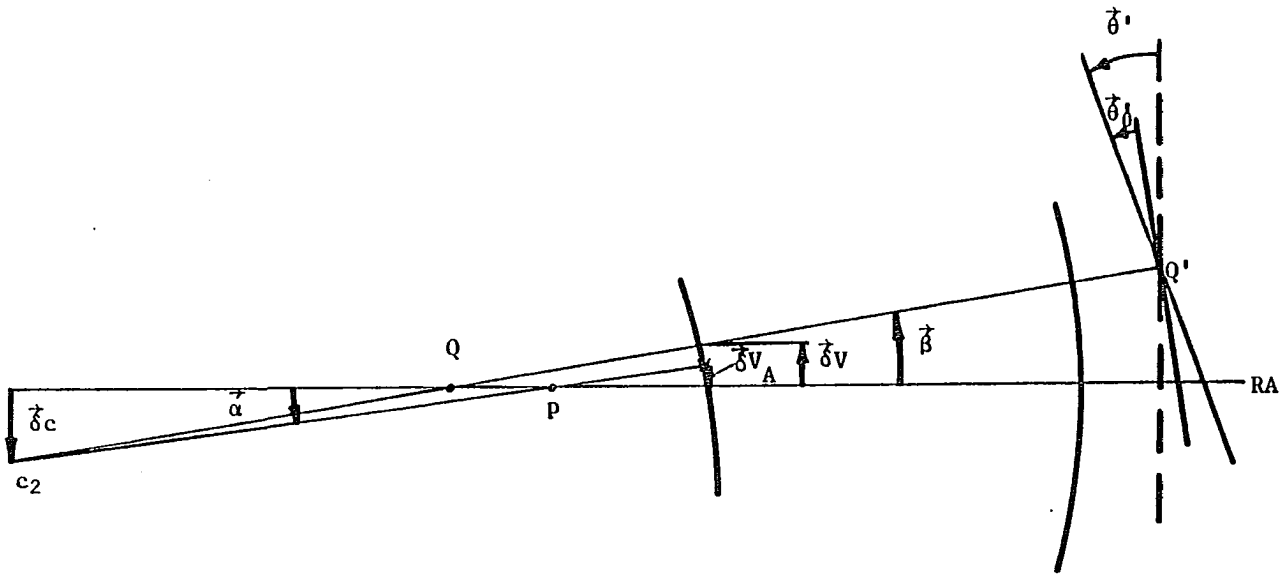

Fig. 7.10. **Misaligned Ritchey-Chretien telescope.**

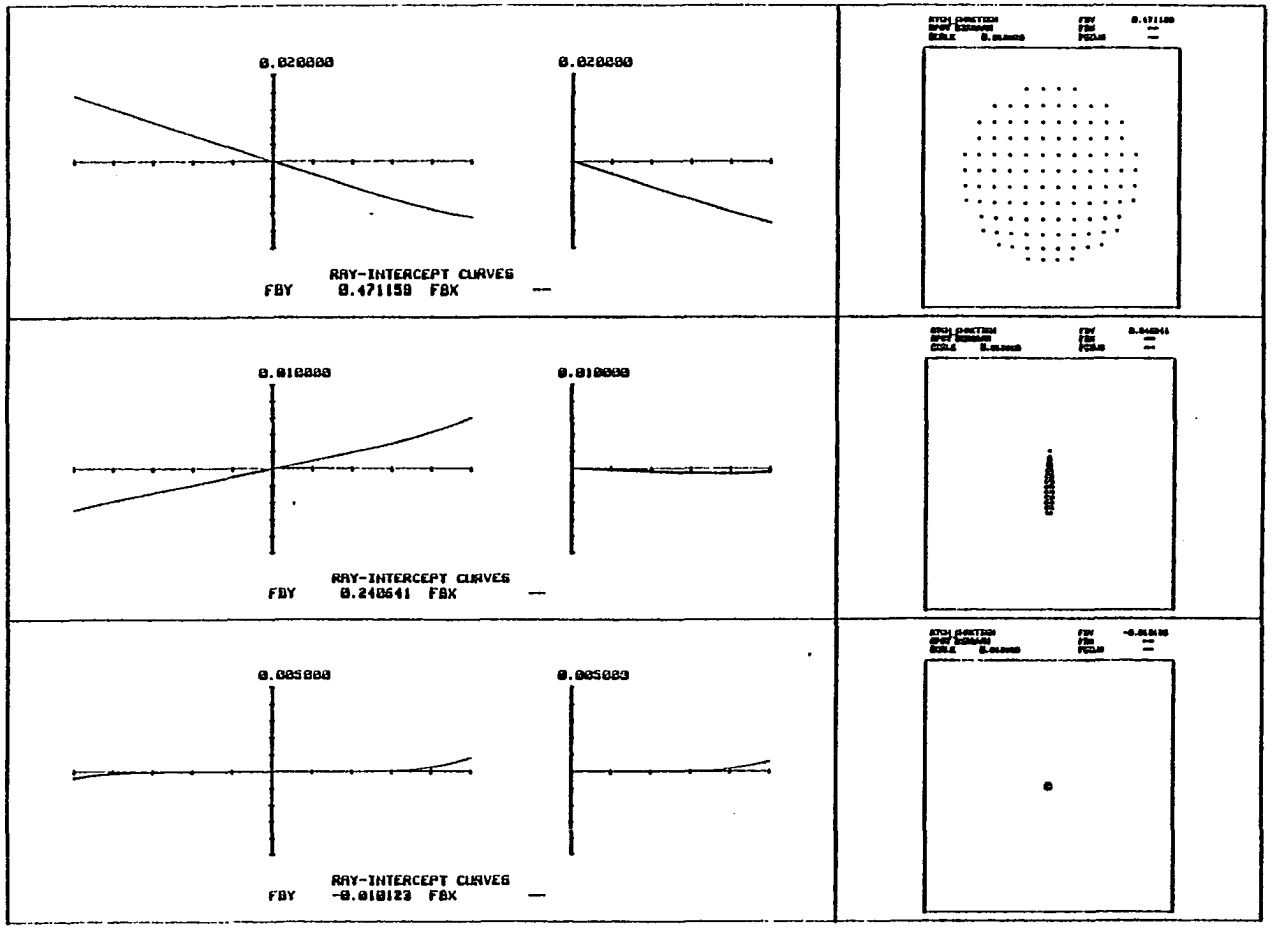

Fig. 7.11. Ray fans and spot diagrams of misaligned Ritchey-Chretien telescope.

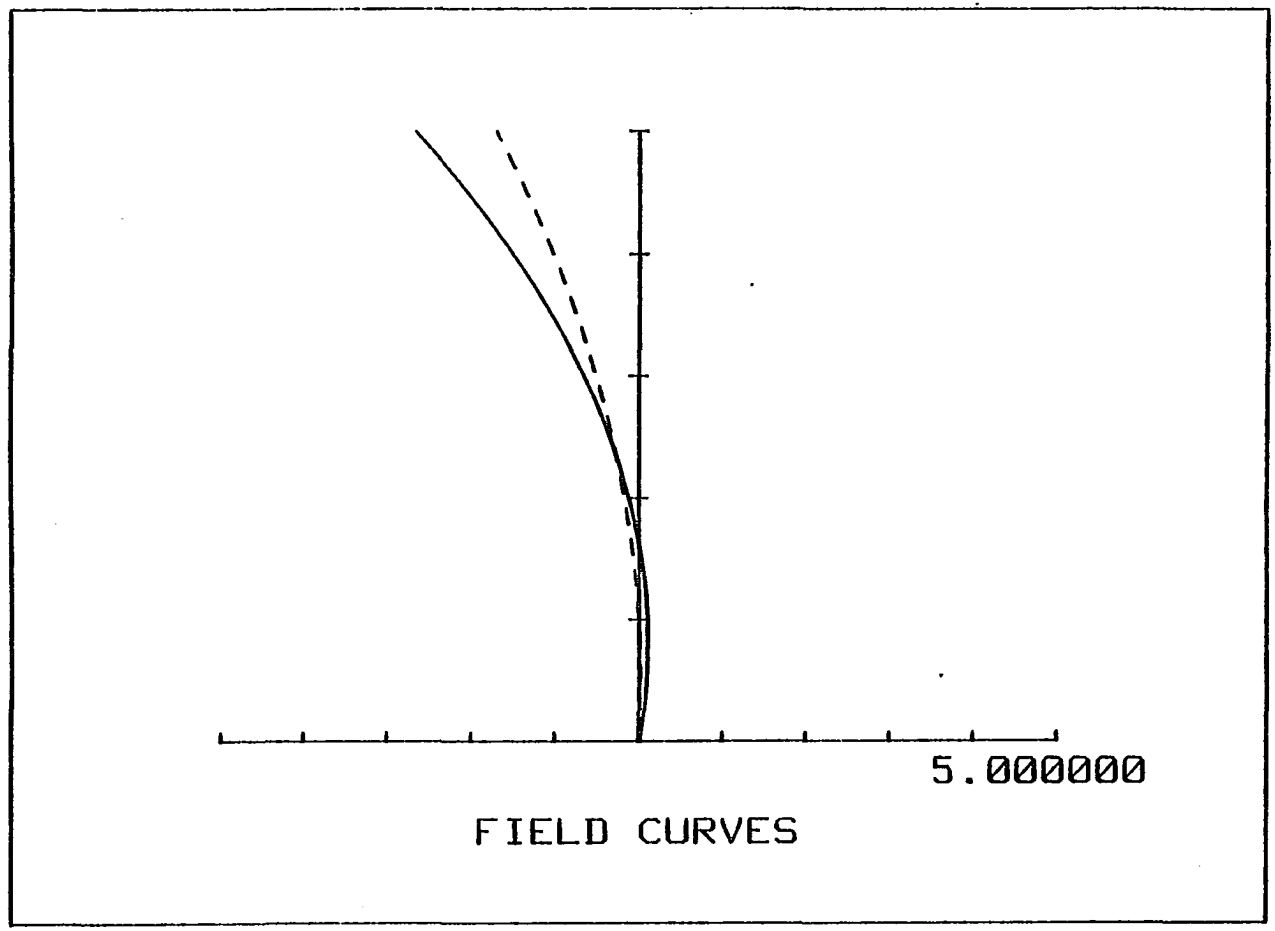

Fig. 7.12. Field curves for misaligned Ritchey-Chretien telescope.

CHAPTER 8

CONCLUSIONS

We have applied the theory of perturbed optical systems to each of the basic components of any optical system and established the relations between the aberrations of each component and its parameters. The emphasis has been on developing insights into the behavior of aberrations of a system having tilted and decentered components.

Insights on how to use plane-parallel plates in the system were developed. We established that with one or two tilted plane-parallel plates we cannot have both axial coma and astigmatism zero in the system (it will require a minimum of three plates).

We established that the aberrations of the wedge depend not only on the tilt and thickness of the wedge (along the reference axis), but also on the position of the wedge in the system, therefore with the wedge the designer has more parameters influencing the aberrations than with the plane-parallel plate.

We also showed that a combination of two wedges, properly tilted and placed in the system, practically does not change the system aberrations. Therefore we can say that by using wedged beamsplitters rather than plane-parallel plates, fewer elements are required to have the system aberrations unaltered.

We also discussed the problem of a misaligned telescope and showed that in order to align the system it is not enough just to eliminate axial coma and astigmatism, but it is necessary to examine either the astigmatic field or the image plane tilt.

In a system with tilted and decentered components, such as unobscured aperture telescopes, the designer should be able to predict systematically what the aberrations for a proposed system would be.

We showed that the components with an axis (a thin lens or a system of two spherical mirrors) when tilted and decentered, can be treated as centered systems with a decentered pupil. In the case of a thin lens, we found this approach to be simpler than a tilted and decentered system approach.

By comparing a few examples with corresponding real ray traces, we showed that the theory developed here is accurate enough to provide the designer with a system which can be used as a starting point in an optimization process.

One area which may be pursued further is the aberration fields in eccentric aperture systems from a design perspective. The system aberration dependence on the transverse stop shift of eccentric pupil systems may be investigated. The problem in this case is simpler because the behavior of the design is independent of the surface contributions and depends only on the aberration totals.

In this analysis, we considered only monochromatic aberrations; it can be extended to cover chromatic aberration as well.

APPENDIX

THIRD-ORDER ABERRATIONS OF A SYSTEM WITH DECENTERED PUPIL

Here we will examine the third-order aberration fields in eccentric aperture systems. In these systems, the pupil dependence in the wave aberration expansion is expanded rather than the field dependence.

The wave aberration expansion up to the third order for the rotationally symmetric system in vector form is given by

$$W = W_{040}(\vec{\rho} \cdot \vec{\rho})^2 + W_{131}(\vec{H} \cdot \vec{\rho})(\vec{\rho} \cdot \vec{\rho})$$

$$+ W_{222}(\vec{H} \cdot \vec{\rho})(\vec{H} \cdot \vec{\rho}) + W_{220}(\vec{H} \cdot \vec{H})(\vec{\rho} \cdot \vec{\rho})$$

$$+ W_{311}(\vec{H} \cdot \vec{H})(\vec{H} \cdot \vec{\rho}) \ , \qquad \text{(A.1)}$$

where $W_{K\ell m}$ are the wave aberration coefficients of the system. If the relative (normalized by the aperture radius) displacement of the system aperture stop from the axis is given by $\vec{c}$, then Eq. A.1 can be modified as follows

$$W = W_{040}[(\vec{\rho} - \vec{c}) \cdot (\vec{\rho} - \vec{c})]^2$$

$$+ W_{131}[\vec{H} \cdot (\vec{\rho} - \vec{c})][(\vec{\rho} - c) \cdot (\vec{\rho} - \vec{c})]$$

$$+ W_{222}[\vec{H} \cdot (\vec{\rho} - \vec{c})]\,[\vec{H} \cdot (\vec{\rho} - \vec{c})]$$

$$+ W_{220}(\vec{H} \cdot \vec{H})[(\vec{\rho} - \vec{c}) \cdot (\vec{\rho} - \vec{c})]$$

$$+ W_{311}(\vec{H} \cdot \vec{H})[\vec{H} \cdot (\vec{\rho} - \vec{c})] \,. \qquad \text{(A.2)}$$

All of the above terms will generate aberration terms with lower power field dependence than the generating aberrations.

After expanding each term above and collecting the terms with the same pupil dependence in each type, we will obtain

Spherical aberration:

$$W_{040}(\vec{\rho} \cdot \vec{\rho})(\vec{\rho} \cdot \vec{\rho})$$

Coma:

$$W_{131}(\vec{H} \cdot \vec{\rho})(\vec{\rho} \cdot \vec{\rho}) - 4W_{040}(\vec{c} \cdot \vec{\rho})(\vec{\rho} \cdot \vec{\rho})$$

Astigmatism:

$$W_{222}(\vec{H} \cdot \vec{\rho})^2 - 2W_{131}(\vec{c} \cdot \vec{\rho})\,(\vec{H} \cdot \vec{\rho}) + 4W_{040}(\vec{c} \cdot \vec{\rho})^2$$

Field Curvature:

$$W_{220}(\vec{H} \cdot \vec{H})(\vec{\rho} \cdot \vec{\rho}) - W_{131}(\vec{H} \cdot \vec{c})(\vec{\rho} \cdot \vec{\rho}) + 2W_{040}(\vec{c} \cdot \vec{c})(\vec{\rho} \cdot \vec{\rho})$$

Distortion:

$$W_{311}(\vec{H} \cdot \vec{H})\,(\vec{H} \cdot \vec{\rho}) - 2W_{220}(\vec{H} \cdot \vec{H})(\vec{c} \cdot \vec{\rho}) - 2W_{222}\,(\vec{H} \cdot \vec{c})\,(\vec{H} \cdot \vec{\rho})$$

$$+ W_{131}\,(\vec{c} \cdot \vec{c})(\vec{H} \cdot \vec{\rho}) + 2W_{131}(\vec{H} \cdot \vec{c})(\vec{c} \cdot \vec{\rho}) - 2W_{040}(\vec{c} \cdot \vec{c})(\vec{c} \cdot \vec{\rho})$$

Constant term (piston error):

$$W_{040}(\vec{c}\cdot\vec{c})^2 - W_{131}(\vec{H}\cdot\vec{c})(\vec{c}\cdot\vec{c}) + W_{222}(\vec{H}\cdot\vec{c})^2 + W_{220}(\vec{H}\cdot\vec{H})(\vec{c}\cdot\vec{c}) - W_{311}(\vec{H}\cdot\vec{H})(\vec{H}\cdot\vec{c}) \qquad (A.3)$$

First let us examine <u>coma</u>.

$$W = \left[W_{131}(\vec{H}\cdot\vec{\rho}) - 4W_{040}(\vec{c}\cdot\vec{\rho})\right](\vec{\rho}\cdot\vec{\rho})$$

$$= W_{131}\left[(\vec{H}-\vec{k}_{131})\cdot\vec{\rho}\right](\vec{\rho}\cdot\vec{\rho}) , \qquad (A.4)$$

where

$$\vec{k}_{131} = \frac{4W_{040}\vec{c}}{W_{131}} . \qquad (A.5)$$

This is the usual linear coma shifted in the image plane to the point located by the vector $\vec{k}_{131}$.

Eq. A.4 is essentially the same as Eq. 2.15. The difference is only in the expressions for perturbation vectors.

Astigmatism and field curvature are given by

$$W = \Delta W_{20}(\vec{\rho}\cdot\vec{\rho}) + W_{222}(\vec{H}\cdot\rho)^2 - 2W_{131}(\vec{c}\cdot\vec{\rho})(\vec{H}\cdot\vec{\rho}) + 4W_{040}(\vec{c}\cdot\vec{\rho})^2$$
$$+W_{220}(\vec{H}\cdot\vec{H})(\vec{\rho}\cdot\vec{\rho}) - W_{131}(\vec{H}\cdot\vec{c})(\vec{\rho}\cdot\vec{\rho})$$
$$+2W_{040}(\vec{c}\cdot\vec{c})(\vec{\rho}\cdot\vec{\rho}) . \qquad (A.6)$$

Here to retain the same pupil dependence we should apply the vector identity (Thompson 1980)

$$2(\vec{A}\cdot\vec{B})(\vec{A}\cdot\vec{C}) = (\vec{A}\cdot\vec{A})(\vec{B}\cdot\vec{C}) + \vec{A}^2\cdot\vec{B}\,\vec{C} , \qquad (A.7)$$

so that

$$2W_{131}(\vec{c}\cdot\rho)(\vec{H}\cdot\vec{\rho}) = W_{131}(\vec{c}\cdot\vec{H})(\vec{\rho}\cdot\vec{\rho}) - W_{131}\vec{H}\,\vec{c}\cdot\vec{\rho}^2 . \qquad (A.8)$$

We will consider the properties of the medial focal surface first.

We know that

$$W_{220}(\vec{H}\cdot\vec{H})(\vec{\rho}\cdot\vec{\rho}) + W_{222}(\vec{H}\cdot\vec{\rho})^2$$

$$= W_{220M}(\vec{H}\cdot\vec{H})(\vec{\rho}\cdot\vec{\rho}) + \frac{1}{2}W_{222}(\vec{H}\cdot\vec{\rho})^2 \ . \qquad (A.9)$$

Therefore the medial focal surface is given by

$$-\Delta W_{20} = W_{220M}(\vec{H}\cdot\vec{H}) - 2W_{131}(\vec{c}\cdot\vec{H}) + 2W_{040}(\vec{c}\cdot\vec{c})$$

$$= W_{220M}\left[(\vec{H} - \vec{k}_{220M})\cdot(\vec{H} - \vec{k}_{220M}) + \ell_{220M}\right] \ , \qquad (A.10)$$

where

$$\vec{k}_{220M} = \frac{W_{131}\vec{c}}{W_{220M}} \qquad (A.11)$$

and

$$\ell_{220M} = \left[\frac{2W_{040}}{W_{220M}} - W_{131}^2/(W_{220M}^2)\right]\vec{c}^2 \ . \qquad (A.12)$$

The medial focal surface varies quadratically with the field. The vertex is located transversely from the center of the image field by the vector $\vec{k}_{220M}$. There is a longitudinal shift along the optical axis due to the term $W_{220M}\ell_{220M}$.

Astigmatism with respect to the medial surface is given by

$$W = \frac{1}{2}W_{222}\vec{H}^2\cdot\vec{\rho}^2 - W_{131}\vec{H}\vec{c}\cdot\vec{\rho}^2 + 4W_{040}\vec{c}^2\cdot\vec{\rho}^2$$

$$= \frac{1}{2}W_{222}\left[(\vec{H} - \vec{k}_{222})^2 - \vec{\ell}_{222}^2\right]\cdot\vec{\rho}^2 \ , \qquad (A.13)$$

where

$$\vec{k}_{222} = \frac{W_{131}}{W_{222}}\vec{c} \qquad (A.14)$$

and

$$\vec{\ell}_{222}^{\,2} = \left[\frac{W_{131}^2}{W_{222}^2} - \frac{8W_{040}}{W_{222}}\right]\vec{c}^{\,2} \quad . \tag{A.15}$$

This is binodal astigmatism with the nodes located by the vectors $\vec{k}_{222} + \vec{\ell}_{222}$ and $\vec{k}_{222} - \vec{\ell}_{222}$.

Distortion is given by

$$\begin{aligned} W = {} & W_{311}(\vec{H}\cdot\vec{H})(\vec{H}\cdot\vec{\rho}) - 2W_{220}(\vec{H}\cdot\vec{H})(\vec{c}\cdot\vec{\rho}) \\ & -2W_{222}(\vec{H}\cdot\vec{c})(\vec{H}\cdot\vec{\rho}) + W_{131}(\vec{c}\cdot\vec{c})(\vec{H}\cdot\vec{\rho}) \\ & + 2W_{131}(\vec{H}\cdot\vec{c})(\vec{c}\cdot\vec{\rho}) - 2W_{040}(\vec{c}\cdot\vec{c})(\vec{c}\cdot\vec{\rho}) \quad . \end{aligned} \tag{A.16}$$

The transverse ray aberration for distortion will be

$$\begin{aligned} (n'u')\vec{\varepsilon} = {} & W_{311}(\vec{H}\cdot\vec{H})\vec{H} - 2W_{222}(\vec{H}\cdot\vec{c})\vec{H} + W_{131}(\vec{c}\cdot\vec{c})\vec{H} \\ & -2W_{220}(\vec{H}\cdot\vec{H})\vec{c} + 2W_{131}(\vec{H}\cdot\vec{c})\vec{c} - 2W_{040}(\vec{c}\cdot\vec{c})\vec{c} \quad . \end{aligned} \tag{A.17}$$

This is a third-degree equation and will have three roots. The easiest way to find the roots of this equation is to use the approximation methods such as one would use to find the roots of a scalar polynomial.

From Eqs. A.4, A.13, and A.17 we can see that there are no new types of aberrations, i.e., they are the same as those described in Chapter 2.

Here we described the aberrations of the rotationally symmetric system with the decentered pupil. In general, the system does not have to be rotationally symmetric, it can have tilted and decentered surfaces or components. In this case the wave aberration expansion will have to include the perturbations of the system as well as the transverse shift of the pupil.

LIST OF REFERENCES

Buchroeder, R. A., "Tilted component telescopes. Part I: Theory," Appl. Optics, **9**, 9, 2169 (1970).

Buchroeder, R. A., "Tilted component optical systems," PhD dissertation, Optical Sciences Center, University of Arizona (1976).

Gelles, Rubin, "Unobscured aperture stigmatic telescope," Opt. Eng. 13, 6, 534 (Nov./Dec. 1974).

Gelles, Rubin, "Unobscured aperture two mirror systems," J. Opt. Soc. Am. **65**, 10 1141 (Oct. 1975).

King, W. B., "Unobscured laser-beam-expander pointing system with tilted spherical mirrors," Appl. Opt. (L), **13**, 1, 21 (1974).

Kingslake, R., Lens Design Fundamentals, Academic Press, New York (1978).

Prasad, J., G. Mitra, and P. K. Jain, "Aberrations of a system of arbitrarily inclined planar surfaces placed in non-collimated light beam," Nouv. Rev. Optique **6**, 6, 345 (1975).

Shearer, J., "Geometrical optics of concave mirrors and of combinations of mirrors," Australian J. Sci. Res. A. **3**, 532 (1950).

Smith, W. J., Modern Optical Engineering; the Design of Optical Systems, McGraw-Hill, New York (1966).

Thompson, K. P., "Aberration fields in tilted and decentered optical systems," PhD dissertation, Optical Sciences Center, University of Arizona (1980).

Welford, W. T., Aberrations of the Symmetrical Optical System, Academic Press, New York (1974).